MASTER'S THESIS

Evaluation of the controllable flexibility reserve of the power transformers for short-term planning and real-time operation of power system

For the achievement of the academic degree
Diplom-Ingenieur (Dipl.-Ing.)

supervisor
Univ.-Prof. Dr.-Ing. Wolfgang Gawlik
and
assistant
Dipl. -Ing. Irina Lupandina

submitted at

Institute of Energy Systems and Electric Drives
Technische Universität Wien

by

Gaini Seitzhanova (01429950)

Vienna, February 2023

Forschungsbereich Energiesysteme und Netze
A-1040 Wien, Gusshausstr. 25, Internet: http://www.ea.tuwien.ac.at

Die approbierte gedruckte Originalversion dieser Diplomarbeit ist an der TU Wien Bibliothek verfügbar
The approved original version of this thesis is available in print at TU Wien Bibliothek.

Die approbierte gedruckte Originalversion dieser Diplomarbeit ist an der TU Wien Bibliothek verfügbar
The approved original version of this thesis is available in print at TU Wien Bibliothek.

Eidesstattliche Erklärung

Hiermit erkläre ich, dass die vorliegende Arbeit ohne unzulässige Hilfe Dritter und ohne Benutzung anderer als der angegebenen Hilfsmittel angefertigt wurde. Die aus anderen Quellen oder indirekt übernommenen Daten und Konzepte sind unter Angabe der Quelle gekennzeichnet. Die Arbeit wurde bisher weder im In- noch im Ausland in gleicher oder in ähnlicher Form in anderen Prüfungsverfahren vorgelegt.

Wien, 28. Februar 2023

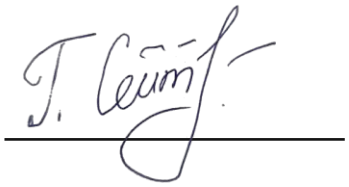

Die approbierte gedruckte Originalversion dieser Diplomarbeit ist an der TU Wien Bibliothek verfügbar
The approved original version of this thesis is available in print at TU Wien Bibliothek.

Acknowledgments

I would like to thank Univ. -Prof. Dr. -Ing. Wolfgang Gawlik for his professional advises and participation in discussions regarding this thesis.

Also I would like thank my supervisor -Dipl. Ing. Irina Lupandina for her guidance throughout this work. Her immense dedication and optimism helped me a lot.

I cannot express how much I am thankful to my mother Balsheker Yermagambetova and my father Sabyrzhan Iskakov for their endless love and support and for this great opportunity to study abroad.

Further I would like to thank my cousin Elmira Lechat for contributing in my personal and professional development. You are a role model and inspiration for me.

Thanks to my grandfather Sakhtaganov Sharip, not only for teaching me math, but for being my friend.

Thanks to my grandmother Zhaikova Ziken for educating me as a child.

Thanks to my friends, especially to Dijana Sibenik for always being there for me.

And finally I would like to thank all the other people who supported my journey.

Die approbierte gedruckte Originalversion dieser Diplomarbeit ist an der TU Wien Bibliothek verfügbar
The approved original version of this thesis is available in print at TU Wien Bibliothek.

Kurzfassung

Ein Leistungstransformator ist ein maßgebliches Element eines Stromversorgungssystems und gleichzeitig eine große Investition. Ein Transformatorausfall führt zu kostspieligem Engpassmanagement-Maßnahmen, die man durch erhöhte Flexibilität des Netztes vermeiden kann.

Das Hauptziel dieser Arbeit ist die Integration eines Kühlsystems in das existierende Temperatur der obersten Ölschichten Modell, um die Auslastungsreserve und Flexibilität von Ölgefüllten Transformatoren zu analysieren. Hierfür wird das Modell aus dem Leitfaden für die Belastung von mineralölgefüllten Leistungstransformatoren (IEC 60076-7) herangezogen und um das Modell von M.Djamali erweitert. Last und Umgebungstemperatur (für Winter und Sommer) werden als Eingangsgröße verwendet. Der Referenztransformator ist ein 58/45/40 MVA-Leistungstransformator mit ONAF/ONAF/ONAN Kühlsystem. Verschiedene Kühlungssystems-Steuerungsstrategien, werden, in folgenden Szenarien, miteinander verglichen: Windkraftwerks-Sammeltransformator (zwei Lastprofile), Solarkraftwerks-Sammeltransformator (ein Lastprofil), Umspannwerkstransformator (ein Lastprofil), sowie Ventilator-Vorkühlung mit unterschiedlichen Aktivierungszeiten, vor einem Netzengpass. Zusätzlich wurde die Zeit, welche das System benötigt, um die vollständig verfügbare, thermische Reserve zu erreichen, sowie das Verbrauch der Reserve nach dem Ereignis im Netz, berechnet.

Die Ergebnisse der beiden Windlast-Szenarien zeigen, dass die mit Auslastung, beziehungsweise Heißpunkttemperatur, gesteuerten Kühlanlage, eine optimale Kühlungssystems-Steuerungsstrategie, für Sommer- und Winterumgebungstemperaturen aufweisen. Im PV-last-Szenario zeigt sich, dass alle Steuergrößen eine ausreichend gute Kühlung im Sommer aufweisen, im Winter ist keine Kühlung notwendig. Im Falle des Umspannwerkstransformators ist, für Sommerumgebungstemperaturen, das Heißpunkttemperatur gesteuerte System, sowie jenes mit Temperatur der obersten Ölschichten-Steuerung, optimal. Im Winter ist auch hier keine Kühlung notwendig. Das System mit Ventilator-Vorkühlung benötig zwischen 94 und 96 Minuten bei Bemessungsölzeitkonstante von 150 min des untersuchten Transformators, um die volle thermische Reserve zu erreichen, unabhängig von der Umgebungstemperatur und der Einschaltzeitpunkt der Ventilatoren. Ventilator-Vorkühlung ist nur bei kurzfristiger Spitzenlast effektiv. Der maximale lineare Temperaturanstieg beträgt 0,03 °C/Minute bei mittlerer Dauer von 125 Minuten. Allgemein ist eine Vorkühlung im Winter nicht notwendig.

Die approbierte gedruckte Originalversion dieser Diplomarbeit ist an der TU Wien Bibliothek verfügbar
The approved original version of this thesis is available in print at TU Wien Bibliothek.

Abstract

A power transformer is a large capital asset and a critical element of a power system. A failure of a transformer leads to costly grid congestion measures, which can be avoided by increasing grid flexibility.

The main aim of this work is to implement a cooling system into the existing top-oil temperature model to analyse the available loading reserve and flexibility of the power transformers. For this purpose the IEC 60076-7 loading guide model is complemented by model suggested by M.Djamali. load, winter and summer ambient temperatures are used as inputs. The reference transformer is a 58/45/40 MVA power transformer with ONAF/ONAF/ONAN cooling system.

The comparison of the different cooling control system strategies is conducted for the following scenarios: Wind Farm Collector Transformer (two load profiles), Solar Farm Collector Transformer (one load profile), interconnecting transformer (one load profile) and pre-cooling with different fan activation time, prior to grid emergency. Additionally, the time that the pre-cooled system required to achieve full temperature reserve is estimated together with linear temperature gain.

The results show that for both wind load profiles, the system controlled by load and the system controlled by hottest-spot temperature, are the optimal cooling control strategies, for winter and summer ambient temperature. For the solar load profile, by summer ambient temperature, the system controlled by top-oil temperature is sufficient or all three governing variables can be applied and by winter ambient temperature no additional cooling is required. For the interconnecting transformer, operating in normal conditions, by summer ambient temperature, the systems controlled by top-oil and by hottest-spot temperature are optimal and no additional cooling is required during the winter at (n-1)-design criterion for normal grid operation.

Time that the pre-cooled system required to achieve the full temperature reserve ranges between 94-96 minutes irrespective of the ambient temperature and fan activation start, with a rated oil time constant of 150 min for the specified transformer. Overall, it can be concluded that pre-cooling is effective only by short-term peaks. Maximum achievable linear temperature gain is $0.03°C/min$ by mean duration of 125 minutes. Pre-cooling by winter is not required.

Die approbierte gedruckte Originalversion dieser Diplomarbeit ist an der TU Wien Bibliothek verfügbar
The approved original version of this thesis is available in print at TU Wien Bibliothek.
TU Bibliothek Your knowledge hub WIEN

Contents

Kurzfassung iii

Abstract iv

List of abbreviations viii

1 Introduction 1
- 1.1 Motivation of the work . . . 2
- 1.2 Research questions . . . 2
- 1.3 Structure of thesis . . . 2

2 Theoretical background 3
- 2.1 Classification of transformers . . . 3
  - 2.1.1 Classification of transformers by power rating . . . 3
  - 2.1.2 Classification of transformers by placement . . . 4
  - 2.1.3 Classification of transformers by type of electrical circuits . . . 4
    - 2.1.3.1 Autotransformers . . . 5
    - 2.1.3.2 Solid-state transformer . . . 5
    - 2.1.3.3 Conventional transformers . . . 6
- 2.2 Wind farm collector transformers . . . 6
- 2.3 Solar farm collector transformers . . . 7
- 2.4 Transformer cooling methods . . . 8
  - 2.4.1 Transformer radiators . . . 9
  - 2.4.2 Oil natural air natural cooling . . . 9
  - 2.4.3 Oil natural air forced cooling . . . 11
  - 2.4.4 Fan arrangement . . . 13
- 2.5 Cooling control methods . . . 14
  - 2.5.1 Automatic control system . . . 14
  - 2.5.2 Pre-cooling or smart cooling . . . 16
- 2.6 Transformer temperature monitoring . . . 16

3 Dynamic thermal modelling 20
- 3.1 Fundamental principles of heat transfer . . . 20
  - 3.1.1 Similitude . . . 20
    - 3.1.1.1 Nusselt number . . . 21
    - 3.1.1.2 Reynolds number . . . 21
    - 3.1.1.3 Grashof number . . . 21
    - 3.1.1.4 Pradntl number . . . 22
    - 3.1.1.5 Dynamic viscosity . . . 22
- 3.2 Thermal models . . . 22
  - 3.2.1 The models from loading guides . . . 23

Die approbierte gedruckte Originalversion dieser Diplomarbeit ist an der TU Wien Bibliothek verfügbar
The approved original version of this thesis is available in print at TU Wien Bibliothek.
TU Bibliothek Your knowledge hub WIEN

3.2.2 Basic principles . . . 23
3.2.2.1 IEC 60076-7 model . . . 25
3.2.2.2 Steady-state model . . . 26
3.2.2.3 IEEE C57 91. Annex G . . . 26
3.3 The thermo-electric analogy theory . . . 26
3.3.1 The model of Swift . . . 28
3.3.2 The model of Susa . . . 29
3.3.2.1 The model for the calculation of top-oil temperature . . . 29
3.3.2.2 The model for the calculation of hottest-spot temperature . 30
3.3.3 The model of Djamali . . . 31

4 Model and methodology 33
4.1 Input data . . . 33
4.1.1 Reference transformer . . . 33
4.1.2 Ambient temperature . . . 34
4.1.3 Load profiles . . . 35
4.2 The hottest-spot temperature model . . . 37
4.3 Oil time constant . . . 37
4.4 Oil side equations . . . 38
4.5 Air side equations . . . 39
4.5.1 Radiation . . . 39
4.5.2 Natural convection . . . 40
4.5.3 Forced convection . . . 41
4.6 Determination of reference temperatures . . . 42
4.6.1 Oil side reference temperature . . . 42
4.6.2 Air side reference temperature . . . 43
4.7 Simulation of control systems . . . 43
4.7.1 System controlled by Top-Oil Temperature . . . 43
4.7.2 System controlled by load . . . 43
4.7.3 System controlled by Hottest-Spot Temperature . . . 44
4.8 Simulation of pre-cooling . . . 44
4.9 Cooling methods . . . 44

5 Determination of optimal cooling method for different loading scenarios 45
5.1 Scenario wind farm collector transformer 1 . . . 45
5.1.1 Summer . . . 45
5.1.2 Winter . . . 48
5.2 Scenario wind farm collector transformer 2 . . . 50
5.2.1 Summer . . . 50
5.2.2 Winter . . . 53
5.3 Scenario solar farm collector transformer . . . 55
5.3.1 Summer . . . 55
5.3.2 Winter . . . 56
5.4 Scenario grid transformer . . . 57
5.4.1 Summer . . . 57
5.4.2 Winter . . . 59

Die approbierte gedruckte Originalversion dieser Diplomarbeit ist an der TU Wien Bibliothek verfügbar
The approved original version of this thesis is available in print at TU Wien Bibliothek.
TU Bibliothek Your knowledge hub WIEN

6 The analysis of the pre-cooling effect **61**
6.1 Summer 61
6.1.1 Scenario 1. Pre-cooling 400 minutes prior grid emergency 61
6.1.2 Scenario 2. Pre-cooling 200 minutes prior grid emergency 62
6.1.3 Scenario 3. Pre-cooling 100 minutes prior grid emergency 63
6.1.4 Scenario 4. Cooling after reported emergency 64
6.2 Winter 65
6.2.1 Scenario 1. Pre-cooling 400 minutes prior grid emergency 65
6.2.2 Scenario 2. Pre-cooling 200 minutes prior grid emergency 66
6.2.3 Scenario 3. Pre-cooling 100 minutes prior grid emergency 67
6.3 Pre-cooling and automatic control systems 67
6.3.1 Summer 67
6.3.2 Winter 69
6.4 Interpretation of the results 72

7 Conclusion **74**

Bibliography **84**

Die approbierte gedruckte Originalversion dieser Diplomarbeit ist an der TU Wien Bibliothek verfügbar
The approved original version of this thesis is available in print at TU Wien Bibliothek.

List of abbreviations

BOT	bottom-oil temperature
EHV	extra high voltage
ETM	Electronic Temperature Monitors
HST	hottest-spot temperature
HV	high voltage
HVDC	high-voltage direct current
HVMV	high-voltage middle voltage
IEC	International Electrotechnical Commission
IEEE	Institute of Electrical and Electronics Engineers
OFAF	Oil Forced Air Forced
OFWF	Oil Forced Water Forced
ON	Oil Natural
ONAF	Oil Natural Air Forced
ONAN	Oil Natural Air Natural
OTI	Oil Temperature Indicators
PV	Photovoltaic
SFCT	Solar Farm Collector Transformer
SPP	Solar Power Plants
SST	solid-state transformer
TFOT	total fan operation time
TOT	top-oil temperature
TTC	thermal time constant
WFCT	Wind Farm Collector Transformer
WPP	Wind Power Plants
WTG	Wind Turbine Generators
WTI	Winding Temperature Indicators
ZAMG	Zentralanstalt für Meteorologie und Geodynamik

Die approbierte gedruckte Originalversion dieser Diplomarbeit ist an der TU Wien Bibliothek verfügbar
The approved original version of this thesis is available in print at TU Wien Bibliothek.

1 Introduction

A power transformer is a large capital asset and a critical element of a power system. The transformer failure leads to violation of (n-1)-criterion, which in turn leads to costly grid congestion managements measures, as for example re-dispatch. According to Austrian Power Grid (Transmission System Operator) alone in June 2022 14 million euro were invested in re-dispatch. A more flexible grid is a solution to prevent frequent grid congestion. One of the measures for increasing the grid flexibility is the consideration of the dynamic loading limits of power transformer. These limits are influenced by the following factors: construction of transformer, cooling system, ambient temperature etc.

With more and more renewable energy sources being integrated into the grid, the topic of transformer overload is gaining importance. However, overloading of transformer accelerates the aging rate of its insulation. By overload the winding and oil temperatures are reaching or even exceeding the loading limits, given by technical norms. Hence it must be ensured, that the heat generated in transformer is dissipated properly. In this regard thermal monitoring of transformer plays a key role.

The transformer insulation aging is directly assessed using the winding hottest-spot temperature (**HST**). For this purpose both steady HST under different load and dynamic HST under varying loads are suitable. The steady HST is obtained during the heat run test and the dynamic HST is estimated using the thermal models. According to the IEC 60076-7 loading guide, maximum allowed steady HST temperature for long and -short term overload are 140 °C and 160 °C respectively [1].

While recently produced transformers are equipped with sensors, direct temperature measurement of winding's HST for already operating transformer could be challenging and price inefficient. Usually for the transformers in operation the top-oil temperature (**TOT**) is measured and the HST is simulated. The most commonly known models used for the HST simulation are the models provided in IEC 60076-7 and IEEE loading guides, as they are quite simple and mostly require data available from standard factory tests or easily obtained during the transformer's operation. The major drawback of these models is that they do not consider many factors, which potentially might have impact on HST value. As for example, variation of thermal resistance with temperature, variation of oil time constant and how the operation of fans and heat pumps influences heat transfer processes inside the transformer.

Another way to prolong the winding insulation life is to pre-cool the transformer. Modern monitoring systems have built-in "Smart Cooling" option, based on pre-cooling method. This means, that transformer fans can be activated in a predictive manner, before the winding is heated. Additionally monitoring system controls current state of the cooling system e.g. it "knows" how many fans are actually available. This allows, to determine the exact amount of cooling required. However, there are still no clear answers to the following questions: how long prior to grid contingency the fans must be activated and how effective is pre-cooling method compared to conventional cooling methods.

Die approbierte gedruckte Originalversion dieser Diplomarbeit ist an der TU Wien Bibliothek verfügbar
The approved original version of this thesis is available in print at TU Wien Bibliothek.
TU Bibliothek Your knowledge hub WIEN

1.1 Motivation of the work

The major objective of this work is to implement cooling system control into existing top-oil temperature model to analyze the available loading reserve and flexibility of oil-immersed power transformers.

1.2 Research questions

In this work the following research questions were analyzed:

- Which cooling control strategy is optimal for power transformer depending on the loading and ambient temperature pattern?
- How the choice of cooling control strategy influences the maintenance and repair costs of the cooling system?
- What is the effective time of pre-cooling and how high is the achievable temperature reserve by using the pre-cooling?
- What is the pre-cooling exposure time and maximum achieved temperature gain?

1.3 Structure of thesis

To answer these questions the following methods were used: the HST rise was calculated using the model provided in IEC 60076-7 loading guide and the TOT was calculated using the thermo-electrical analogy based on the model of M. Djamali. Load, winter ambient temperature and summer ambient temperature were used as input. The load data were retrieved from SimBench data base and the ambient temperature data were extracted from Zentralanstalt für Meteorologie und Geodynamic (ZAMG). The following scenarios were studied: Wind Farm Collector Transformer with a peak load during the mid-day and steadily increasing load, Solar Farm Collector Transformer and interconnecting transformer, which will be referred as Grid Transformer in this work, pre-cooling with fan activation 400, 200 and 100 minutes prior the grid emergency.

This master thesis has the following structure: in the following chapter the information about the transformers (such as: transformer types and scope of their application, monitoring of oil temperature, transformer cooling methods etc.) is provided.

The third chapter gives an overview of dynamic thermal models and fundamental principles of heat transfer. The fourth chapter describes method and methodology, which were applied in this work. The fifth chapter contains simulation results for different scenarios followed by analysis of pre-cooling effect. And in the last chapter conclusions and the outlook are provided.

Die approbierte gedruckte Originalversion dieser Diplomarbeit ist an der TU Wien Bibliothek verfügbar
The approved original version of this thesis is available in print at TU Wien Bibliothek.
TU Bibliothek Your knowledge hub WIEN

2 Theoretical background

This chapter contains an overview of transformer types and scope of their application. Transformers can be classified as power transformers and distribution transformers. While power system comprises transformers from generation station to the first distribution points, distribution system is a chain of transformers to final distribution points. Here should be mentioned, that the classification is constantly changing due to the growing connections of generator in low voltage grid.

2.1 Classification of transformers

Transformers used in substations can be subdivided into: transformers that transfer energy between different voltage level grids and transformers used for supply of auxiliary equipment. Power transformers can be classified by their size, scope of application and placement, voltage type. This is explained in the following chapters.

2.1.1 Classification of transformers by power rating

The power transformers can be classified by power rating as: large, medium and distribution transformers according to the iEC 60076-7 loading guide [1].

- **Large power transformers**

  According to the IEC 60076-7 the three-phase power transformers with a maximum rating up to 100 MVA and single-phase transformers with a maximum rating up to 33.3 MVA are large power transformers [1]. They can be further subdivided into generator and system interconnecting transformers [2]. Generator power transformer in turn, are frequently called step-up transformers.

- **Medium power transformers**

  Three-phase power transformers with a maximum rating of 100 MVA or single-phase transformers with a power rating of 33.3 MVA are called medium power transformers [1]. They are used as generator step-up transformers and grid transformers.

- **Distribution transformers**

  A power transformer can be referred as small, when it does not have radiators, coolers or tubes. In IEC 60076-7 loading guide the definition small transformer was replaced by distribution transformer[1].

  A distribution transformer is used to supply power for general purposes at final distribution voltage level from a higher-voltage distribution system. The rating of such transformers varies from 5 kVA to 3 MVA (for industry). Distribution transformers are usually -ON cooled. They can be installed indoors or outdoors, however

Die approbierte gedruckte Originalversion dieser Diplomarbeit ist an der TU Wien Bibliothek verfügbar
The approved original version of this thesis is available in print at TU Wien Bibliothek.
TU Bibliothek Your knowledge hub WIEN

the construction of both of these transformer types does not differ a lot. Distribution transformers can be further classified as installed directly on a pole or with a pole-mounted platform, the latter is used for rural distribution [3].

2.1.2 Classification of transformers by placement

The transformers can be further classified by placement as generator step-up/down, interconnecting, wind- and PV collector transformers, HVDC, traction transformers etc.

- **Generator step-up transformers**

  While generator step-down transformers transform voltage from transmission to distribution system level, generator step-up transformers are used to step-up voltage of the generators to the voltage of the transmission system. Usually they are connected in delta on the low-voltage side and in star on the high voltage side. The generator transformers can feed both conventional and the generators from renewable energy sources. The information regarding wind farm collector transformers and solar farm collector transformers is provided in sections 2.2 and 2.3 respectively.

  The other common cooling methods are Oil Forced Air Forced (OFAF) and Oil Forced Water Forced (OFWF). The OFWF cooled transformers allow to save more space on the substation, as they are less bulky due to the less oil volume required. Water is used on the power plant for cooling, so it is commonly available cooling medium [3].

  Usually one transformer is fed by one generator. However in the hydroelectric power plants it is a common practice to feed one transformer with the output of two generators, instead of using two transformers. This allows to enhance the efficiency and save some costs.

- **System interconnecting transformers**

  System interconnecting transformers serve to connect different voltage systems and allow exchange of active and reactive power between the systems [2]. These are usually two/three-winding transformers or autotransformers (autotransformers also can be with three windings)[3].

  The substation transformers vary in range from less than 10 MVA to 150 MVA. Often substation transformers have tap-changing mechanisms for voltage control [4].

  In many substations two transformers are connected parallel. The rating of the transformer is chosen the way, that when one transformer is out of operation the second transformer can support the entire substation load. In larger substations usually more than two transformers are connected parallel, in order to fulfil even stricter network security standards [3].

  For substations it is common to have transformer with dual rating e.g. with ONAN and additional ONAF cooling, because the transformers usually are not fully loaded (the load is shared by two transformers) and the load varies during 24 hours [3].

2.1.3 Classification of transformers by type of electrical circuits

Transformers can be classified by electrical circuits types as: autotransformers, conventional transformers and solid-state transformer or **SST**.

Die approbierte gedruckte Originalversion dieser Diplomarbeit ist an der TU Wien Bibliothek verfügbar
The approved original version of this thesis is available in print at TU Wien Bibliothek.
TU Bibliothek Your knowledge hub WIEN

2.1.3.1 Autotransformers

In autotransformers a primary and secondary circuits share one part of a winding. This gives certain advantages and disadvantages. Their rating usually ranges from 120 to 1000 MVA [5].

Autotransformers compared to any other transformers have the following advantages [5]:

- Lower costs
- Greater efficiency
- Better regulation
- Smaller size
- Smaller excitation current

While in the transformers all the kVA is transformed from the primary to the secondary lines in the autotransformers only a part of kVA is transformed, the rest flows directly from the primary to the secondary lines without transformation. This gives the autotransformers the advantages stated above. A significant disadvantage of the autotransformers is their limited ability to withstand short-circuit current. Another disadvantage or limitation is insulation problem. Due to the metallic connection between the high- and low-voltage circuits, each circuit is affected by electric disturbances occurring in the other[5]. The autotransformers often serve as interconnecting transformers, which connect different high-voltage system levels [2].

2.1.3.2 Solid-state transformer

The solid-state transformers (SST) are a common subject in the power system studies. They can connect AC/AC, DC/DC and AC/DC grids. The circuit consists of the power electronic converters and medium-/high-frequency transformer. The SST provide the galvanic separation of the connected grids [6].

The SST can offer multiples advantages compared to the conventional transformers:

- Less bulky due to its high-frequency transformer
- Ability to correct power factor
- Better control options
- Instant voltage regulation
- Improve sag and swell voltage
- The output and input of the SST can be in different frequencies

However, the SST have certain disadvantages as for example high costs and their limited ability to operate under harsh environmental conditions [6].

Die approbierte gedruckte Originalversion dieser Diplomarbeit ist an der TU Wien Bibliothek verfügbar
The approved original version of this thesis is available in print at TU Wien Bibliothek.
TU Bibliothek Your knowledge hub WIEN

2.1.3.3 Conventional transformers

The conventional transformers are the most commonly used transformers. They operate based on the Faradey's law and provide galvanic separation of the connected networks. The three winding transformers separate three networks and the two winding transformers separate two networks [3].

2.2 Wind farm collector transformers

Nowadays, big wind parks are interconnected to the utility gird at the transmission level and smaller generation is connected to the distribution grid[7].

WPP consist of many Wind Turbine Generators (**WTG**). Each WTG is connected via a step-up transformer to a medium-voltage collector system operating at 12 kV to 34.5 kV. The collector system has one or more feeders connected together at a collector system station and a collector step-up transformer to achieve transmission system voltage [8]. Figure 2.1 represents the grid topology of WPP.

These transformers must reliably transfer power to the transmission system, provide ground sources for the transmission grid and collector system and maintain acceptable collector system voltage. WPP transformers have a lot in common with conventional power plant step-up transformer and primary distribution substation transformers, however the following factors need to be considered [7]:

- Frequent wind turbine transformers energisation will lead to mechanical and thermal stresses caused by inrush currents [9].
- Variable loading pattern, due to the intermittency in the primary energy sources (wind speed).
- Higher losses compared to conventional transformers. Wind energy that is converted and dissipated by the transformer results in higher loss compared to normal transformer use because of incentives and regulations supporting the production of clean energy.
- When it comes to wind energy, the importance of transformer reliability (how often it fails) becomes less important than its availability. This is because the grids usually rely less on the renewable energy sources by planning the generator's system capacity needs. However, poor transformer reliability can result in low availability if it takes a long time to repair or replace. The replacement and major repair for transformers might be a long process, and wind plants located in remote or offshore areas may experience particularly long outages.

Die approbierte gedruckte Originalversion dieser Diplomarbeit ist an der TU Wien Bibliothek verfügbar
The approved original version of this thesis is available in print at TU Wien Bibliothek.

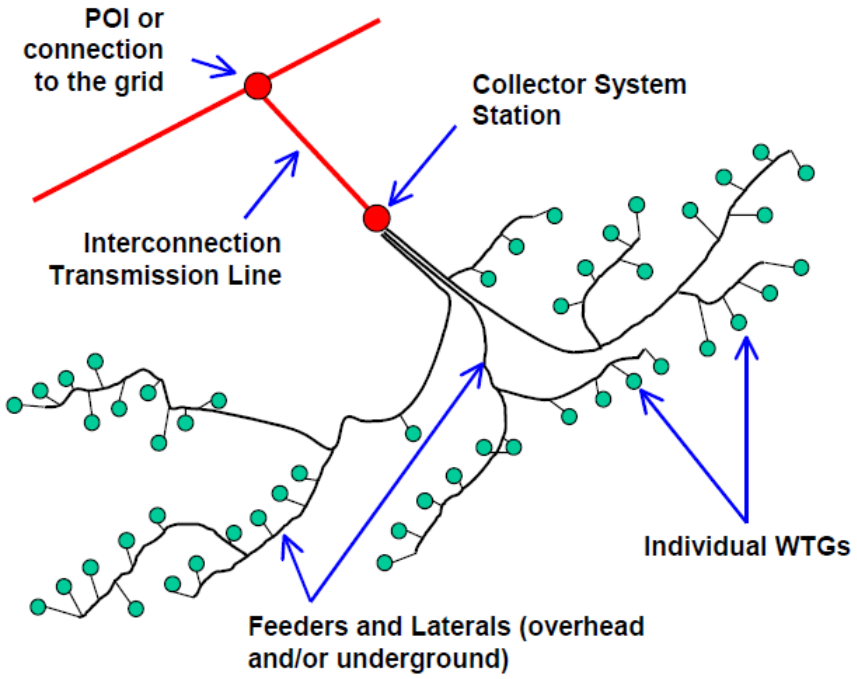

Figure 2.1: WPP grid topology [8]

2.3 Solar farm collector transformers

Figure 2.2 represents the grid topology of Solar Power Plant. It can be seen, that photovoltaic modules are connected to inverter transformers, which are primarily used as a step-up transformers to change input voltage. Usually they step-up voltage up to 36 kV or higher if needed. This voltage is further supplied to a collector bus. Further either the distribution system can be fed by this voltage or it will be connected to the substation collector transformer at the utility substation. The collector substation collects the power output of the multiple distributed sources of generation and steps-up the voltage to transmission or distribution system's voltage level. The substation transformers have power rating ranging from 20 MVA to 40 MVA with a nominal voltage of the respective grid level. Larger SPP might require a larger substation transformer [10].

Typical transformers used in SPP are: inverter transformers, auxiliary transformers and substation collector transformers.

Die approbierte gedruckte Originalversion dieser Diplomarbeit ist an der TU Wien Bibliothek verfügbar
The approved original version of this thesis is available in print at TU Wien Bibliothek.

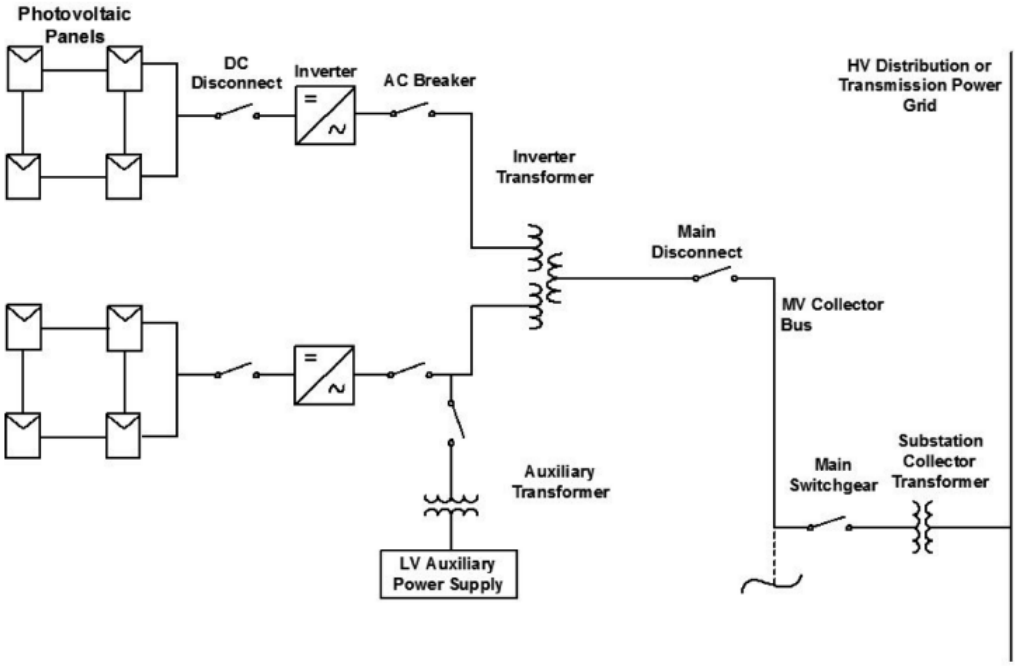

Figure 2.2: SPP grid topology [10]

2.4 Transformer cooling methods

In order to identify the cooling method of oil-immersed transformers, an international code consisting of 4 letters was introduced. The first letter indicates the type of the internal cooling medium: A-air, O-oil, G-gas, C-cryo, K- not mineral oil (synthetic, natural ester or natural oil), L-liquid with immeasurable combustion point [11].

The second letter indicates its circulation mechanism, e.g. how the cooling medium was put into motion: N-natural, F-forced by fan or pump, D-directed through channels in the windings. The classification of transformer cooling methods can be seen in figure 2.3. The third letter indicates the type of the outer medium, which could be A-air or W-water and the fourth letter indicates the circulation mechanism of the outer cooling medium [12]. Here should be noted, the inner cooling medium is in contact with the winding, whereas the outer cooling medium is in contact with the outer system (air in most cases) [11].

Die approbierte gedruckte Originalversion dieser Diplomarbeit ist an der TU Wien Bibliothek verfügbar
The approved original version of this thesis is available in print at TU Wien Bibliothek.

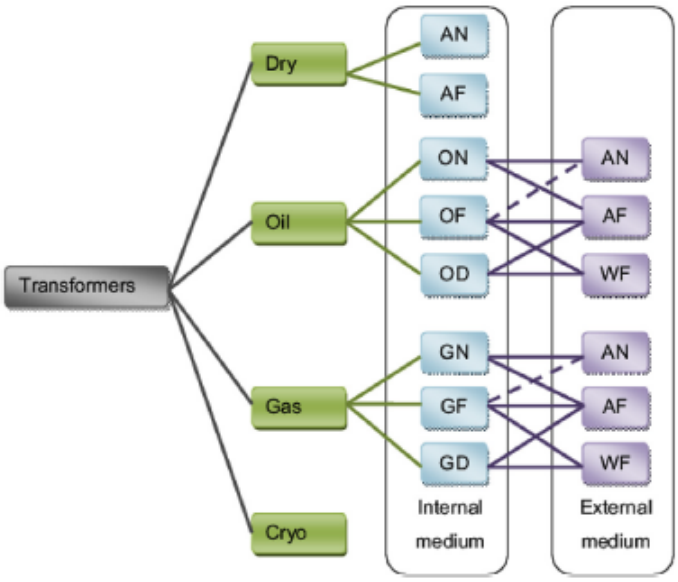

Figure 2.3: Transformer cooling modes [12]

2.4.1 Transformer radiators

The two types of transformer radiators can be distinguished [13]:

- plate
- tubular

The formulas for calculation of air side equations depend on the radiator type. For the plate radiator type vertical, horizontal or vertical and horizontal fan arrangements are common and for the tubular only horizontal fan arrangement is possible. The fans can be positioned in different ways along the plate radiators, this results in zones of surface being cooled by natural or forced air flow.

Convection heat transfer coefficients in these zones differ strongly. For the air forced zone heat transfer coefficient depends on air velocity, which can be determined as the velocity by which equilibrium between the pressure produced by the fan and pressure drop in the air stream flowing over the radiators can be reached. The fan arrangement and positioning together with the radiator type have impact on the value of this pressure drop [13].

2.4.2 Oil natural air natural cooling

Oil Natural Air Natural (**ONAN**) cooling is the simplest cooling method from the construction point, as it does not require any additional equipment and is based fully on thermosiphon principle. Thermosiphon effect is a natural circulation of oil occurring due to the convection [11].

Figure 2.4 demonstrates the dependency of oil density from the temperature. It can be seen, that oil density increases with the lower temperature.

Die approbierte gedruckte Originalversion dieser Diplomarbeit ist an der TU Wien Bibliothek verfügbar
The approved original version of this thesis is available in print at TU Wien Bibliothek.
TU Bibliothek Your knowledge hub WIEN

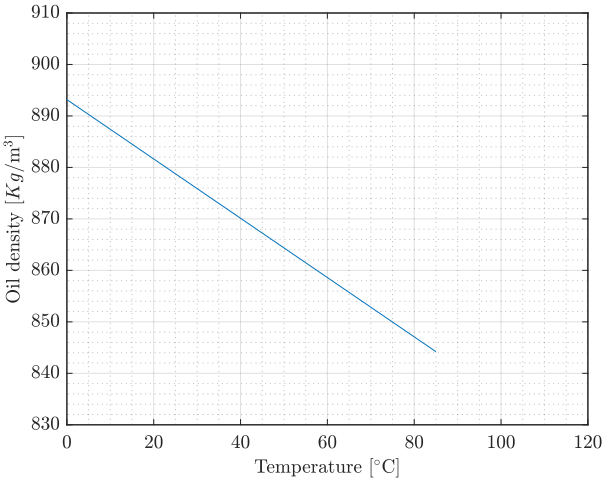

Figure 2.4: Dependency of oil density from the temperature [14]

When the oil passes by the windings it is heated and becomes lighter, this leaves less space for cold oil to fill. While oil flows up its temperature keeps increasing due to the continuous heating from the winding until it reaches maximum temperature at the winding top. Then oil flows into the cooler inlet. In the cooler (radiator) it dissipates the heat and gets cooled. The greater density makes cold oil heavier and it drops down to the bottom valve, the cycle then is repeated. This results in uneven temperature distribution along the windings. The oil at the bottom of the winding has usually the lowest temperature, then the temperature gradually increases on its way to the winding top until it reaches the maximum there [14].

It should be mentioned, that for natural cooling the height of the radiator mounting related to the winding is a crucial factor, as this cooling mode fully relies on the gravitational buoyancy. The higher the radiator is mounted above winding the higher is the buoyancy. As a result the oil circulates faster. Placing the radiator center and the winding center at the same altitude will not create gravitational buoyancy, this prevents oil from the circulation. The radiators mounted above the winding center can be seen in figure 2.5.

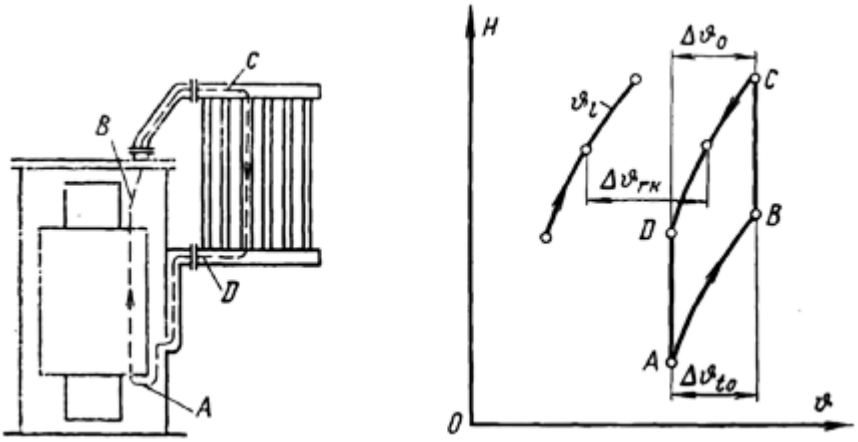

Figure 2.5: High mounted radiator [15]

Die approbierte gedruckte Originalversion dieser Diplomarbeit ist an der TU Wien Bibliothek verfügbar
The approved original version of this thesis is available in print at TU Wien Bibliothek.
TU Bibliothek Your knowledge hub WIEN

Hence this reduces the radiator's cooling ability notably. Worth to mention, that radiators must not be mounted to high either. If the radiator is installed too high the oil leaving the radiator bottom will not reach the winding bottom and will flow up through the wingdings. It will bypass the windings and flow to the winding top through the gap between the winding and the tank wall [14].

ONAN transformers operate better in short-term conditions than other cooling methods, as they have higher heat storage capacity due to the larger amount of oil. However in a hotter climate the cooling efficiency of ONAN transformers drops significantly, since the ambient temperature has a direct influence on it [6].

The operational principle of ONAN cooling is illustrated in figure 2.6. The physical processes are explained using the $\theta - H$ coordinate system. In the point A the oil is heated in the winding. Then oil is lifted and it moves towards the top of the winding, where it leaves the winding in point B. On the way from point B to point C, before flowing into the radiator inlet the oil temperature drops insignificantly, due to the heat transfer from the tank top to the upper part of the tank wall. Between the points C and D the oil is cooled and it moves to the lower part of the tank. The cooled oil moves from point D to point A then the cycle is repeated [15].

The following symbols were used on the right part of the figure 2.6:

- θ_{rk} logarithmic average temperature, between the cooling air and cold oil
- θ_{to} axial temperature drop of the oil in the winding
- θ_o axial temperature drop of the oil in the radiator (equals to θ_{to})

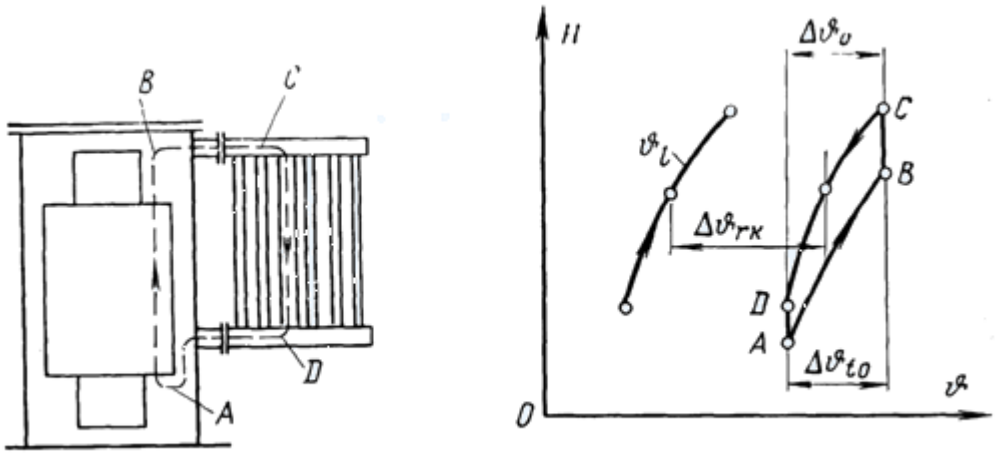

Figure 2.6: Operation principle of ONAN cooling method [15]

2.4.3 Oil natural air forced cooling

The operation principle of Oil Natural Air Forced cooling method is shown in figure 2.7.

The fans mounted under the radiators force the air in the channels between the radiator's individual sections. The increased air speed improves the heat transfer coefficient of the radiator from the air side, thanks to that the same amount of loss is dissipated by

Die approbierte gedruckte Originalversion dieser Diplomarbeit ist an der TU Wien Bibliothek verfügbar
The approved original version of this thesis is available in print at TU Wien Bibliothek.
TU Bibliothek Your knowledge hub WIEN

less temperature drop from the air side than by -ON cooling. The better heat transfer coefficient of the radiator from the air side, by the same amount of dissipated by radiator losses, leads to faster than by -ON oil circulation cooling of the oil in the tubes. On the right part of the figure 2.7 the diagram representing the physical processes inside the ONAF transformer is provided. By comparing the figures 2.6 and 2.7, it can be seen that the curve C-D has become "more prominent", this can be connected to the faster oil circulation. However, the value of the axial temperature drop in the winding $\Delta\theta_{to}$ will remain unchanged [15].

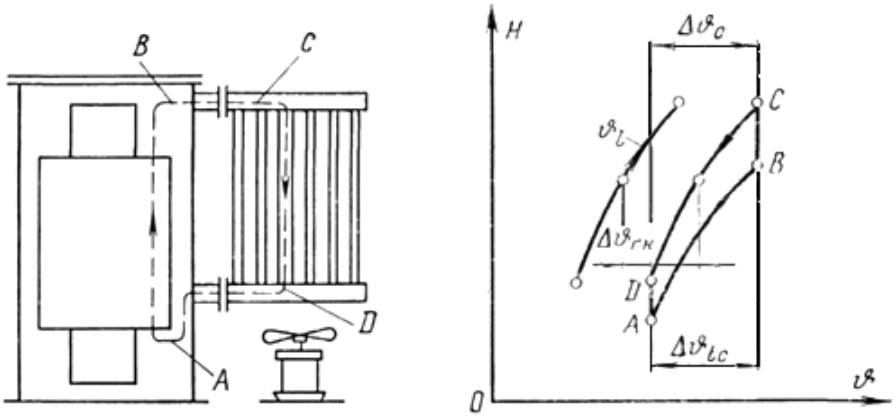

Figure 2.7: Operation principle of ONAF cooling method [15]

Figure 2.8 is a simplified temperature diagram of the same transformer with ONAN and additional ONAF cooling modes.

The solid line represents a transformer with ONAN cooling mode and the dashed line is a transformer in ONAF cooling mode. It must be ensured, that upper winding temperature is about the same for both cooling methods if it is a transformer with two cooling methods.

Die approbierte gedruckte Originalversion dieser Diplomarbeit ist an der TU Wien Bibliothek verfügbar
The approved original version of this thesis is available in print at TU Wien Bibliothek.

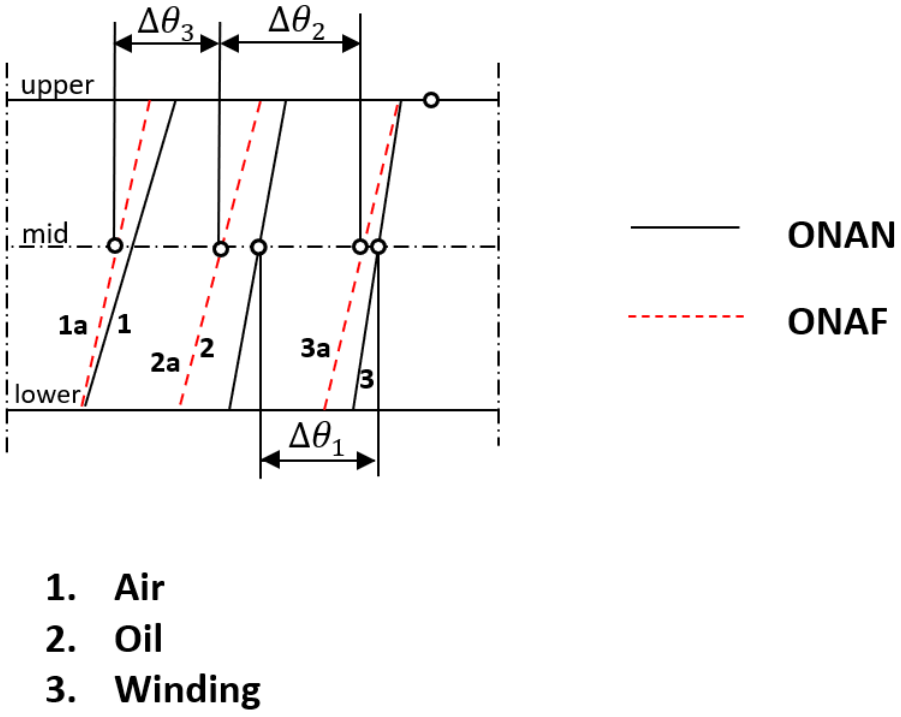

Figure 2.8: Thermal diagram of a transformer with ONAN and additional ONAF cooling methods [11]

The main temperature differences are marked on the diagram. The temperature difference $\Delta\theta_3$ between the cooling air in radiator and the oil in radiator is marked only for ONAF operation mode. However, it still can be seen that, despite the higher losses, the improvement of the heat transfer coefficient is so great, that the oil is colder in ONAF operation. Since the air volume passing through the air-side radiator ducts increased compared to ONAN, the air temperature did not heat much despite the greater amount of heat. Temperature difference between the winding and the oil in ONAF operation mode ($\Delta\theta_2$) is higher than in ONAN operation mode ($\Delta\theta_1$), this allows to dissipate more heat by the same radiator surface. Switching from the ONAN to ONAF cooling mode allows to increase cooling efficiency up to 2.6 times by the same ambient temperature [11].

2.4.4 Fan arrangement

The fans of a transformer can be mounted either on the side or under the radiator. There are two ways to mount the fans:

- vertical
- horizontal

Both vertical and horizontal fan arrangements can be seen in figure 2.9.

By vertical ventilation, the air flow moves in opposite to the oil direction which reduces the cooling efficiency. By horizontal fan arrangement the freshly sucked-in air flow meets the points with the hottest oil temperature, whereas by vertical fan arrangement already

Die approbierte gedruckte Originalversion dieser Diplomarbeit ist an der TU Wien Bibliothek verfügbar
The approved original version of this thesis is available in print at TU Wien Bibliothek.

heated air flow ventilates the upper hottest area of the radiator. On the other hand, the vertical upward flow is supported by natural buoyancy force and by horizontal fan arrangement the required air mass can only be provided by higher individual fan output. More powerful fan produced more noise [11].

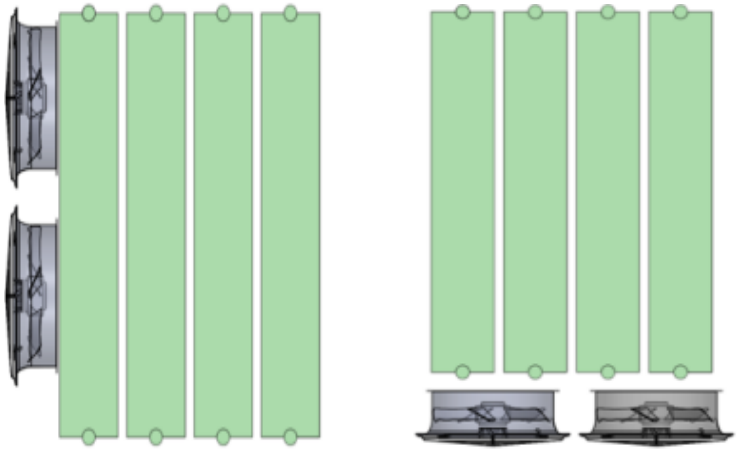

(a) Vertical fan arrangement

(b) Horizontal fan arrangement

Figure 2.9: Vertical and horizontal mounted fans [16]

2.5 Cooling control methods

In this section the existing cooling control methods are presented. The fans can be switched on/off manually or using the automatic control systems.

2.5.1 Automatic control system

The electrical energy for the operation of fans and pumps is supplied via control cabinets attached to the transformer or the cooling system. The control cabinet contains the main circuits for motor feeding, the control circuits and the monitoring circuits. Depending on the size of transformer the clumping strips for the connection to the switching elements are included in these cabinets or installed in separate cabinets [11].

Figure 2.10 demonstrates the construction of the fan control cabinet of ONAF transformer with a radiator.

Die approbierte gedruckte Originalversion dieser Diplomarbeit ist an der TU Wien Bibliothek verfügbar
The approved original version of this thesis is available in print at TU Wien Bibliothek.

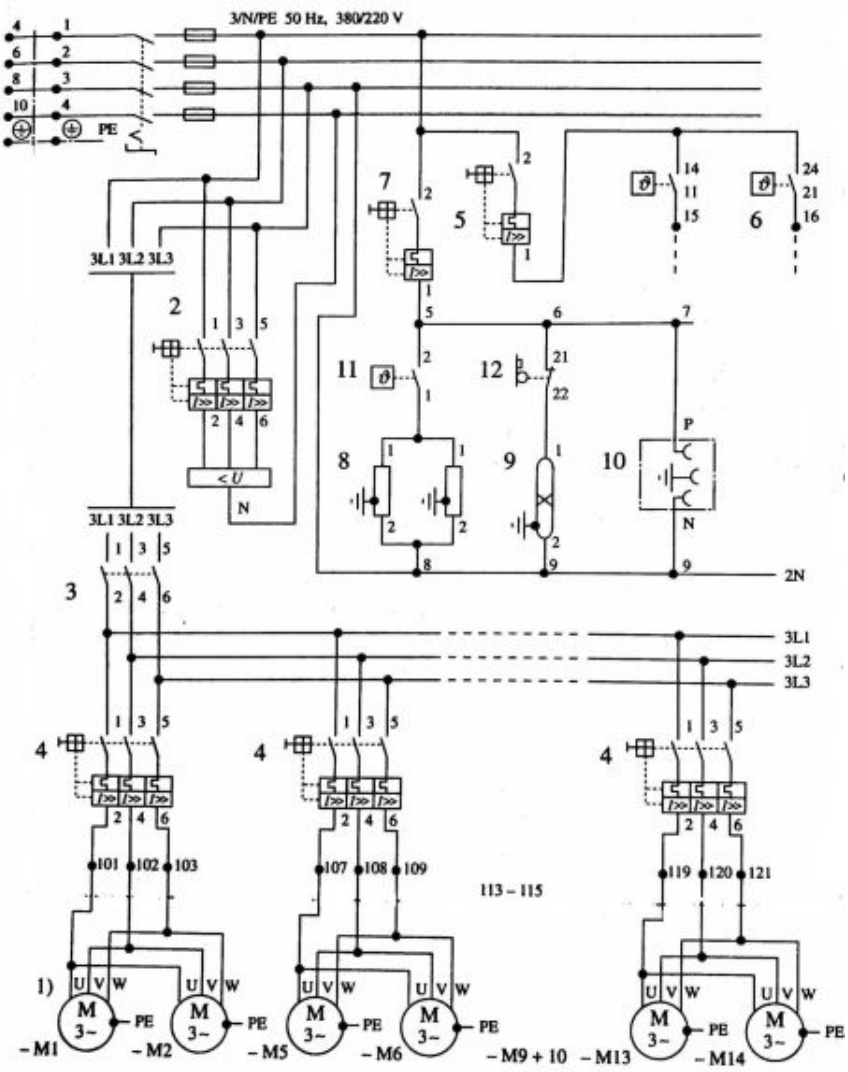

Figure 2.10: The scheme of a control cabinet [11]

The three-phase current feed (1) is routed via cables from the outside into the cabinet to clumping strips. From there the main circuit is continued via the main switch and fuses. The voltage is monitored by Relay (2) connected to overcurrent switch. The three-phase motors are supplied by main circuit breaker (3). The supply line then expands by individual motor protection switches (4). The control voltage is switched on via controllers (5). The temperature measuring device automatically switches on and -off the fans via the sensors (6) [11] using the following signals:

- Load
- Hottest-spot temperature
- Top-oil temperature

Regardless the temperature fans can be manually switched on/off manually from the control room for continuous operation. For indication of the faulty fans there is a lamp in the cabinet. Additional sensor sends the information to the room [11].

Die approbierte gedruckte Originalversion dieser Diplomarbeit ist an der TU Wien Bibliothek verfügbar
The approved original version of this thesis is available in print at TU Wien Bibliothek.

The heating (8), the lighting (9) and the socket (10) are supplied via the circuit breaker (7), additionally a fault current circuit breaker can be installed in the same circuit. The cabinet heating switches on by thermostat (11) or hygrostat. And the lighting switches on by the sensor installed in the door [11].

The construction of cooling systems with fans and pumps can be more complicated. The two or more cooling groups can form cooling stages, each stage has individual circuit. When needed the stages can be equipped with time relay. If cooling groups are switched by stages, this can be done by a dial thermometer equipped with sensors.

2.5.2 Pre-cooling or smart cooling

Some monitoring systems have a "Smart Cooling" function. The implementation of this function helps to reduce the aging rate of the insulation by using the so-called pre-cooling method. This means, that the transformer's fans are switched on in a predictive manner in response to forecast of TOT and winding HST. The smart cooling system considers ambient temperature and current state of the cooling system and determines how much cooling is required. In figure 2.11 it can be seen how "Smart cooling" reduces the insulation aging [17].

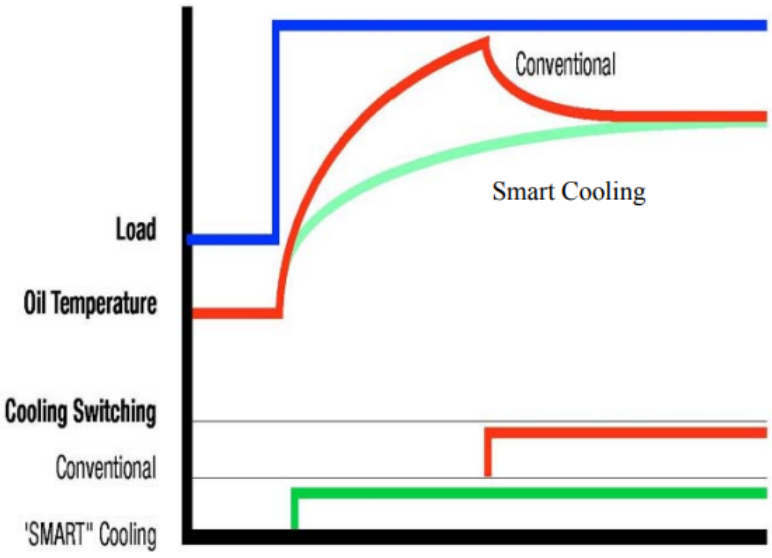

Figure 2.11: The effect of pre-cooling on the insulation aging [17]

2.6 Transformer temperature monitoring

The following temperatures are commonly measured in the transformers [18]:

- Top-oil temperature
- Bottom-oil temperature
- Winding hottest-spot temperature
- Thermal image of the winding hottest-spot temperature

Die approbierte gedruckte Originalversion dieser Diplomarbeit ist an der TU Wien Bibliothek verfügbar
The approved original version of this thesis is available in print at TU Wien Bibliothek.

The following methods for temperature measurement are commonly used: temperature measurements using traditional thermometers like Oil Temperature Indicators and Winding Temperature Indicators, electronic thermometers and direct temperature measurement with the help of Fiber Optic Temperature Probes.

Figure 2.12 illustrates traditional oil temperature thermometer. As traditional temperature gauges Oil Temperature Indicators and Winding Temperature Indicators can be named. They were invented in 1940 and it is a common practice nowadays for newly produced transformers to have OTI and WTI. A regular maintenance check or calibration must be executed to ensure accurate measurements. WTI and OTI are prone to mechanical damages, this might lead to incorrect function of the devices and as a result less efficient cooling and tripping control [19].

Figure 2.12: Traditional gauge [20]

1. **Oil Temperature Indicators**

   Oil Temperature Indicators or OTI are mounted on the top of a transformer tank. They are equipped with a sensing bulb immersed into a thermometer pocket and connected to the instrument housing via flexible connecting tubing. The instrument housing contains two capillary tubes. One is connected to the operating bellow and the other to a compensating bellow. Since the temperature inside the pocket might deviate from the actual temperature (up to 6 K) the compensating bellow is required. It compensates the variation of ambient temperature. There is a steel carriage with attached pointer and four mercury switches. One mercury switch operates the fans, one mercury switch operates the pumps, one mercury switch is required to alarm the high temperature, and the last one can inter-trip the transformer when the oil temperature is critical [20].

   Additionally the dial of the oil indicator is equipped with a dummy pointer. The main pointer pushes the dummy pointer by temperature increase. After the oil temperature drops the main pointer will move backwards, however the dummy pointer will stay on the highest temperature position of the main pointer. This allows to register the maximum temperature rise of the transformer during preset period of

Die approbierte gedruckte Originalversion dieser Diplomarbeit ist an der TU Wien Bibliothek verfügbar
The approved original version of this thesis is available in print at TU Wien Bibliothek.
TU Bibliothek Your knowledge hub WIEN

time. The liquid inside the sensing bulb rises (due to expansion) through a capillary line and moves towards the operating mechanism. A link and lever mechanism amplifies the movement, so it reaches the mercury switches and pointer. The liquid volume changes at operating mechanism make the bellow contract and expand. A lever linkage mechanism transmits this movement of below to the pointer in the temperature indicator [20].

2. **Winding Temperature Indicators**

   Since the winding temperature cannot be measured directly, a method commonly known as a "thermal image" is used [11]. The operation principle of OTI and WTI can be seen in figure 2.13.

   Winding Temperature Indicator (**WTI**) has a sensing bulb immersed in the dry well placed inside the top layer of the insulating fluid. The operation principle of OTI and WTI is the same, with the only difference that the sensing bulb of OTI is heated by surrounding oil, whereas the sensing bulb of WTI is heated by a heater coil. A heater coil (also called heating element) is fed by a sample of load current, which is directly proportional to the current in the windings. The current makes sensing bulb to sense the TOT plus a temperature increment. The temperature increment is equivalent to the winding temperature rise over the TOT. There are capillary tubes connected to the dial of the temperature indicators as by the OTI. The liquid expands and moves through the capillary tubes towards the dial gauges equipped with switches [21].

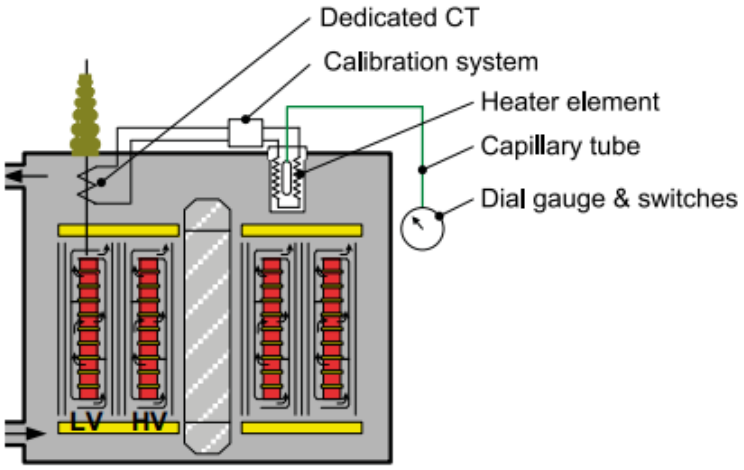

Figure 2.13: Scheme of WTI and OTI [21]

3. **Electronic Temperature Monitors**

   These electronic device can replace up to three analogue gauges. It consolidates temperature data and cooling control into one communication point. Using the transformer design information ETM can calculate winding hottest-spot temperature, this allows more accurate measurement results. The ETM can monitor all three phases by connecting to the multiple bushing CTs. Additionally ETM are helpful for estimating the transformer loss of life, as they can calculate the insulation loss of

Die approbierte gedruckte Originalversion dieser Diplomarbeit ist an der TU Wien Bibliothek verfügbar
The approved original version of this thesis is available in print at TU Wien Bibliothek.
TU Bibliothek Your knowledge hub WIEN

life. The ETMs are equipped with electronic communication, which enables remote monitoring [21].

4. **Fiber Optic Temperature Probes**

   The commonly used sensors for the winding temperature measurements are: RTD thermocouples, PT100, fiber optic, infrared [22].

   Direct Measurement with Fiber Optic Temperature Probes are used when real-time winding temperature monitoring is required. The end of the sensor, which is a measurement point is usually placed between the windings. The light pulse signal from the tip is sent down the fiber. The results are shown on the transformer monitor. This measurement method is usually used in critical transformers as for example the interconnecting power transformers, because it is quite expensive and difficult to install [22]. Since the sensor does not measure temperature directly, additionally there must be equipment to convert sensor signal into a value in degrees.

Die approbierte gedruckte Originalversion dieser Diplomarbeit ist an der TU Wien Bibliothek verfügbar
The approved original version of this thesis is available in print at TU Wien Bibliothek.

3 Dynamic thermal modelling

3.1 Fundamental principles of heat transfer

The generated heat is transferred from winding or from other transformer components. The three modes of heat transfer can be distinguished namely, conductivity, radiation and convection [23].

- **Thermal conductivity**

  With the help of thermal conductivity heat flow transportation within the material can be explained. The thermal conductivity number indicates how good or bad the thermal conductivity of material is. It is denoted by λ and has the following untis: $(W/cm \cdot K)$ or $(W/m \cdot K)$ [11]. The interaction between the solid boundary and inertial media causes the transfer of energy. Different solid boundaries have different temperature, which means different kinetic energy. While solid bodies are inherent to heat conduction, the gases and liquids transfer energy due to the natural convection, when they are heated. The thermal conductivity of liquids ranges between 0.1 and 0.2 $(W/K \cdot m)$ and the thermal conductivity of gases varies between 0.01 and 0.03 $(W/m \cdot K)$ [24].

- **Convection**

  Convection is the mechanism of heat transfer through a fluid in the presence of bulk fluid motion. The following types of convection are distinguished: natural (also known as free) and forced convection. Whether the convection is natural or forced depends on the mechanism, that initiated the medium motion. By natural convection the fluid motion is initiated by buoyancy force and by forced convection the fluid is artificially forced to flow by external means such as fans or pumps [25]. This process can be quantitatively estimated by calculating heat transfer coefficient α. The unit of the heat transfer coefficient is $(W/cm^2 \cdot K)$ or $(W/m^2 \cdot K)$ [11].

- **Radiation**

  By radiation the heat is transferred as an electromagnetic wave. α_s denotes heat transfer coefficient $(W/m^2 \cdot K)$[11] .

3.1.1 Similitude

For the calculation of the complicated thermal processes in the similitude theory a dimensionless group of parameters was introduced, such as: Prandtl number (Pr), Nusselt number (Nu), Grashof Number (Gr) etc. These parameters were used in this work to calculate the heat transfer coefficient.

Die approbierte gedruckte Originalversion dieser Diplomarbeit ist an der TU Wien Bibliothek verfügbar
The approved original version of this thesis is available in print at TU Wien Bibliothek.

3.1.1.1 Nusselt number

Nusselt number (Nu) is a dimensionless parameter. Depending on the convection type Nusselt number can be calculated using the equation 3.1 or 3.2. Nusselt number helps to improve the heat transfer coefficient [26].

Nusselt number for natural convection can be defined as:

$$Nu = f(Gr \cdot Pr) \tag{3.1}$$

For forced convection Nusselt number is calculated as:

$$Nu = f(Re \cdot Pr) \tag{3.2}$$

- Re Reynolds number
- Pr Prandtl number
- Gr Grasshof number

3.1.1.2 Reynolds number

The ratio of inertial forces to viscous forces can be defined as the Reynolds number (Re) [26]. The equation for calculation of Reynolds number is:

$$Re = \frac{\rho \cdot v \cdot d}{\mu} \tag{3.3}$$

- ρ density (kg/m^3)
- d area of the surface (m^2)
- v speed of flow (m/s)
- μ viscosity $kg/(s \cdot m)$

The Reynolds number is used to determine the fluid flow type. If Reynolds number equal to 2100 indicates laminar flow and Reynolds number greater than 2100 indicates turbulent flow [26].

3.1.1.3 Grashof number

The Grashof number is defined as a ratio of buoyant forces to viscous forces. It is used to determine the flow regime of fluid boundary layers in laminar systems. The Grashof number for incompressible liquids is given as follows [23]:

$$Gr = \frac{g \cdot L_c^3 \cdot \beta \cdot \Delta T}{\nu^2} \tag{3.4}$$

- L_c characteristic length, which is frequently chosen as the vertical distance, where the buoyancy occurs (s_{oil} in equation 4.15)
- g gravitational acceleration (m/s^2)

Die approbierte gedruckte Originalversion dieser Diplomarbeit ist an der TU Wien Bibliothek verfügbar
The approved original version of this thesis is available in print at TU Wien Bibliothek.
TU Bibliothek Your knowledge hub WIEN

- β volumetric thermal expansion coefficient $(1/K)$
- ΔT temperature difference (K)
- ν $kg/(s \cdot m)$

The coefficient of thermal expansion is given as follows:

$$\beta = \frac{1}{V} \cdot \frac{\partial V}{\partial T} \tag{3.5}$$

For many liquids the coefficient of thermal expansion β $(1/K)$ is tabulated as a value of 10^{-3} or 10^{-4} order [23].

3.1.1.4 Pradntl number

The Prandtl number can be defined as a dimensionless quantity, it describes the correlation between the fluid viscosity and thermal conductivity. In another words Prandtl number is a ratio between momentum transport and thermal transport capacity of a fluid. The lower the Prandtl number is the higher is the thermal conductivity of fluid [27].

3.1.1.5 Dynamic viscosity

The viscosity is a value that describes momentum transfer in a fluid perpendicular to the flow direction. It is especially important for calculation pressure drop. Additionally it is used to calculate Prandtl and Grashof number, which in turn are used for determination of the heat transfer coefficient. There are two types of viscosity, namely dynamic (ν) and kinematic (ρ). The equation 3.6 connects both types of viscosity [24].

$$\eta = \nu \cdot \rho \tag{3.6}$$

3.2 Thermal models

In order not to exceed loading capability of the transformers a winding temperature must be kept in an allowed range. For example, by exceeding winding temperature every 6 °C the isolation aging is accelerated twice, this is a so called 6 degree rule. Considering all the named factors the measurement of hottest-spot and winding temperature is essential. However, since the fiber optic sensor in some cases cannot be installed these values are not always representative for estimation of transformer's life losses. It is a common practice to estimate HST using the models [28]. These are:

- **Physical and semi-physical models**

  In these models complicated physical processes are expressed by simple mathematical equations. The inputs are values measured during the real-time operation. This type of models are widely used in online monitoring [29].

- **Computational fluid-dynamics approach**

  These method usually requires vast amount of data and high-performance computers. Computations might last up to few days [29].

Die approbierte gedruckte Originalversion dieser Diplomarbeit ist an der TU Wien Bibliothek verfügbar
The approved original version of this thesis is available in print at TU Wien Bibliothek.
TU Bibliothek Your knowledge hub WIEN

While measurement of HST and winding temperature are expensive and complicated processes, the TOT measurement is cost-effective and installation of the measurement equipment can be executed on the operating transformer [28].

3.2.1 The models from loading guides

The IEC 60076-7 [1] model and IEEE loading guides [30] models are generally very similar. The difference can be seen in expression of the thermal time constant and TOT rise over the ambient. The following assumptions and explanations are valid for both models.

The equations 3.7 and 3.8 represent the solution of the equation 3.20. The equation 3.8 is a difference equation used when the data set is discrete.

$$\Delta\theta = (\Delta\theta_u - \Delta\theta_i) \cdot (1 - e^{-\frac{t}{\tau_{to}}}) \tag{3.7}$$

where $\Delta\theta_u$ (°C) is the ultimate temperature rise caused by the loss P, $\Delta\theta_i$ is initial temperature rise (°C), t is time (min) and τ_o is the oil time constant (min).

$$D\theta_o = \frac{Dt}{k_{11} \cdot \tau_0}(\Delta\theta_u - \theta_{to} + \theta_a) \tag{3.8}$$

where k_{11} is the oil time constant correction factors, θ_{to} is the top-oil temperature at the considered condition (°C) and θ_a is ambient temperature (°C), Dt is time difference between the sequential measurements.

Final temperature rise from equation 3.8 is given as follows:

$$\Delta\theta_u = \Delta\theta_{or} \cdot \left[\frac{1 + R \cdot K^2}{1 + R}\right]^x \tag{3.9}$$

where $\Delta\theta_{or}$ (°C) is a temperature rise at the full load, K is a load factor, R is a ratio of short circuit loss to no load loss.

3.2.2 Basic principles

The sum of the three temperature rises represents a temperature rise of a winding above ambient, these are:

(a) the temperature rise of the inlet cooling oil above ambient

(b) the temperature rise of the cooling oil as it passes through the transformer

(c) and the temperature rise of the winding above the cooling oil

This temperatures in turn are derived from measured temperatures: inlet and outlet oil temperatures and the mean winding temperature. The temperature increase of the oil passing through the transformer is simplified and taken as the difference between the inlet and outlet oil. However this is a rough approximation, which does not consider the existence of more parallel oil paths inside the transformer. Usually there are more than one parallel oil paths, at least one for each winding, with their own temperature rise. The parallel oil paths have a common inlet temperature, but different outlet temperatures until they mix on the top. The TOT is measured using the temperature pockets [13].

Figure 3.1 demonstrates the simplified linear diagram of oil cooled transformer.

Die approbierte gedruckte Originalversion dieser Diplomarbeit ist an der TU Wien Bibliothek verfügbar
The approved original version of this thesis is available in print at TU Wien Bibliothek.
TU Bibliothek Your knowledge hub WIEN

- A TOT derived as the average of the tank outlet oil temperature and the tank pocket temperature
- B Mixed oil temperature in the tank at the top of the winding
- C Temperature of the average oil in the tank
- D Oil temperature at the bottom of the winding
- E Bottom of the tank
- gr Average winding to average oil (in tank) temperature gradient at rated current
- H Hotspot factor
- P Hottest-spot temperature
- Q Average winding temperature determined by resistance measurement
- y-axis representing relative position (height) and x-axis representing temperature

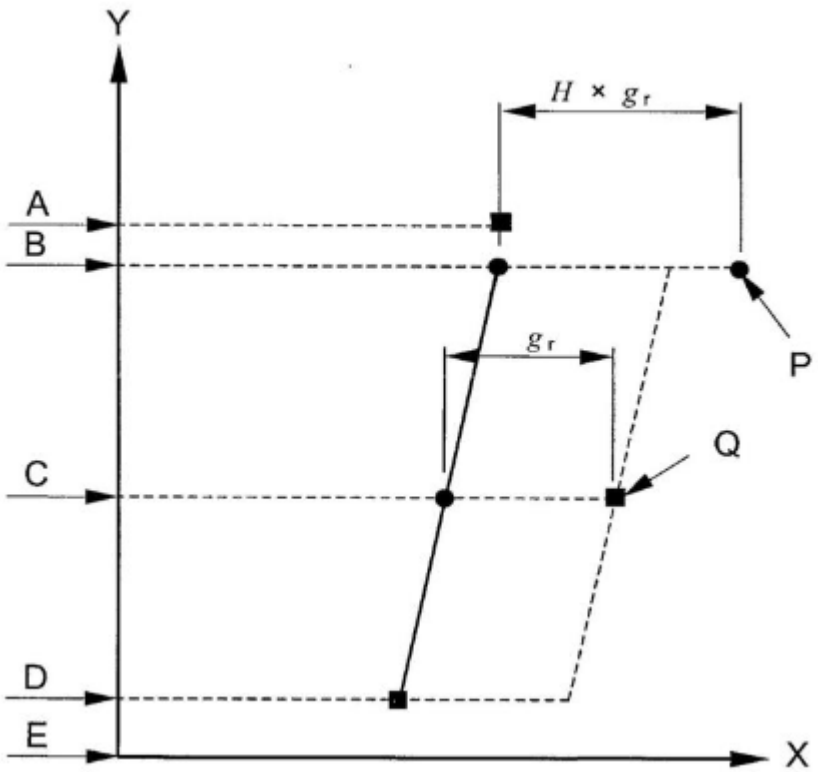

Figure 3.1: Linear thermal diagram of oil cooled transformer [1]

Summarizing all the information, the following assumptions and simplification were made:

Die approbierte gedruckte Originalversion dieser Diplomarbeit ist an der TU Wien Bibliothek verfügbar
The approved original version of this thesis is available in print at TU Wien Bibliothek.

- The winding coil to duct-oil temperature between the bottom and top winding parts increases linearly irrespective of the cooling mode
- The winding coil to duct- oil temperature gradient is constant with height.
- The HST rise is higher than the temperature rise of the oil at the top of a winding, because allowance has to be made for the increase in stray losses. To consider these non-linearities, the temperature difference between the HST and the oil at the top of the winding equals to $H \times g_r$.

3.2.2.1 IEC 60076-7 model

The TOT model from IEC 60076-7 is given as follows [1]:

$$\left(\frac{1+K^2 \cdot R}{1+R}\right)^x \cdot \Delta\theta_{or} = k_{11} \cdot \tau_{to} \frac{d\theta_{to}}{dt} + (\theta_{to} - \theta_a) \tag{3.10}$$

- K load factor
- R no-load loss ratio to load loss ratio
- $\Delta\theta_{or}$ top-oil temperature rise by rated current (K)
- k_{11} correction factor
- τ_{to} oil time constant (min)
- θ_a ambient temperature (°C)
- θ_{to} TOT (°C)
- x oil exponent

the oil time constant (τ_{to}) is corrected by implementing the factor (k_{11}). This factor reflects the stagnation of the oil in the bottom of the tank [13].

In the IEC 60076-7 loading guide the HST is a linear equation of the second order, which can be presented as two first-order differential equations. The factors k_{21} and k_{22} were implemented to consider overshoot, which imitates mass inertia in natural convection based oil flow. $\Delta\theta_{h1}$ and $\Delta\theta_{h2}$ can be derived from equations 3.11 and 3.12 and used to calculate the equation 3.13 [6][13].

$$k_{21} \cdot \Delta\theta_{hr} \cdot K^y = k_{22} \cdot \tau_w \frac{d\theta_{h1}}{dt} + \Delta\theta_{h1} \tag{3.11}$$

$$(k_{21} - 1) \cdot \Delta\theta_{hr} \cdot K^y = \frac{\tau_{to}}{k_{22}} \cdot \frac{d\theta_{to}}{dt} + \Delta\theta_{h2} \tag{3.12}$$

where

- k_{21} and k_{22} are the overshoot factors
- K is the load factor
- y winding exponent
- $\Delta\theta_{h1}$ and $\Delta\theta_{h2}$ are HST calculated in separated equations (K)
- τ_w winding time constant (s)
- $\Delta\theta_{hr}$ is the rated winding oil temperature rise (K)

$$\Delta\theta_h = \Delta\theta_{h1} - \Delta\theta_{h2} \tag{3.13}$$

Die approbierte gedruckte Originalversion dieser Diplomarbeit ist an der TU Wien Bibliothek verfügbar
The approved original version of this thesis is available in print at TU Wien Bibliothek.
TU Bibliothek Your knowledge hub WIEN

3.2.2.2 Steady-state model

In this section a steady-state model for IEC 60076-7 presented in section 3.2.2.1 is derived. In steady state the value does not change with time. So the derivatives are equal to zero. By omitting the derivations of the equations 3.11, 3.12 and 3.25, the formulas for the calculation of HST rise and TOT rise are 3.14 and 3.15 respectively. Another way to derive steady-state model is to substitute value of t by $t \to \infty$ in exponential forms of equations for calculation of HST and TOT.

$$\Delta\theta_h = \Delta\theta_{h,r} \cdot K^y \tag{3.14}$$

$$\Delta\theta_{tu} = \left[\frac{1 + K^y \cdot R}{1 + R}\right] \cdot \Delta\theta_{to,r} \tag{3.15}$$

3.2.2.3 IEEE C57 91. Annex G

Annex G model [30] is based on energy balance equation. In this model the HST temperature is the sum of the following temperatures: ambient temperature (θ_a), bottom-oil rise ($\Delta\theta_{b.oil}$), bottom-oil to top-duct-oil gradient ($\Delta\theta_{wo/b.oil}$) and top-duct-oil to hottest-spot gradient ($\Delta\theta_{hs/wo}$). Unlike in IEC 60076-7 model [1], in this model variation of ambient temperature, oil viscosity, winding resistance and related losses changes are considered. The equation 3.16 is used for calculation of HST in Annex G model.

$$\theta_{hs} = \theta_a + \Delta\theta_{b.oil} + \Delta\theta_{wo/b.oil} + \Delta\theta_{hs/wo} \tag{3.16}$$

The equation for calculation of temperature rise is given as follows:

$$\Delta\theta(\Delta t) = \frac{Q_{gen} - Q_{diss}}{M_w \cdot C_p} \tag{3.17}$$

where

- $\Delta\theta$ is a transient temperature increase of particular transformer element (core, coils, tank etc.) (K)
- Δt is a period of time (min)
- Q_{gen} and Q_{diss} generated and dissipated losses (W)
- M_w winding mass (kg)
- C_p winding capacity ($W/s \cdot K$)

3.3 The thermo-electric analogy theory

The thermo-electric analogy theory is based on the mathematical similarity of the Fourier law, which is a fundamental law of thermodynamics and of the Ohm's law, which is a fundamental law of electrical circuit [31].

The equation for calculation of the heat flow is given as follows:

$$Q = \frac{kS\Delta T}{\delta} = \frac{\Delta T}{R_{th}} \tag{3.18}$$

- Q heat flow (W)

Die approbierte gedruckte Originalversion dieser Diplomarbeit ist an der TU Wien Bibliothek verfügbar
The approved original version of this thesis is available in print at TU Wien Bibliothek.
TU Bibliothek Your knowledge hub WIEN

- ΔT temperature difference (K)
- R_{th} heat resistance (K/W)
- S area in contact with heat (m^2)
- k thermal conductivity $(W/K \cdot m)$
- δ length of heat flow path (m)

And the electrical current according to the Ohm's law is given as follows:

$$I = \frac{E}{R_e} \tag{3.19}$$

where E is a potential difference (V) and R_e is the electrical resistance (Ω).

It can be concluded, that the equation for the calculation of heat transfer and the equation for calculation of the current in electrical circuit are analogous. This makes the description of heat transfer processes similar to these of electrical systems. The equivalent electrical circuit can be used to solve complicated heat transfer problems. Some analogous variables are summarized in the table 3.1.

Table 3.1: Analogy between the thermal and electrical variables [32]

Thermal		**Electrical**	
Generated heat	q	**Current**	I
Temperature	θ	**Voltage**	U
Resistance	R_{th}	**Resistance**	R
Capacitance	C_{th}	**Capacitance**	C_e

Dynamic calculation of the temperature rise can be described using the exponential law. The loss generation in transformer causes rapid temperature increase. This loss cannot be entirely dissipated, so it is stored. As the temperature increases loss dissipation increases too, until the rest of the heat is entirely transferred to the outer medium. These physical processes can be explained using the analogues circuit presented in figure 3.2.

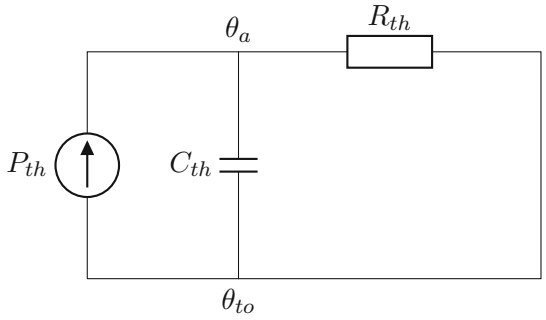

Figure 3.2: Thermo-electric analogy [29]

These processes inside the transformer can be described by first-order differential equation [29]:

$$P = C_{th} \cdot \frac{\mathrm{d}\Delta\theta}{\mathrm{d}t} + \frac{\Delta\theta}{R_{th}} \tag{3.20}$$

Die approbierte gedruckte Originalversion dieser Diplomarbeit ist an der TU Wien Bibliothek verfügbar
The approved original version of this thesis is available in print at TU Wien Bibliothek.

where P is the total loss (no-load loss and load loss), C_{th} $(W \cdot s/K)$ is a thermal capacity and R_{th} (K/W) is a thermal resistance, $\Delta\theta$ is a temperature rise (K).

3.3.1 The model of Swift

The model proposed by Swift is based on the natural heat convection. Here current source represents copper loss heat source, voltage source is used as the ambient air heat source. Worth to note, that Swift considered the ambient temperature influence on calculation of HST and TOT. Additionally, Swift introduced parameter exponent n for calculation of the temperature rise.

For the calculation of TOT a simplified circuit illustrated in 3.3 was used [32] [29].

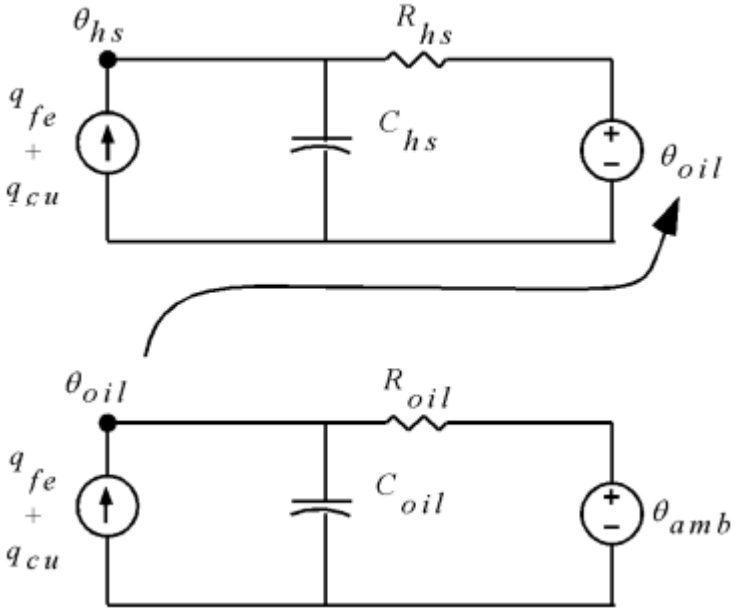

Figure 3.3: Circuit for calculation of TOT in Swift model [32]

In the model of Swift the equation for the calculation of TOT is given as follows:

$$\tau_{to,r} \cdot \frac{d\theta_{to}}{dt} + (\theta_{to} - \theta_a)^{\frac{1}{n}} = \Delta\theta_{to,r}^{\frac{1}{n}} \left(\frac{1 + R \cdot K^2}{1 + R} \right) \tag{3.21}$$

where

- $\tau_{to,r}$ rated oil time constant (s)
- $\theta_{to,r}$ TOT, rated (K)
- θ_a ambient temperature (K)
- h exponent
- $\theta_{to,r}$ rated top-oil rise (K)
- K load factor
- R ratio of no-load loss to load loss

Die approbierte gedruckte Originalversion dieser Diplomarbeit ist an der TU Wien Bibliothek verfügbar
The approved original version of this thesis is available in print at TU Wien Bibliothek.

3.3.2 The model of Susa

Susa suggested models for calculation of HST and TOT. Their principles are based on on heat transfer theory, application of the lumped capacitance method, the thermal-electrical analogy. Additionally the author introduced a nonlinear thermal resistance. The models consider variations in oil viscosity and winding resistance. Reference temperature for the oil viscosity estimation is the TOT used for both models. Additionally he introduced an exponent n, which depends on the fluid flow type [33]. In his further works [34], [35] Susa proposed a bottom winding temperature rise over bottom-oil temperature (BOT) model and BOT rise over ambient temperature based on the law of energy conservation [29].

3.3.2.1 The model for the calculation of top-oil temperature

The interim calculations for the calculation of TOT are omitted in this work. In order to calculate the TOT in Susa model the circuit presented in figure 3.4 was used. The TOT calculation model is a differential equation given as follows [33]:

$$\frac{1+R\cdot K^2}{1+R}\cdot\mu_{pu}^{n}\cdot\Delta\theta_{to,r}=\mu_{pu}^{n}\tau_{to,r}\cdot\frac{d\theta_{to}}{dt}+\frac{(\theta_{to}-\theta_a)^{1+n}}{\Delta\theta_{to,r}^{n}} \tag{3.22}$$

where

- K load factor
- R ratio of no-load loss to load loss
- $\mu_{p.u.}$ oil viscosity per unit value
- $\theta_{t.oil}$ TOT (°C)
- θ_{amb} ambient temperature (°C)
- n is empirical factor for laminar flow type, different depending on the cooling method of transformer
- $\Delta\theta_{t.oil.r}$ rated TOT rise over ambient temperature (K)
- $\tau_{t.oil.r}$ rated oil time constant (s)

In this model load factor K, viscosity $\mu_{p.u.}$ and ambient temperature θ_a are used as inputs. The output is TOT θ_{to}. The calculation can be conducted using the numerical method as for example Runge-Kutta.

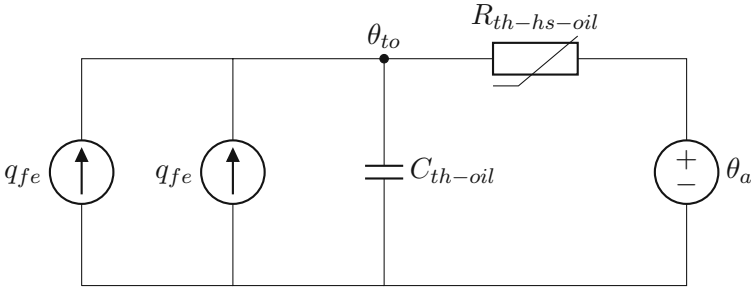

Figure 3.4: Circuit for calculation of TOT in Susa model [33]

- q_fe heat generated by no-load losses (W)
- q_{cu} heat generated by load losses (W)

Die approbierte gedruckte Originalversion dieser Diplomarbeit ist an der TU Wien Bibliothek verfügbar
The approved original version of this thesis is available in print at TU Wien Bibliothek.

- C_{th-oil} thermal capacitance of the oil $(W \cdot h/K)$
- θ_{oil} TOT (K)
- R_{th-oil} non-linear thermal resistance (K/W)

As it was already mentioned before, the author suggested implementation of the viscosity temperature variation. Which can be defined as follows:

$$\mu = \mu_{pu}\mu_r \tag{3.23}$$

Where (μ_{pu}) is a viscosity temperature variation and (μ_r) is a rated oil viscosity $(kg/(ms)$. From equation 3.22, it can be seen that this value impacts both oil thermal resistance and the top-oil time constant.

Additionally, the author implemented the non-linear thermal resistance, which is reciprocal to the heat transfer coefficient and area [33].

$$R_{th-oil} = \frac{1}{\alpha \cdot A} \tag{3.24}$$

where

- α $(W/m^2 \cdot K)$ heat transfer coefficient
- A (m^2) surface of heat transfer

3.3.2.2 The model for the calculation of hottest-spot temperature

The model for the calculation of HST was implemented similar way as the model for the calculation of TOT. The electric circuit used for calculation of HST can be seen on the figure 3.5. In this model load factor (K), variable viscosity (μ_{pu}), TOT (θ_{to}) calculated in the previous subsection are used as input and HST (θ_{hs}) is the output [33].

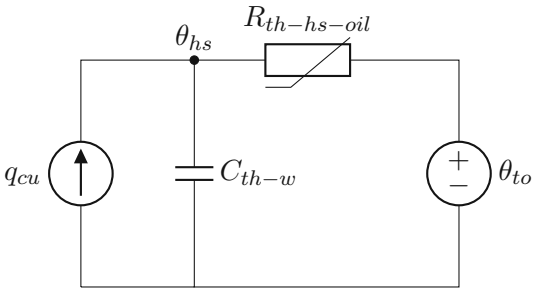

Figure 3.5: Circuit for calculation of HST in Susa model [33]

The circuit consists of the following elements:

- q_{cu} heat generated by load losses (W)
- θ_{hs} HST (K)
- $R_{th-hs-oil}$ (K/W)
- θ_{to} TOT (K)
- C_{th-w} winding thermal capacitance $(W \cdot s/K)$

Die approbierte gedruckte Originalversion dieser Diplomarbeit ist an der TU Wien Bibliothek verfügbar
The approved original version of this thesis is available in print at TU Wien Bibliothek.

The equation for the calculation of the HST is given as follows:

$$[K^2 \cdot P_{cu,pu}(\theta_{hs})]\mu_{pu}^n \cdot \Delta\theta_{hs,r} = \mu_{pu}^n \cdot \tau_{w,r} \cdot \frac{d\theta_{hs}}{dt} + \frac{(\theta_{hs} - \theta_{to})^{n+1}}{\Delta\theta_{hs,r}^n} \tag{3.25}$$

where

- K is a load factor
- $P_{cu,pu}(\theta_{HS})$ is load-loss, depending on the temperature
- μ_{pu} oil viscosity per unit value
- n empirical factor, depending on the flow type
- $\theta_{hs,r}$ HST, rated (K)
- $\tau_{w,r}$ winding time constant (s)
- θ_{to} TOT, (K)

In analogy to TOT model, the variable thermal viscosity is implemented in this model as well. This impacts thermal resistance and the winding time constant [33].

3.3.3 The model of Djamali

The model of M. Djamali was used for calculation of TOT in this work. M. Djamali and S. Tehnbohlen suggested a model suitable for online monitoring of a transformer cooling system. The model is supposed to help to detect the faulty fans in real-time operation and offers more accurate calculation of TOT using different heat transfer modes. It operates based on the IEC 60076-7 loading guide model, however some changes were introduced. In the presented model a method for calculation of the thermal resistance with a consideration of operating fans was introduced [36].

The heat generated in the windings is dissipated to the surrounding ambient using the oil in the tank and air outside of the tank. Considering this the corresponding equations for calculation of thermal resistance were calculated from both air and oil side [36].

In this work the thermal resistance corresponding to the natural convection of oil was calculated. For the calculation of thermal resistance of the air, three thermal resistances were determined namely, resistance corresponding to the radiation, natural convection and forced convection due to the operation of fans.

Reference temperature for the calculation of the air-side equations is logarithmic average temperature. The reference temperature for the calculation of the oil-side equations is average oil temperature. In order to determine average oil temperature, bottom-oil temperature needs to be calculated. The calculation method is provided in section 4.2. The equivalent circuit used for the calculation of TOT is illustrated in figure 3.6 .

Die approbierte gedruckte Originalversion dieser Diplomarbeit ist an der TU Wien Bibliothek verfügbar
The approved original version of this thesis is available in print at TU Wien Bibliothek.

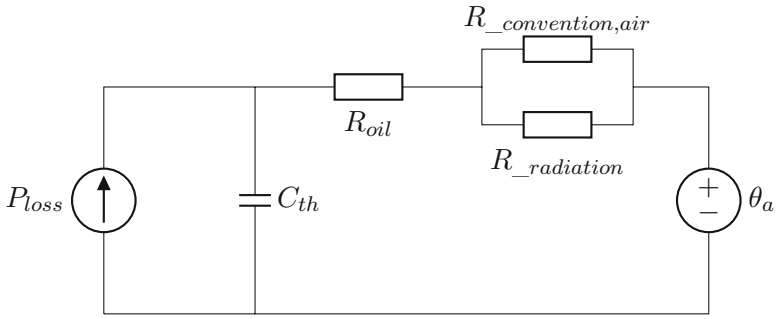

Figure 3.6: Circuit for calculation of TOT in Djamali model [36]

Die approbierte gedruckte Originalversion dieser Diplomarbeit ist an der TU Wien Bibliothek verfügbar
The approved original version of this thesis is available in print at TU Wien Bibliothek.

4 Model and methodology

Figure 4.1 represents a simplified block diagram of the model used in this work. The information about methods used for simulation of ambient temperature and load profiles can be found in sections 4.1.2 and 4.1.3 respectively. The top-oil simulation is based on the model offered by M. Djamali, which is in turn based on the thermo-electrical analogy. The equations provided in this model can be found in section 4.2 and the theoretical background in section 3.3.3. Simulation of HST-rise is based on IEC 60076-7, the equations for the calculation of HST rise are provided in section 3.2.2.1. Fan control threshold values are calculated based on the steady-state model. Calculation of the bottom-oil temperature (BOT) is described in section 4.6.1.

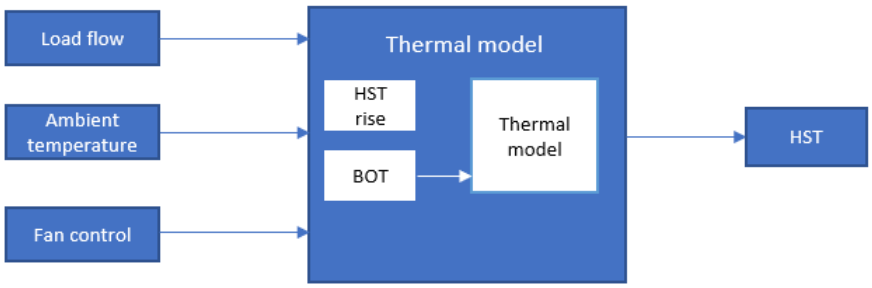

Figure 4.1: Simplified model block diagram

4.1 Input data

This section contains data used as input variables.

4.1.1 Reference transformer

As a reference transformer, the oil-immersed two-winding power transformer with a rated power of 58/45/40 MVA and nominal voltage 225/26.4 kV was used. Maximum rated power is by 4 operation of 4 fans [13]. For control purposes number of fans is divided in two groups (2 fans for each ventilator group).

Die approbierte gedruckte Originalversion dieser Diplomarbeit ist an der TU Wien Bibliothek verfügbar
The approved original version of this thesis is available in print at TU Wien Bibliothek.

4.1.2 Ambient temperature

The temperature measurements for summer and winter day simulations were extracted from ZAMG open access database. The data set contains measurement data from 1992 to the present day with a 10-minute resolution. ZAMG weather stations form comprehensive meteorological measuring network in Austria with approximately 260 measuring stations (mostly semi-automatic). They cover all climatic regions and altitudes. Weather stations record basic weather elements and forward them to Hohe Warte in Vienna in real time [37].

In order to observe transformer oil temperatures in various weather conditions, it was decided to use daily measurements representing summer and winter days of a region. Maximum, minimum and average ambient temperatures are summarized in table 4.1.

- Temperature for simulation of winter day corresponds to 24 hours air measurements conducted every 10 minutes on 6.01.2020 at the meteorological station, located at Schwechat (Lower Austria).
- The measurements for summer day were conducted on 5.08.2022. Both temperature profiles can be seen in figure 4.2.

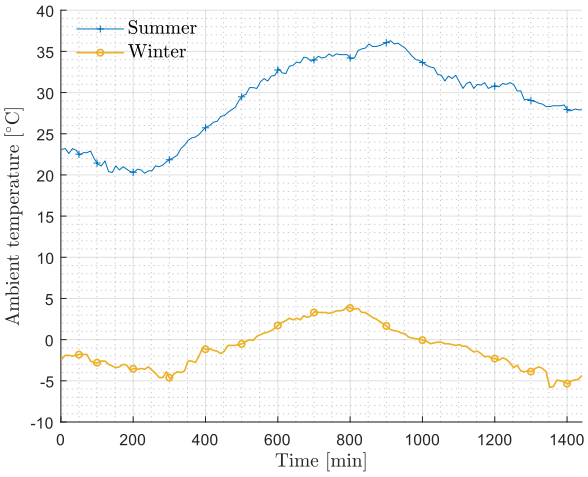

Figure 4.2: Ambient temperature in winter and summer

Table 4.1: Minimum, maximum and average temperatures for winter and summer temperature profiles

Ambient temperature,°C	Summer	Winter
Maximum	36.3	4
Minimum	20.2	-6.8
Average	29.04	-1.22

Die approbierte gedruckte Originalversion dieser Diplomarbeit ist an der TU Wien Bibliothek verfügbar
The approved original version of this thesis is available in print at TU Wien Bibliothek.

4.1.3 Load profiles

The steadily increasing number of the renewable energy sources fed-in into the grid is changing the grid topology. Hence the calculation of the grid needs to be adjusted accordingly. The grid data must be adapted or updated to these requirement. To help with these new challenges research project SimBench was introduced. The major aim of this project was a creation of a benchmark network [38].

This benchmark network, i.e. electricity network offers an extensive simulation database for areas of network analysis, network planning and network management. The seasonal time series of industrial and agricultural load profiles are load measurements performed in 2016 and provided as an anonymous data base [39].

According to technical documentation of the project the time series for wind and photovoltaic were generated with the help of simulation tool SIMONA, using the ambient temperature data from Deutscher Wetterdient from year 2011 and 2012 as input [39].

Load profiles for the simulation in this work were extracted from SimBench database [40], 1-HVMV-mixed-all-0-s grid model, where HVMV indicated grid voltage level[1].

In order to activate all automatic systems load profiles must be scaled. Load profiles were scaled the following way: in system controlled by TOT by full load (e.g. load factor equals to one) and constant ambient temperature $\theta_a = 40°C$, load factor was increased until the HST reached critical 120 °C. Load profiles are illustrated in figure 4.3. Since wind demonstrated stochastic behavior during the year, the simulation was conducted for two different wind profiles: increasing (profile 2) and decreasing (profile 1) load. Maximum, minimum and average load factors are summarized in table 4.2.

For scenarios WFCT 1, WFCT 2 and SFCT (both summer and winter) the reactive power value was omitted, as it can have different reactive power control scheme.

- **Wind load**

  For scenario Wind Farm Collector Transformer 1 or **WFCT1** is a Wind Profile 4 from 1-HVMV-mixed-all-0-sw. For the simulation daily load profile with 15 minute resolution from the 5th April was used, load was scaled 1.6 times.

- **Wind load**

  For scenario **WFCT 2** is a Wind profile 5 from the fore-mentioned grid model. Load profile represents daily load profile with 15 minute resolution from the 5th April. Initial load was scaled 1.8 times.

- **Photovoltaic** (PV)

  Summer load profile for scenario Solar Farm Collector Transformer by summer ambient temperature or **SFCT** is a PV 6 profile, dated by 26th July. Since the PV module generates lower energy volumes during the winter time, it was decided to consider seasonal time series. Photovoltaic in winter is PV4 profile, load data from the 3rd January.

- **Grid load**

  Grid load profile is an industrial load profile G_0-A[2]. Load was caclulated using the equation 4.1.

[1] High Voltage, Medium Voltage
[2] G denotes Gewerbe, *Ger.* business

Die approbierte gedruckte Originalversion dieser Diplomarbeit ist an der TU Wien Bibliothek verfügbar
The approved original version of this thesis is available in print at TU Wien Bibliothek.

- **Grid emergency**

  Grid emergency represents a grid load profile, scaled twice after minute 600.

Each time series of load contains values for active (P) and reactive power (Q). Load equation is given as follows:

$$S = \sqrt{P^2 + Q^2} \tag{4.1}$$

For the calculation of load factor K the rated current of ONAN transformer was used.

Table 4.2: Maximum, minimum and average load factors

	Value [p.u.]		
Load profile	**Maximum**	**Minimum**	**Average**
WFCT 1	1.48	0.73	1.01
WFCT 2	1.55	0.26	0.83
SFCT	1.5	0	0.43
SFCT winter	0.34	$2.8 \cdot 10^{-4}$	$3.7 \cdot 10^{-4}$
Grid Transformer	0.72	0.39	0.58
Grid Emergency	1.44	0.41	0.93

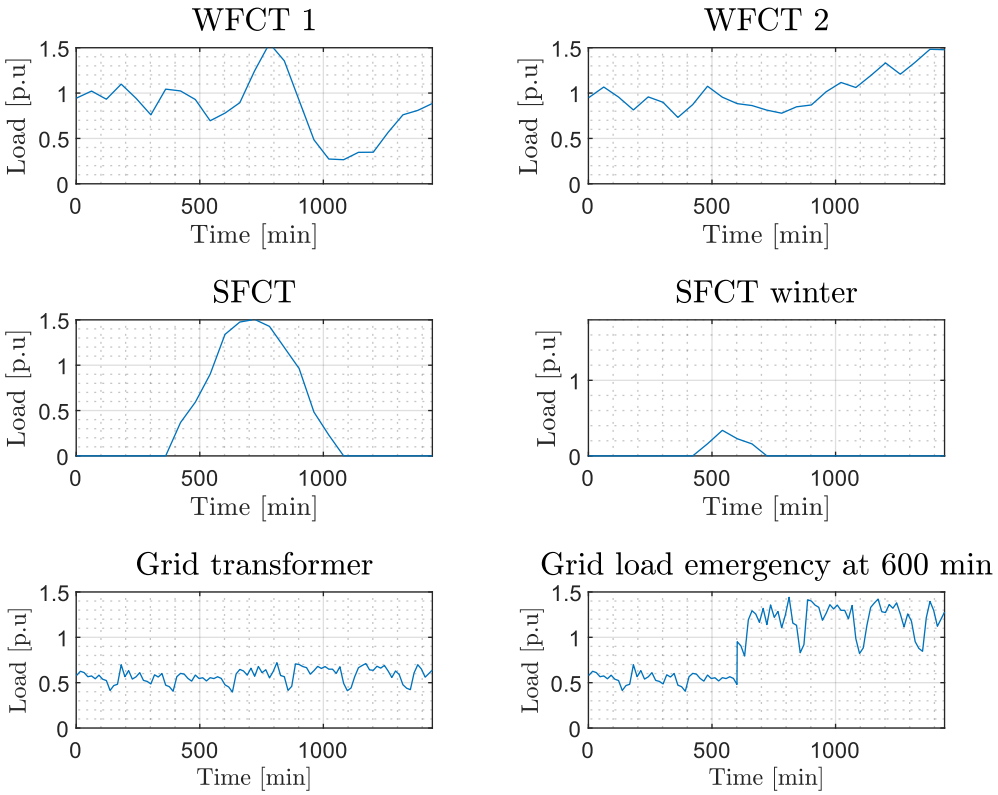

Figure 4.3: Load profiles used for different scenarios

Die approbierte gedruckte Originalversion dieser Diplomarbeit ist an der TU Wien Bibliothek verfügbar
The approved original version of this thesis is available in print at TU Wien Bibliothek.

4.2 The hottest-spot temperature model

In this work the hottest-spot temperature model was used (see the equation 4.2).

$$\theta_h = \Delta\theta_h + \theta_{to} \tag{4.2}$$

The HST-rise was calculated based on the IEC 60076-7 model and the TOT based on the model suggested by M.Djamali, which in turn is based on the circuit 3.6. The differential equation for the calculation of TOT of oil-immersed transformers according to IEC 60076-7 is [1]:

$$\theta_{to}^{(i+1)} = \theta_{to}^{(i)} \frac{Dt^{(i)}}{\tau_{to}^{(i)}} (\Delta\theta_{to}^{(i)} - \theta_{to}^{(i)} + \theta_a^{(i)}) \tag{4.3}$$

The equation 4.3 can also be written as:

$$k_{11} \cdot \tau_{to} \frac{\mathrm{d}\theta_{to}}{\mathrm{d}t} + \theta_{to} - \theta_a = \Delta\theta_{to} \tag{4.4}$$

where θ_a is ambient temperature (°C), $\Delta\theta_{to}$ is a TOT rise over the ambient temperature (K), τ_{to} is the oil time constant (hours) and k_{11} is oil time constant correction factor.

The top-oil temperature rise $\Delta\theta_{to}$ at considered load is:

$$\Delta\theta_{to} = (P_0 + P_k \cdot K^2) \cdot R_{total} \tag{4.5}$$

where P_k is the short-circuit loss (W), P_0 no load loss (W), R_{total} is a total thermal resistance (K/W), K is a load factor (%).

The equation for calculation of total thermal resistance (R_{total}) can be calculated as:

$$R_{total} = R_{oil} + \frac{R_{convection} \cdot R_{radiation}}{R_{convection} + R_{radiation}} \tag{4.6}$$

where (R_{oil}) is a thermal resistance of oil, ($R_{convection}$) is a thermal resistance corresponding the convection (both natural and forced) and ($R_{radiation}$) is a thermal resistance corresponding the radiation.

4.3 Oil time constant

Thermal time constants (TTC) of a thermal dynamic model are used to reflect the change rate of temperature [41]. The oil time constant in IEC 60076-7 is a constant value, however in reality it is affected by many factors such as load current, oil temperature etc. In this work the oil time constant is a temperature dependent value. Temperature dependence is expressed by multiplying rated oil constant ($\tau_{to.r}$) by total thermal resistance at a considered load (R_{total}). Total thermal resistance is normalized by dividing it to rated thermal resistance (R_{th_n}), this in turn was obtained by rated load and constant ambient temperature ($20°C$) in steady-state.

$$\tau_{to}^{(i)} = \frac{R_{total}^{(i)}}{R_{th_n}} \cdot \tau_{to.r} \tag{4.7}$$

Die approbierte gedruckte Originalversion dieser Diplomarbeit ist an der TU Wien Bibliothek verfügbar
The approved original version of this thesis is available in print at TU Wien Bibliothek.
TU Bibliothek Your knowledge hub WIEN

4.4 Oil side equations

R_{th} in a suggest model is a temperature dependent value [36]. This section contains equations, used for determination of thermal resistance of oil. The thermal resistance was calculated reverse. Firstly, the heat transfer coefficient needs to be estimated. In order to the estimate heat transfer coefficient α_{oil}, thermal conductivity λ_{oil}, Grashof (Gr) and Prandtl (Pr) numbers are required. Note, that the reference temperature for oil side $T_{ref.oil}$ is the average temperature of oil (K), calculated in section 4.6.

The formula for the calculation of the thermal resistance of oil is given as follows:

$$R_{oil} = \frac{1}{A_{oil} \cdot \alpha_{oil}} \tag{4.8}$$

- A_{oil} is the surface of heat transfer (m^2) of the oil
- α_{oil} is the heat transfer coefficient of oil $(W/m^2 \cdot K)$

The thermal conductivity of oil is given as:

$$\alpha_{oil} = \frac{\lambda_{oil}}{s_{oil}} \cdot (q_{oil} \cdot (Gr_{oil}(T_{ref.oil}) \cdot Pr_{oil}(T_{ref.oil})^{p_{oil}}) \tag{4.9}$$

- λ_{oil} is the thermal conductivity of oil $(W/m \cdot K)$
- Gr_{oil} is the Grashof number
- Pr_{oil} is the Prandtl number
- q_{oil}, p_{oil} are empirical factors
- s_{oil}, characteristic length of convection (m)

The Prandtl number can be found from:

$$Pr_{oil}(T_{ref.oil}) = \frac{\nu_{oil}(T_{ref.oil}) \cdot \rho_{oil}(T_{ref.oil}) \cdot cp_{oil}(T_{ref.oil})}{\lambda_{oil}(T_{ref.oil})} \tag{4.10}$$

- ν_{oil} is kinematic viscosity (m^2/s)
- cp_{oil} specific heat $(W \cdot s/kg \cdot K)$
- λ_{oil} is a thermal conductivity $(W/m \cdot K)$
- ρ_{oil} fluid density (kg/m^3)

Thermal conductivity of oil is:

$$\lambda_{oil}(T_{ref.oil}) = 0.124 - 1.525 \cdot 10^{-4} \cdot T_{ref.oil} \tag{4.11}$$

And the kinematic viscosity of oil can be estimated as follows:

$$\nu_{oil}(T_{ref.oil}) = (e^{e^{24.736 \cdot (T_{ref.oil})^{-4.136}}} - 0.7) \cdot 10^{-6} \tag{4.12}$$

The equation for calculation of fluid density is:

$$\rho_{oil}(T_{ref.oil}) = 887 - 0.659 \cdot T_{ref.oil} \tag{4.13}$$

The specific heat of oil can be calculated as:

$$cp_{oil}(T_{ref.oil}) = 1960 + 4.005 \cdot T_{ref.oil} \tag{4.14}$$

Die approbierte gedruckte Originalversion dieser Diplomarbeit ist an der TU Wien Bibliothek verfügbar
The approved original version of this thesis is available in print at TU Wien Bibliothek.
TU Bibliothek Your knowledge hub WIEN

To calculate the Prandtl number the values from 3.9-3.12 were substituted into the equation 4.10.

The Grashof number is defined as:

$$Gr_{oil}(T_{ref.oil}) = s_{oil}^3 \cdot \frac{g \cdot \beta_{oil} \cdot \Delta\theta_w}{(\nu_{oil}(T_{ref.oil})^2)} \tag{4.15}$$

- s_{oil} is the characteristic length of heat transfer on the oil side (m)
- g is acceleration due to the gravity, $g = 9.8m/s^2$
- β_{oil} is the volumetric thermal expansion coefficient $(1/K)$
- $\Delta\theta_w$ is the temperature gradient between the winding at the middle height and the oil at the top of the winding (K).

The volumetric thermal expansion coefficient of oil β_{oil} is equal to $8.6 \cdot 10^{-4}$ $1/K$.

4.5 Air side equations

Since air mass movement is influenced by fans, there are 2 types of convection: natural and forced. For determination of air side parameters average logarithmic temperature determined in section 4.6.2 was used.

As it can be seen in figure 3.6, the thermal resistances are connected parallel analogues to the electrical resistances, so the equation for calculation of the air resistance becomes:

$$R_{air} = \frac{R_{convection} \cdot R_{radiation}}{R_{convection} + R_{radiation}} \tag{4.16}$$

where $R_{radiation}$ (K/W) is a thermal resistance corresponding to radiation and $R_{convection}$ (K/W) is a thermal resistance corresponding to both natural and forced convection.

The temperature dependent resistance of air can be calculated as follows:

$$R_{air} = \frac{1}{A_{air} \cdot \alpha_{convection}} \tag{4.17}$$

where $A_{air}(m^2)$ is a surface of heat transfer and $\alpha_{air}(W/m^2 \cdot K)$ is the heat transfer coefficient.

The heat transfer coefficient is given as follows:

$$\alpha_{convection} = (\alpha_{natural}^4 + \alpha_{forced}^4)^{\frac{1}{4}} \tag{4.18}$$

where $\alpha_{natural}(W/m^2 \cdot K)$ is the heat transfer coefficient for the natural convection and $\alpha_{forced}(W/m^2 \cdot K)$ is the heat transfer coefficient for forced convection.

4.5.1 Radiation

The process of heat transfer from the steel plate of the transformer's tank to its surrounding by radiation can be described using the Stephan-Bolzmann's law. Note, that the transformer's tank represents the gray body and surrounding ambient represents the black body.

According to the law of conservation of energy the sum of reflectance R and of adsorbtion A equals to one. A black body can be defined as ideal body that has zero reflectance and

Die approbierte gedruckte Originalversion dieser Diplomarbeit ist an der TU Wien Bibliothek verfügbar
The approved original version of this thesis is available in print at TU Wien Bibliothek.

highest degree of absorption (e.g. perfect absorber) [42]. Hence the black body emits maximum possible radiation for a given temperature. However, radiation emitted by real surfaces ranges between 0 and 1 [24]. In approximation the real surfaces can be assumed as grey bodies e.g. constant emissivity.

The equation for calculation of resistance corresponding to radiation is:

$$R_{radiation} = \frac{1}{\sigma \cdot \epsilon \cdot A_{radiation}(T_{ref.air}^2 + \theta_a^2)(T_{ref.air}^2 + \theta_a)} \tag{4.19}$$

- σ Stefan-Bolzmann constant, $\sigma = 5.67 \cdot 10^{-8} \frac{W}{m^2 \cdot K^4}$
- ϵ Emissivity grade
- $A_{radiation}$ Effective surface area of radiation (m^2)

4.5.2 Natural convection

Heat transfer coefficient for resistance corresponding the air natural convection is given as follows:

$$\alpha_{air}(T_{ref.air}) = \frac{\lambda_{air}}{s_{air}} \cdot (q_{air}(Gr_{air}(T_{ref.air}) \cdot Pr_{air}(T_{ref.air}))^{p_{air}}) \tag{4.20}$$

- λ_{air} thermal conductivity of air $(W/m \cdot K)$
- q_{air} and p_{air} empirical factors
- s_{air} characteristic length of convection (m)
- Gr_{air} Grashof number
- Pr_{air} Prandtl number

The equation for calculation of Grashof number from the air side is given as follows:

$$Gr_{air}(T_{ref.air}) = s_{air}^3 \cdot \frac{g \cdot \beta_{air}(T_{ref.air}) \cdot (T_{ref.air} - \theta_a)}{(\nu_{air}(T_{ref.air})^2} \tag{4.21}$$

- s_{air} characteristic length of convection from air side (m)
- g gravitational constant (m/s^2)
- ν_{air} kinematic viscosity of air (m^2/s)
- β_{air} volumetric expansion coefficient of air (1/K)

The formula for calculation of volumetric thermal expansion coefficient of the air β_{air} is given as :

$$\beta_{air}(T_{ref.air}) = 0.004 - 1.3 \cdot 10^{-5} \cdot T_{ref.air} \tag{4.22}$$

similar to:

$$\beta_{air}(T_{ref.air}) = (5 \cdot 10^{-5} \cdot (T_{ref.air})^2 - 0.0428 \cdot T_{ref.air} + 11.658) \cdot 10^{-3} \tag{4.23}$$

Kinematic viscosity of air can be found as:

$$\nu_{air}(T_{ref.air}) = (2.25 \cdot T_{ref.air}^2 + 0.1 \cdot T_{ref.air} + 13.68) \cdot 10^{-10} \tag{4.24}$$

Prandtl number for air side can be calculated using the following equation:

$$Pr_{air}(T_{ref.air}) = \frac{\eta_{air}(T_{ref.air}) \cdot cp_{air}(T_{ref.air})}{\lambda_{air}} \tag{4.25}$$

Die approbierte gedruckte Originalversion dieser Diplomarbeit ist an der TU Wien Bibliothek verfügbar
The approved original version of this thesis is available in print at TU Wien Bibliothek.
TU Bibliothek Your knowledge hub WIEN

- η_{air} dynamic viscosity $(kg/s^2 \cdot m^2)$
- cp_{air} specific heat of air $(W \cdot s/kg \cdot K)$
- λ_{air} thermal conductivity of air $(W/m \cdot K)$

Dynamic viscosity of air η_{air} can be expressed as a product of kinematic viscosity of air ν_{air} (m/s^2) and density of air ρ_{air} (kg/m^3):

$$\eta_{air}(T_{ref.air}) = \nu_{air} \cdot \rho_{air} \tag{4.26}$$

The formula for calculation of specific heat is:

$$cp_{air}(T_{ref.air}) = 4.12 \cdot 10^{-4} \cdot T_{ref.air}^2 + 0.02 \cdot T_{ref.air} + 1006 \tag{4.27}$$

The equation for calculation of thermal conductivity of air is:

$$\lambda_{air} = (0.02382 + 6.478 \cdot 10^{-5} \cdot T_{ref.air}) - 0.015 \tag{4.28}$$

similar to:

$$\lambda_{air} = (0.02382 + 6.478 \cdot 10^{-5} \cdot T_{ref.air}) \tag{4.29}$$

4.5.3 Forced convection

The equation for calculation of heat transfer coefficient corresponding forced convection is:

$$\alpha_{forced} = \frac{\lambda_{air}(T_{ref.air})}{s_{air}} \cdot C_{air} \cdot (Re(T_{ref.air})^m \cdot Pr(T_{ref.air})^n) \tag{4.30}$$

Reynolds number can be calculated as follows:

- Re Reynolds number
- m, n and C_{air} empirical factors

$$Re(T_{ref.air}) = \frac{V_m \cdot d}{\nu_{air}(T_{ref.air})} \tag{4.31}$$

$$V_m = u \cdot n \tag{4.32}$$

- V_m average air velocity depends on a number of running fans (m/s)
- u_{oil} design dependent parameter
- d_{oil} characteristic diameter of oil duct (m)

Die approbierte gedruckte Originalversion dieser Diplomarbeit ist an der TU Wien Bibliothek verfügbar
The approved original version of this thesis is available in print at TU Wien Bibliothek.

4.6 Determination of reference temperatures

4.6.1 Oil side reference temperature

Equations from oil and air sides are temperature dependent. For oil side equations reference temperature is average oil temperature. It was calculated using the formula 4.33. In order to calculate bottom-oil temperature the thermal electrical analogy was introduced (see figure 4.4). The circuit was solved using the Kirchhoff law, where R_{bo} is a non-linear thermal bottom-oil resistance.

$$\theta_{avg} = T_{ref.oil} = \frac{\theta_{to} + \theta_{bo}}{2} \tag{4.33}$$

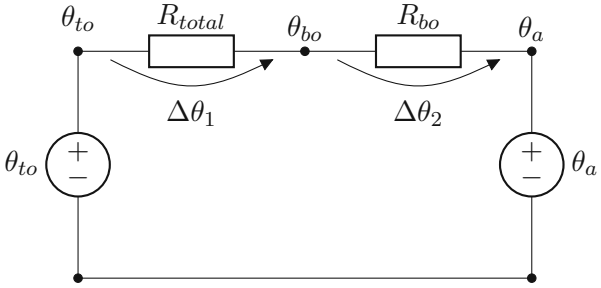

Figure 4.4: Bottom-oil circuit

The circuit was solved using the following equation:

$$\theta_{to} - \Delta\theta_1 - \Delta\theta_2 - \theta_a = 0 \tag{4.34}$$

After substituting the values of $\Delta\theta_1$ and $\Delta\theta_2$ the equation 4.34 becomes:

$$\theta_{to} - R_{total} \cdot P - R_{bo} \cdot P - \theta_a = 0 \tag{4.35}$$

The non-linear bottom-oil resistance can be defined as follows:

$$R_{bo} = \frac{\theta_{bo,r}}{P_{total,r}} \tag{4.36}$$

where $(\theta_{bo,r})$ is a bottom-oil temperature rise over ambient temperature at rated current, obtained from heat-run test and $(P_{total,r})$ is total losses by rated current.

$$\theta_{b.oil} = \theta_{t.oil} - R_{total} \cdot P \tag{4.37}$$

The value of P can be derived from 4.35:

$$P = \frac{\theta_{to} - \theta_a}{R_{total} + R_{bo}} \tag{4.38}$$

After substituting the equation 4.35 in 4.37 the equation for calculation of the bottom-oil temperature can be defined as:

$$\theta_{bo}^{(i+1)} = \theta_{to}^{(i)} + R_{total}^{(i)} \cdot \left(\frac{\theta_{to}^{(i)} - \theta_a^{(i)}}{R_{total}^{(i)} + R_{bo}} \right) \tag{4.39}$$

Die approbierte gedruckte Originalversion dieser Diplomarbeit ist an der TU Wien Bibliothek verfügbar
The approved original version of this thesis is available in print at TU Wien Bibliothek.

4.6.2 Air side reference temperature

As a reference temperature for calculation of the thermal properties of the air a logarithmic average temperature of the oil and the air was used. The logarithmic average temperature θ_{o-a} (K) was calculated using the formula 4.40, where θ_a is ambient air temperature.

$$\theta_{o-a} = T_{ref.air} = \frac{\theta_{avg} - \theta_a}{\ln \frac{\theta_{avg}+273}{\theta_a+273}} \tag{4.40}$$

4.7 Simulation of control systems

The automatic control systems were simulated with the help of double Relay block in Simulink. Double Relay enables switching between two outputs, depending on the specified input parameters. As soon as the relay switches on, it remains on until the specified value drops below the Switch-off point. Once the relay is off, it will remain off until the input exceeds the value of Switch on point parameter. In this work as input for Switch-on and off points load signal, HST and TOT were used. The Switch on and off points can be found in table 4.3.

Table 4.3: Fan switch on and off points for different automatic systems

		Level of cooling	Switch on point	Switch off point
System controlled by	TOT	1	55°C	45 °C
		2	60 °C	56°C
	Load	1	0.7	0.6
		2	0.9	0.7
	HST	1	69 °C	65 °C
		2	80 °C	68°C

It is assumed, that transformer has two level of cooling: when one level of cooling is activated 2 fans are switched on. By increased load second level of cooling is activated and all 4 fans are switched on.

4.7.1 System controlled by Top-Oil Temperature

For system controlled by TOT the Switch on point is 55°C and Switch off point is 45°C. This means once the TOT exceeds 55°C one level of cooling will be automatically switched on, when the temperature drops to 45 °C no additional cooling is required. For second level of cooling the Switch-on and off points are 60°C and 56°C respectively. By 60 °C all levels of cooling are activated, once the TOT drops below 60 °C the system switches back to one level of cooling.

4.7.2 System controlled by load

System controlled by load is parameterized the following way: by load exceeding 0.7 first level of cooling is activated, when load drops to 0.6 no fans are activated. By load values higher than 0.9 both cooling levels are active, once load is 0.7 the automatic system switches back to only one level of cooling.

Die approbierte gedruckte Originalversion dieser Diplomarbeit ist an der TU Wien Bibliothek verfügbar
The approved original version of this thesis is available in print at TU Wien Bibliothek.
TU Bibliothek Your knowledge hub WIEN

4.7.3 System controlled by Hottest-Spot Temperature

Using the steady-state thermal model (see equation 4.41) the Switch on and -off points for system controlled by HST were determined. The HST is defined as a sum of ambient temperature ($\Delta\theta_a = 20°C$), the TOT to HST-rise ($\Delta\theta_h$), and final top-oil temperature rise ($\Delta\theta_{to}$) [43].

$$\theta_h = \Delta\theta_h + \Delta\theta_{to} + \Delta\theta_a \tag{4.41}$$

The TOT to HST-rise ($\Delta\theta_h$) was calculated using the equation 3.14.

For the first level of cooling the Switch on point is 69 °C, once the HST drops below 65 °C no forced cooling is applied. For the second level of cooling the Switch on point is 80 °C. The second level of cooling is deactivated when the temperature is below 68 °C.

4.8 Simulation of pre-cooling

Pre-cooling was simulated using the Switch block. Switch block activates fans before the expected grid emergency, at the pre-defined time. Input signal is a number of fans (1 or 2 fan groups). This means, that before the pre-defined set-point 0 fans are active and after 1 or 2 fan groups are activated.

4.9 Cooling methods

In this work the following cooling methods were simulated:

- **Natural cooling (ONAN)**. By natural cooling fans are not active.
- **Continuous forced cooling (1 or 2 group of fans)**. By continuous forced cooling fans are manually switched on and operate 24 hours.
- **Automatic control system** controlled by different signals, namely by load, HST or TOT signals. Automatic control system activates fans depending on pre-defined value, this allows to activate fans only when it is required.

Die approbierte gedruckte Originalversion dieser Diplomarbeit ist an der TU Wien Bibliothek verfügbar
The approved original version of this thesis is available in print at TU Wien Bibliothek.

5 Determination of optimal cooling method for different loading scenarios

In this chapter the influence of different cooling system control strategies on the behaviour of HST was analyzed. In order to assess the effect of each strategy the resulting average hottest-spot temperatures (**HST**) were compared. For automatic control systems number of fan activations and de-activations was calculated and fan activation pattern was analysed. Additionally, total fan operation time (**TFOT**) was calculated by integrating the area under the fan activation pattern. This is a mean specific value calculated for a unit, where a unit represents half of the system power. The equation for calculation of TFOT is:

$$TFOT = \int_0^{1440} n(t)\,dt \tag{5.1}$$

Where n corresponds to the governing signal and t is time (minutes). These two parameters help to estimate how the cooling system control strategy choice impacts the future maintenance and repair costs of the equipment.

The following types of scenarios were studied: 2 WFCT, 1 SFCT and 1 grid transformer. Each cooling method was studied by winter and summer ambient temperatures.

5.1 Scenario wind farm collector transformer 1

This section contains simulation results for Wind Farm Collector Transformer (**WFCT**) 1. The load profile used as input can be seen in figure 4.3. The profile was chosen due to its peak in the middle of the day. The maximum load is 1.54 and it can be observed on 800 minute (1 p.m.). Average load during the day is 0.83 and minimum load is only 0.26. Figure 4.2 illustrates summer and winter ambient temperatures used as input. Maximum, minimum and average ambient temperatures are summarized in table 4.1. The model used as a basis for simulation is presented in section 4.2.

5.1.1 Summer

Figure 5.1 illustrates the HST of different cooling methods for WFCT 1 by summer ambient temperature. Maximum and average HST together with TFOT are summarized in table 5.1.

Die approbierte gedruckte Originalversion dieser Diplomarbeit ist an der TU Wien Bibliothek verfügbar
The approved original version of this thesis is available in print at TU Wien Bibliothek.

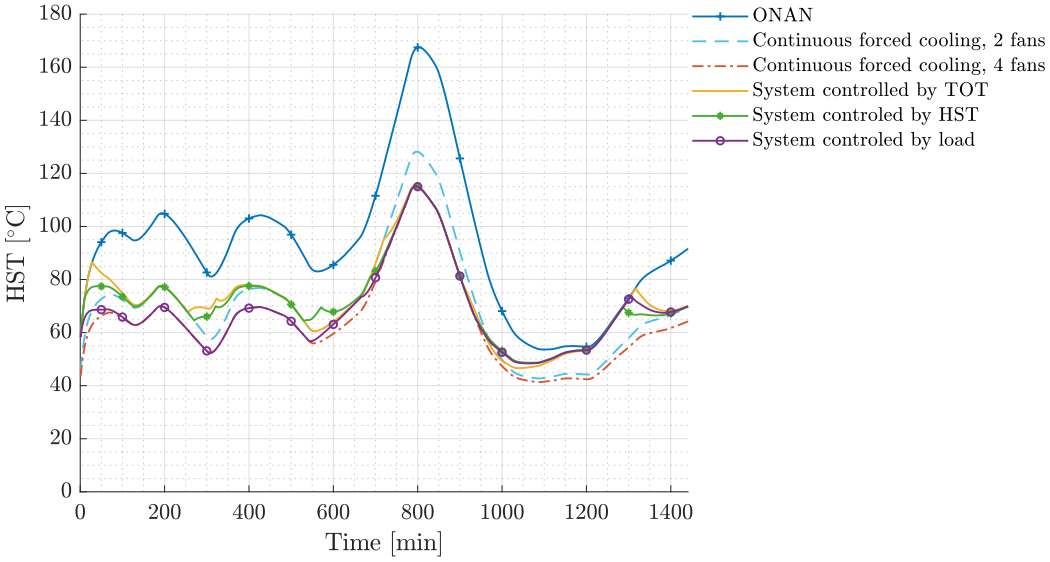

Figure 5.1: HST of different cooling methods. WFCT 1, summer

Table 5.1: Maximum, average HST and TFOT of different cooling methods. Scenario WFCT 1, summer

	Maximum HST,°C	Average HST, °C	TFOT, hrs
ONAN	167.53	93.03	0
Continuous forced cooling 2 fans	128.19	69.98	24
Continuous forced cooling 4 fans	115.11	64.27	48
System controlled by TOT	115.55	71.99	17.5
System controlled by HST	115.21	71.49	19.5
System controlled by load	115.15	68.02	31.5

ONAN is a reference scenario, which can be used when the cooling system does not operate. The best cooling effect was achieved by continuous forced cooling with 4 fans, average HST by this cooling method is 64.27°C, followed by continuous forced cooling with 2 fans with average HST 69.98 °C. Maximum HST for system controlled by load and by HST reached almost the same value. However, average HST is 3°C higher for the latter. This can be connected to TFOT, while the system controlled by load had operating fans during 31.5 hours, the system controlled by HST had only 19.5 hours. Average HST of the system controlled by load is 68.02°C, whereas of the system controlled by HST it is 71.49°C. The system controlled by TOT has the highest HST (71.99 °C) among the automatic control systems and shortest TFOT (17.5 hours).

Figure 5.2 illustrates the fan activation pattern for automatic systems. Total number of fan activations and de-activations can be found in table 5.2.

Die approbierte gedruckte Originalversion dieser Diplomarbeit ist an der TU Wien Bibliothek verfügbar
The approved original version of this thesis is available in print at TU Wien Bibliothek.

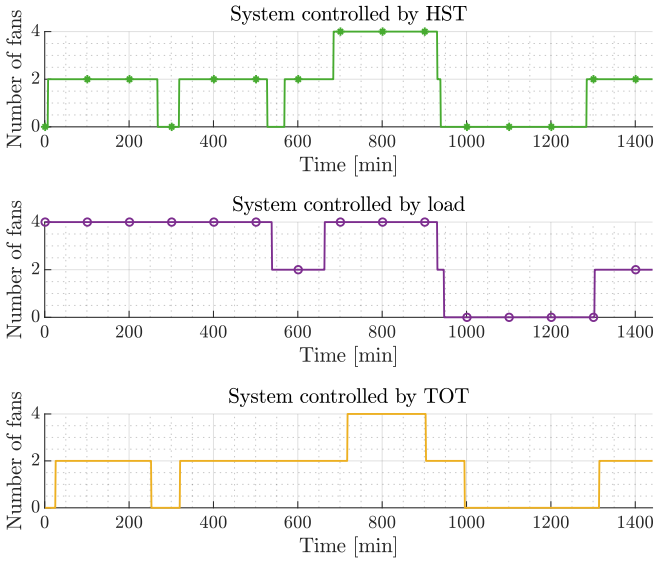

Figure 5.2: Fan activation pattern. Scenario WFCT 1, summer

Table 5.2: Number of fan activations and de-activations. Scenario WFCT 1, summer

	System controlled by		
	Load	**HST**	**TOT**
Number of activations	2	4	3
Number of de-activations	1	3	2
Total	3	7	5

The system controlled by HST signal started cooling with 2 fans. At minute 685 activation of 4 fans was executed, 4 fans remained active until minute 930. Afterwards, the system briefly switched to natural cooling. And from minute 1285 transformer cooling was executed exclusively by 2 fans.

On the contrary, the system controlled by load started cooling with 4 fans, then shortly switched to one level of cooling. At minute 664 both levels of cooling were activated and remained active until minute 931. Between minutes 931 and 1304 by lower load the transformer is cooled via natural convection, then 2 fans are switched on again.

The system controlled by TOT switches on 2 fans after 30 minutes. Then periodically activates and de-activates one level of cooling. From minute 718 activation of the second level of cooling follows and lasts until 903 minute. Between minutes 903 and 995 only one level of cooling is active. Between minutes 996 and 1314 no fans are active. Then activation of one level follows.

From minute 718 all automatic systems activated both levels of cooling, which remained active until minute 903. By lower load all systems switched to natural cooling. The fastest to react to load increase is the system controlled by load, whereas the slowest is the system controlled by TOT. For this particular wind profile in summer it can be recommended to use a fast control system, as system controlled by load.

Although during the first 600 minutes, the system with 2 continuously operating fans

Die approbierte gedruckte Originalversion dieser Diplomarbeit ist an der TU Wien Bibliothek verfügbar
The approved original version of this thesis is available in print at TU Wien Bibliothek.

was more effective, compared to the systems controlled by TOT and HST when peak load occurred the HST of a system with 2 fans was 10°C higher. Remarkably, that HST of continuous forced cooling with 2 and 4 fans only differ in average by 7 °C.

The frequent switching on and -off of the cooling stages might be harmful, however constant operation of fans significantly reduces the life span of the cooling system as well. Hence, there must be a balance between the number of fan activation and de-activation and TFOT.

From table 5.2 it can be seen, that all automatic systems had frequent switchings of cooling levels. System controlled by load had lowest number of switchings and longest total duration of fans operation. This allowed the system controlled by load to achieve average HST 6°C lower than this of the system controlled by TOT. The system controlled by HST had 7 switchings in total and average HST is only 2°C lower than average HST of the system controlled by TOT. The system controlled by TOT in turn switched on and off the cooling system 5 times in total. However, since the system controlled by HST had longer continuous cooling by 4 fans than the system controlled by TOT the resulting average HST is lower by the latter system.

Based on the number of the fan activation/de-activation and TFOT the system controlled by load and TOT can be recommended to keep the cooling system "healthy" for a longer period of time and prevent it from frequent outages.

5.1.2 Winter

Figure 5.3 illustrates HST of different cooling methods for WFCT 1 by winter ambient temperature. Maximum and average HST together with the analysis of TFOT are represented in table 5.3.

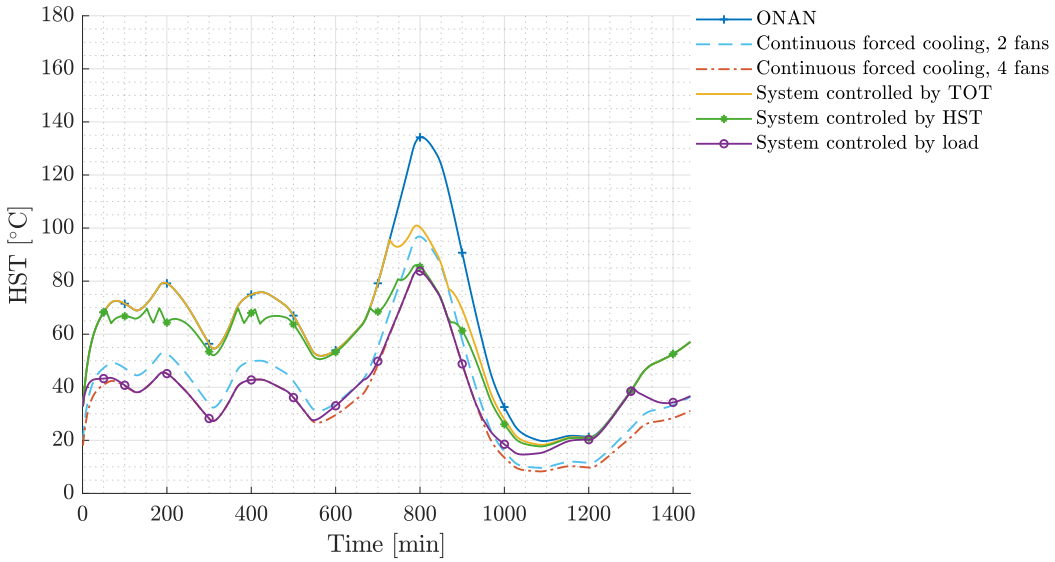

Figure 5.3: HST of different cooling methods. Scenario WFCT 1, winter

Die approbierte gedruckte Originalversion dieser Diplomarbeit ist an der TU Wien Bibliothek verfügbar
The approved original version of this thesis is available in print at TU Wien Bibliothek.

Table 5.3: Maximum, average HST and TFOT of different cooling methods. Scenario WFCT 1, winter

	Maximum HST,°C	Average HST, °C	TFOT, hrs
ONAN	134.27	61.87	0
Continuous forced cooling, 2 fans	96.97	40.11	24
Continuous forced cooling, 4 fans	83.86	34.49	48
System controlled by TOT	100.92	57.49	4.4
System controlled by HST	86.05	53.13	6.2
System controlled by load	83.89	38.11	31.5

The lowest average HST can be observed by continuous forced cooling using 4 fans and the highest by ONAN. Average HST for the first cooling method is 34.49°C, while for the latter it is 61.87°C. System controlled by load is only 4°C lower than the lowest HST (due to the fact that this system mostly used 4 fans). Average HST of the system controlled by HST signal is 53.13°C, followed by the system controlled by TOT with 57.49°C. The latter is the highest HST among the all automatic systems.

The fan activation pattern can be seen in figure 5.4. Total number of fan activations and de-activations is summarized in table 5.4.

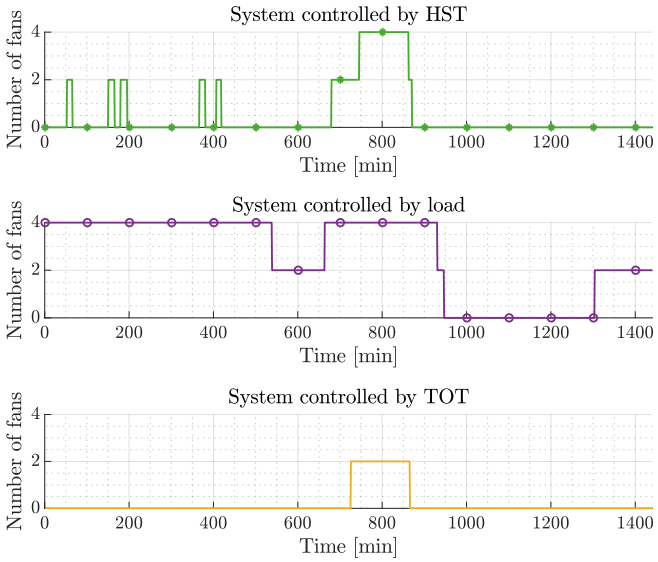

Figure 5.4: Fan activation pattern. Scenario WFCT 1, winter

Die approbierte gedruckte Originalversion dieser Diplomarbeit ist an der TU Wien Bibliothek verfügbar
The approved original version of this thesis is available in print at TU Wien Bibliothek.

Table 5.4: Number of fan activations and de-activations for all automatic systems. Scenario WFCT 1, winter

	System controlled by		
	Load	**HST**	**TOT**
Number of activations	2	6	1
Number of de-activations	1	6	1
Total	3	12	2

From the fan activation pattern it is noticeable, system controlled by HST periodically activates and de-activates one level of cooling. From minute 750 all 4 fans are active until minute 950. The system controlled by load immediately activated both levels of cooling. At minute 550 it shortly switched to one level of cooling then continued with both levels of cooling. The system controlled by TOT mostly used natural cooling, during the peak load it shortly switched on 2 fans.

In table 5.4 it can be seen, that the system controlled by HST has frequent switches and there is a short period of time when one then two levels of cooling operate continuously. TFOT by this system is 6.2 hours. The system controlled by load in total executed 3 switchings, however the duration of fans operation allowed to achieve the best cooling effect. The system controlled by TOT only activated and de-activated one level of cooling and fans were operating for 4.4 hours. Considering the total number of activations and de-activations and TFOT for this wind load profile by lower ambient temperature the system controlled by load can be recommended.

Summarizing simulation results for this wind profile, it can be concluded, that in summer optimal cooling can be achieved using the system, controlled by load. In winter it is better to use the system controlled by HST, since it is not necessary to keep temperature at this low level.

5.2 Scenario wind farm collector transformer 2

In this scenario the second wind load profile was studied by summer and winter ambient temperatures. Figures 4.3 and 4.2 illustrate load and ambient temperatures used as input. The wind load profile was interesting due to its tendency to increase over the day. Maximum load was reached by minute 1440 (1.48). Minimum load value is 0.73 and average load value is 1.01.

5.2.1 Summer

The resulting HST of different cooling methods for scenario WFCT 2 by summer ambient temperature are demonstrated on figure 5.5. Maximum, minimum and average HST together with TFOT are represented in table 5.5.

Die approbierte gedruckte Originalversion dieser Diplomarbeit ist an der TU Wien Bibliothek verfügbar
The approved original version of this thesis is available in print at TU Wien Bibliothek.

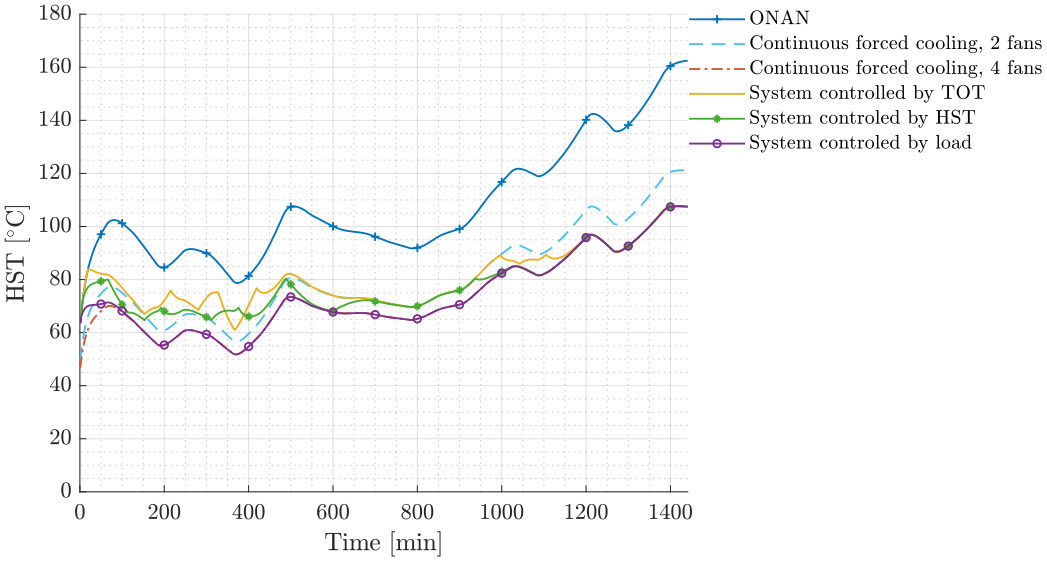

Figure 5.5: HST of different cooling methods. Scenario WFCT 2, summer

Table 5.5: Maximum, average HST and TFOT of different cooling methods. Scenario WFCT 2, summer

	Maximum HST,°C	Average HST, °C	TFOT, hrs
ONAN	161.18	105.85	0
Continuous forced cooling 2 fans	120.12	78.91	24
Continuous forced cooling 4 fans	106.66	71.75	48
System controlled by TOT	106.66	79.27	26.9
System controlled by HST	106.66	77.22	30.7
System controlled by load	106.66	72.07	48

As in previous wind load scenario the transformer with natural cooling has the highest HST, whereas forced cooling by 4 fans has the lowest HST. HST of a transformer with system controlled by load is 72.07°C. This differs from continuous forced cooling with 4 fans by 0.32°C, due to the fact that TFOT is 48 hours e.g. fans are operating non-stop. Average HST of a system controlled by TOT is 79.27°C and of the system controlled by HST is 77.22°C. For continuous forced cooling with 2 fans this value is 78.91°C. Since systems controlled by TOT and HST only differ from continuous forced cooling with 2 fans by few degrees, it can be concluded that they mostly activated 2 fans. This high average HST is directly connected to the TFOT, only 27 hours against 48 hours for the system controlled by load. The system controlled by HST had operating fans during 30.7 hours. Additional 2 hours of fan operation allowed to achieve 2 °C lower average HST compared to the system controlled by HST.

Figure 5.6 demonstrates the fan activation pattern for WFCT 2. Total number of fan

Die approbierte gedruckte Originalversion dieser Diplomarbeit ist an der TU Wien Bibliothek verfügbar
The approved original version of this thesis is available in print at TU Wien Bibliothek.
TU Bibliothek Your knowledge hub WIEN

activations and de-activations of the cooling system can be found in table 5.6. From the fan activation pattern it can be seen, that the system controlled by load has both levels of cooling active from minute 0 to 1440. The system controlled by HST switches between 1 and 2 levels of cooling and from minute 950 4 fans are active constantly. On contrary, the system controlled by TOT mostly uses one level of cooling. Before approximately 410 minute it activates and de-activates 2 fans. At minute 1008 both levels of cooling are active.

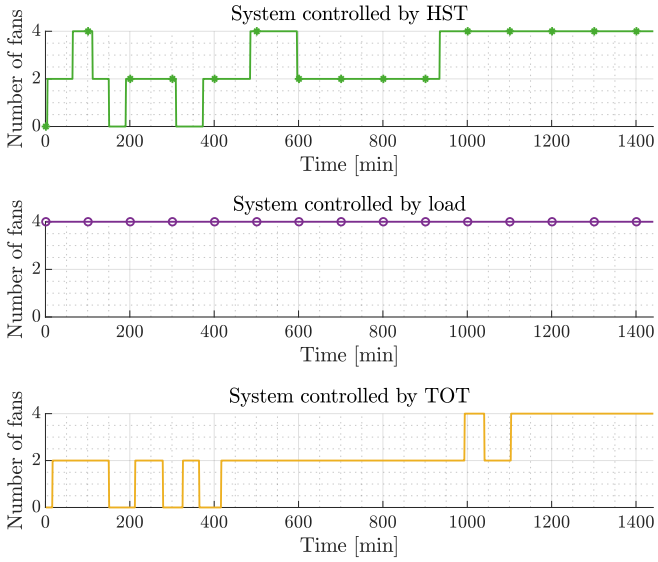

Figure 5.6: Fan activation pattern. Scenario WFCT 2, summer

Table 5.6: Number of fan activations and de-activations. Scenario WFCT 2, summer

	System controlled by		
	Load	**HST**	**TOT**
Number of activations	1	3	4
Number of de-activations	0	2	3
Total	1	5	7

The system controlled by HST requires almost 31 hours of fans in operation.

While the system controlled by TOT only required 3.2 hours of fan operation, the system controlled by load required 48 hours. TFOT for the system controlled by HST is 9.6 hours.

From table 5.6 it can be concluded, that with one switching there is no visible difference between the system controlled by load and continuous forced cooling e.g. both systems have 4 fans operating the entire day. The system controlled by TOT on the contrary had frequent switchings and stable fan operation in the end. Same can be told about the system controlled by HST, frequent switchings (on and off), however longer operation of both cooling systems in the end allowed to achieve lower average HST compared to the system controlled by TOT.

Although the system controlled by load has the lowest average HST, leaving the fans to operate 48 hours might be damaging in long term perspective and cause unnecessary

Die approbierte gedruckte Originalversion dieser Diplomarbeit ist an der TU Wien Bibliothek verfügbar
The approved original version of this thesis is available in print at TU Wien Bibliothek.

expenses. Considering a good cooling effect, total TFOT and number of fan activations/deactivations for this profile system controlled by HST can be named optimal.

5.2.2 Winter

Figure 5.7 illustrates HST of WFCT 2 by winter ambient temperature. Maximum, minimum and average HST together with TFOT are summarized in table 5.7.

The system controlled by load and continuous forced cooling have the lowest average HST, for the first it is 44.19°C and for the latter 43.87°C. Average HST of the system controlled by TOT remained high (72.02°C), this is reflected in TFOT. The fans operation lasts only 6.5 against 48 hours by the system controlled by load. Due to the fact that in total fans were active only for 9.6 hours, average HST of the system controlled by HST is high too.

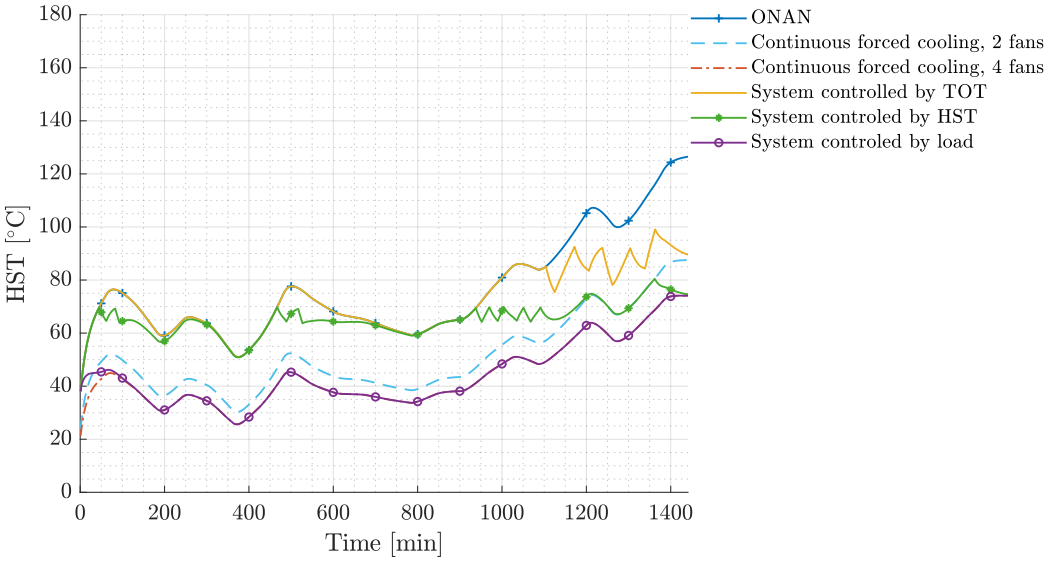

Figure 5.7: HST temperatures of different cooling methods. Scenario WFCT 2, winter

Table 5.7: Maximum, average HST and TFOT of different cooling methods. Scenario WFCT 2, winter

	Maximum HST,°C	Average HST, °C	TFOT, hrs
ONAN	126.49	76.43	0
Continuous forced cooling, 2 fans	87.53	50.91	24
Continuous forced cooling, 4 fans	74.11	43.87	48
System controlled by TOT	99.07	72.02	6.5
System controlled by HST	80.47	65.06	9.6
System controlled by load	74.11	44.19	48

Fan activation pattern can be seen in figure 5.8. Total number of fan activation/ de-

Die approbierte gedruckte Originalversion dieser Diplomarbeit ist an der TU Wien Bibliothek verfügbar
The approved original version of this thesis is available in print at TU Wien Bibliothek.

activations is summarized in table 5.8. Fan activation pattern shows, that the system controlled by load has both level of cooling constantly active. Remarkably, that the system controlled by TOT did not use all 4 fans even during the period of higher load. System controlled by HST activated and de-activated one level of cooling for short period of time. From minute 1134 it used 2 fans for a relatively long period of time and then activated both levels of cooling.

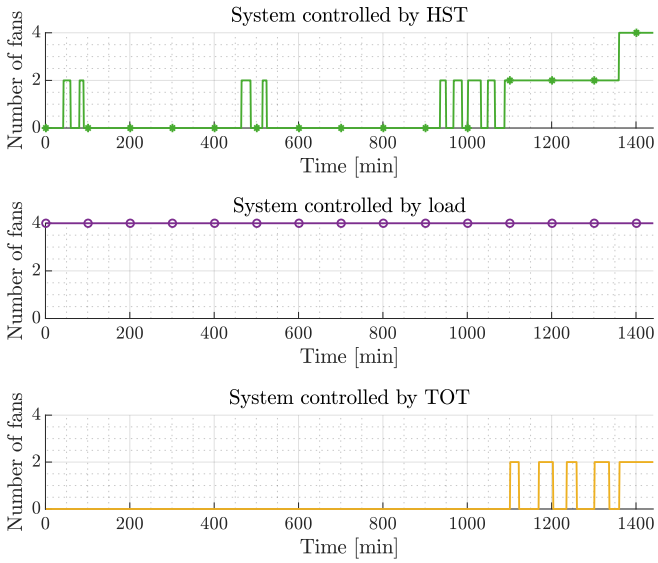

Figure 5.8: Fan activation pattern. Scenario WFCT 2,winter

Table 5.8: Number of fan activations. Scenario WFCT 2, winter

	System controlled by		
	Load	**HST**	**TOT**
Number of activations	1	9	5
Number of de-activations	0	8	4
Total	1	17	9

From figure 5.8 it can be noticed, that the system controlled by load switched on both levels of cooling once and had 4 fans operating during the entire day. This is reflected in the low average HST value. The system controlled by TOT frequently activated and de-activated one level of cooling, however this system did not have continuous fan operation, which could potentially provide better cooling (6.5 hours in total). The most frequent "jumps" can be observed by the system controlled by HST, however some periods of continuous cooling allowed to achieve better results compared to the system controlled by TOT. Although the system controlled by load gives quite good cooling it mostly activates 4 fans, this results in very low oil temperature and might cause additional expenses. Hence, for wind load in winter, the system controlled by HST and TOT can be applied. As system controlled by HST frequently switches on and -off and has longer TFOT, the system controlled by TOT could be a better cooling strategy for this load profile.

Die approbierte gedruckte Originalversion dieser Diplomarbeit ist an der TU Wien Bibliothek verfügbar
The approved original version of this thesis is available in print at TU Wien Bibliothek.

5.3 Scenario solar farm collector transformer

This section contains simulation results for Solar Farm Collector Transformer (**SFCT**). Load values and ambient temperatures used as input can be seen in pictures 4.3 and 4.2.

5.3.1 Summer

Figure 5.9 illustrates HST of different cooling methods by summer ambient temperature and table 5.9 gives an overview of maximum, average HST and TFOT.

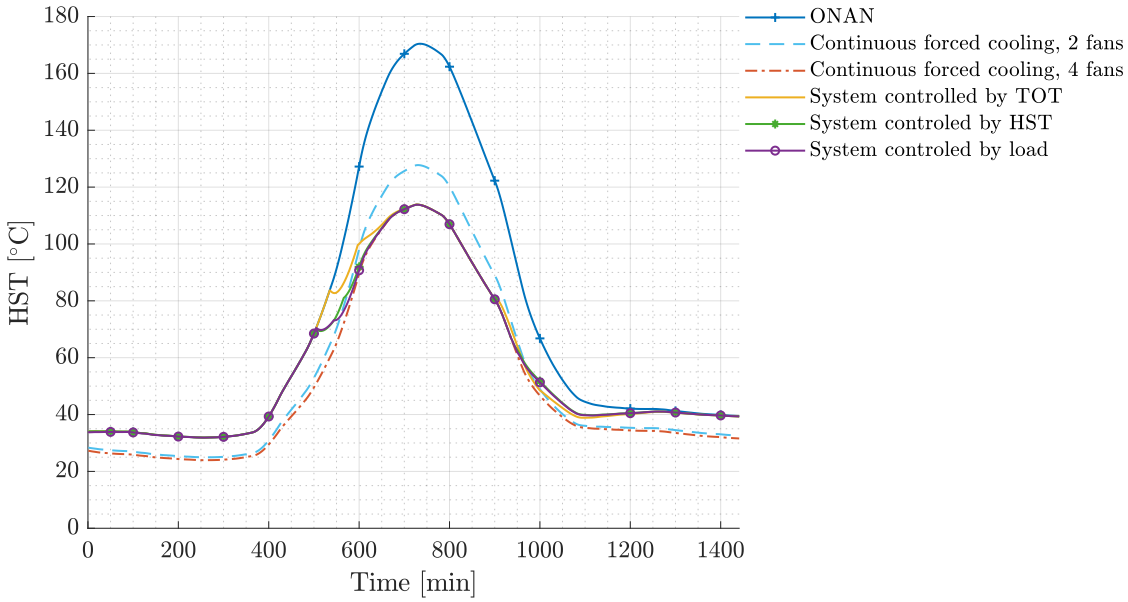

Figure 5.9: HST of different cooling methods. Scenario SFCT, summer

Table 5.9: Maximum, average HST and TFOT of different cooling methods. Scenario SFCT, summer

	Maximum HST, °C	Average HST,°C	TFOT, hrs
ONAN	170.42	71.53	0
Continuous forced cooling, 2 fans	127.74	54.89	24
Continuous forced cooling, 4 fans	113.80	50.88	48
System controlled by TOT	113.87	57.37	11.4
System controlled by HST	113.81	56.87	12.83
System controlled by load	113.80	56.69	13.9

It can be seen, that until peak load the transformer does not require any cooling. Highest average HST was observed by ONAN cooling method, followed by continuous forced cooling with 2 fans. The latter is proven to be less effective against the peaks in previous scenarios. The lowest average HST is 50.88°C and it was achieved by continuous

Die approbierte gedruckte Originalversion dieser Diplomarbeit ist an der TU Wien Bibliothek verfügbar
The approved original version of this thesis is available in print at TU Wien Bibliothek.

forced cooling with 4 fans. Average HST of automatic control systems varies between 56-57°C.

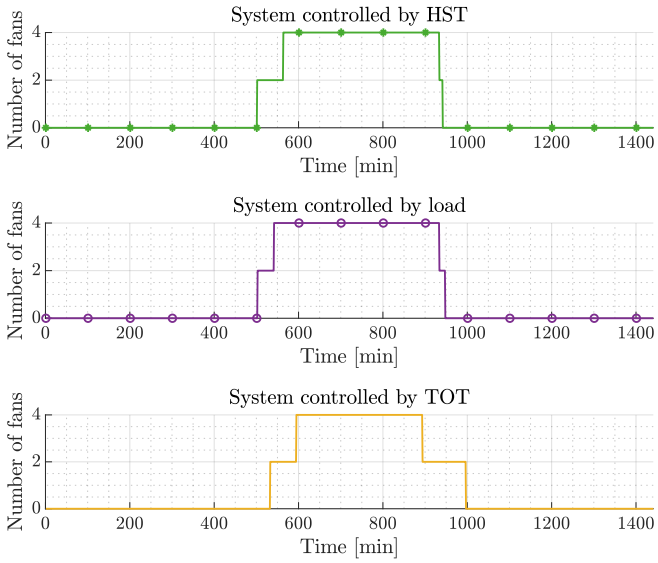

Figure 5.10: Fan activation pattern. Scenario SFCT, summer

Figure 5.10 demonstrates the fan activation pattern for SFCT by summer ambient temperatures. By increasing load, the system controlled by HST and TOT activated one level of cooling from starting at minute 518, while the system controlled by load started cooling with one level earlier (503 minute). System controlled by HST activated both cooling level at minute 575, the system controlled by load at minute 545. Latest to activate both levels was the system controlled by TOT (after 610 minutes). The system controlled by load had longest TFOT with 13.9 hours. TFOT of the system controlled by HST is 12.8 hours. TFOT of the system controlled by TOT is the shortest with 11.4 hours.

It can be concluded, that the cooling system controlled by load gives the best cooling effect with average HST of 54.86 °C. Worth to mention, that PV load is not volatile and does not require a fast reacting system, so system controlled by TOT is sufficient by peak load.

5.3.2 Winter

Figure 5.11 illustrates HST of different cooling methods for scenario SFCT by winter ambient temperature.

Die approbierte gedruckte Originalversion dieser Diplomarbeit ist an der TU Wien Bibliothek verfügbar
The approved original version of this thesis is available in print at TU Wien Bibliothek.

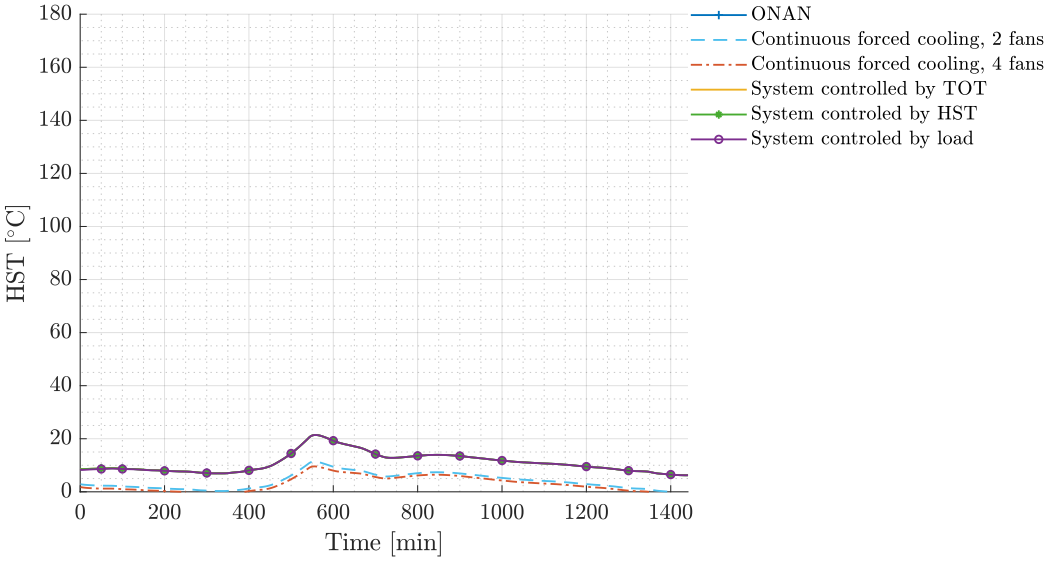

Figure 5.11: HST of different cooling methods. Scenario SFCT, winter

Due to the low photovoltaic module output in winter, none of the cooling levels were activated. Activating one or two levels of cooling results in very low HST levels. Average HST for all automatic systems is 11.5°C and maximum HST is 18.97°C. One level of cooling has maximum HST 9.3°C and average HST 4.49°C. For two levels of cooling average HST is 3.44°C and maximum HST is 7.5°C.

5.4 Scenario grid transformer

In this scenario the HST of interconnecting or Grid Transformer was analyzed by summer and winter ambient temperatures. The chosen load profile represents load of a transformer operating in normal grid conditions. The load profile used as input is illustrated on figure 4.3 and ambient temperatures are illustrated on the figure 4.2.

5.4.1 Summer

Figure 5.12 demonstrates HST of different cooling methods of a grid transformer by summer ambient temperature. Maximum and average HST, together with TFOT are represented in table 5.10.

Die approbierte gedruckte Originalversion dieser Diplomarbeit ist an der TU Wien Bibliothek verfügbar
The approved original version of this thesis is available in print at TU Wien Bibliothek.

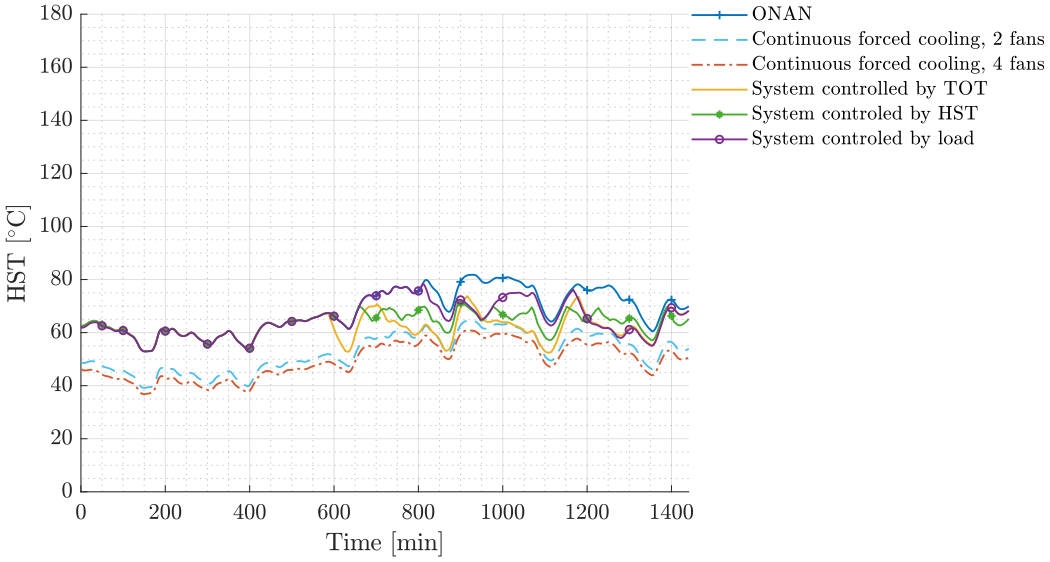

Figure 5.12: HST of different cooling methods. Scenario grid transformer, summer

Table 5.10: Maximum, average HST and TFOT. Scenario grid transformer, summer

	Maximum HST, °C	Average HST,°C	TFOT, hrs
ONAN	81.79	68.17	0
Continuous forced cooling, 2 fans	64.51	52.43	24
Continuous forced cooling, 4 fans	60.85	49.36	48
System controlled by TOT	73.76	61.31	15.3
System controlled by HST	71.04	63.39	9.5
System controlled by load	78.53	65.12	5.9

The highest average HST is 68.17°C and it is resulting from natural cooling. The lowest HST is realised by continuous forced cooling using 4 fans (49.36°C), followed by continuous forced cooling using 2 fans. As it can be seen from table 5.10 the system controlled by TOT has its fans active for the longest period of time 15.3 hours. Due to this, the system controlled by TOT has the lowest HST compared to other automatic control systems. Average HST of the system controlled by load is 65.12°C. This system only has 5.9 hours of TFOT, which explains relatively high average HST.

Die approbierte gedruckte Originalversion dieser Diplomarbeit ist an der TU Wien Bibliothek verfügbar
The approved original version of this thesis is available in print at TU Wien Bibliothek.

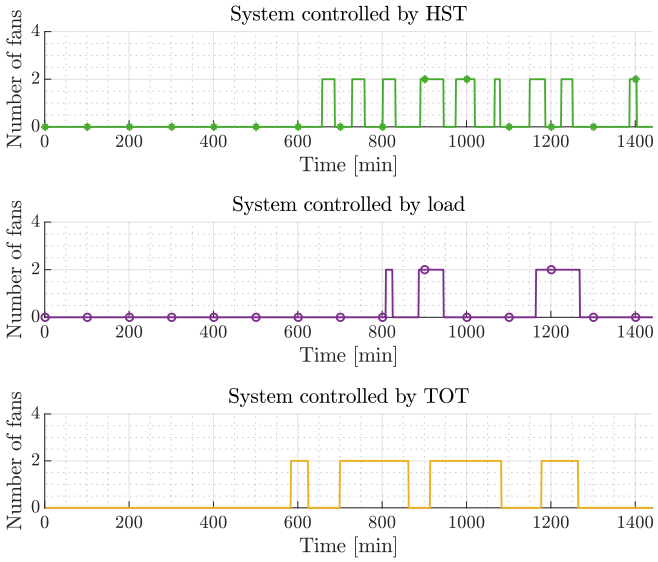

Figure 5.13: Fan activation pattern. Scenario grid transformer, summer

Table 5.11: Number of fans activations and de-activations. Scenario grid transformer, summer

	System controlled by		
	Load	**HST**	**TOT**
Number of activations	3	9	4
Number of de-activations	3	9	4
Total	6	18	8

Table 5.11 contains number of total switch on (and offs) and the fan activation pattern can be seen in figure 5.13. While the system controlled by HST frequently switches on and -off one level of cooling, the system controlled by TOT rather has continuous fan operation. This allows to achieve better a cooling effect. This can be concluded from average HST of both systems. By normal load conditions, the system controlled by load is less effective, during the day it only briefly activated the fans 3 times.

System controlled by TOT activated one level of cooling at minute 810, whereas the system controlled HST temperature activated one level of cooling after 910 minutes. It is noticeable from figure 5.12, that the system controlled by load did briefly switch on one level of cooling after 800 minutes, then after 900 minute and finally after 1175 minutes.

Based on the resulting average HST together with TFOT for the grid operating in normal conditions, the system controlled by TOT and by HST can be recommended.

5.4.2 Winter

Figure 5.14 shows HST of different cooling methods of a grid transformer by winter ambient temperature. It can be seen, that HST remains low even without additional cooling. Only the system controlled by load, activated the fans. Switching on one or two levels of cooling is not reasonable, as generally the transformer does not require additional cooling at this low level of ambient temperature.

Die approbierte gedruckte Originalversion dieser Diplomarbeit ist an der TU Wien Bibliothek verfügbar
The approved original version of this thesis is available in print at TU Wien Bibliothek.

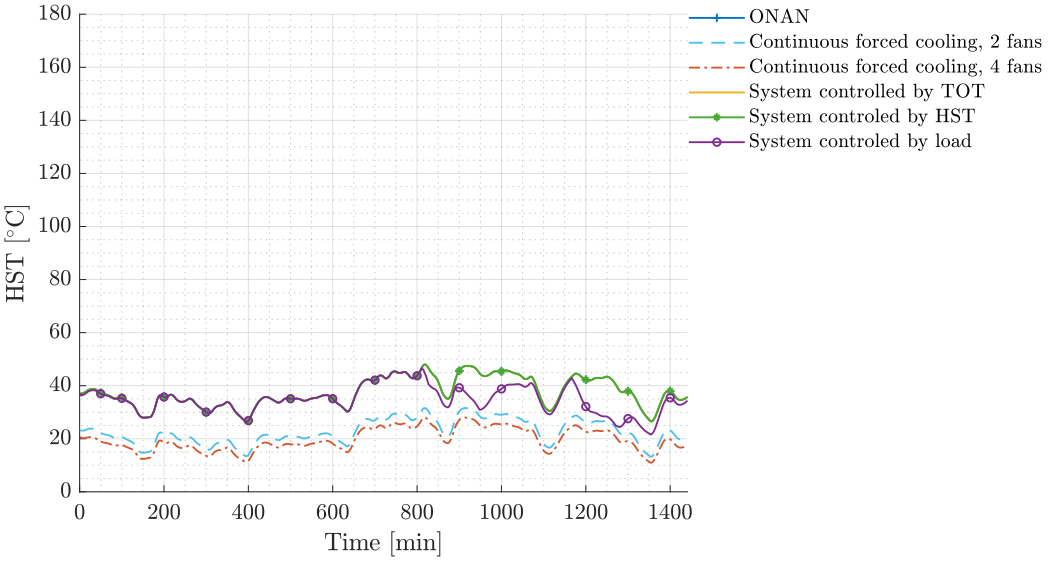

Figure 5.14: HST of different cooling methods. Scenario grid transformer, winter

Die approbierte gedruckte Originalversion dieser Diplomarbeit ist an der TU Wien Bibliothek verfügbar
The approved original version of this thesis is available in print at TU Wien Bibliothek.

6 The analysis of the pre-cooling effect

In this chapter the effective time of pre-cooling was investigated. Effective time of pre-cooling is the time required to reach minimum achievable HST. Since, continuous forced cooling using 4 fans demonstrated the best cooling effect it was decided to use it as a benchmark (minimum achievable HST).

In other words, following the fan activation, the HST drops to the level of continuous forced cooling. The time that pre-cooled system required to reach this level was determined and average HST was estimated.

Additionally the pre-cooling effect was studied for all automatic systems by summer and winter ambient temperatures. For this purpose a scenario with pre-cooling starting 200 minutes prior to grid emergency. The objectives are to determine how long did the automatic system require to reach the HST of a pre-cooled system, to estimate the pre-cooling exposure time after grid emergency and last but not least to estimate resulting temperature gain by comparing average HST of the pre-cooled system and automatic control system during the pre-cooling exposure time. Pre-cooling exposure time is time that the automatic control system required to achieve the HST of pre-cooled system.

Consider a substation with two transformers connected parallel, so that $(n-1)$ criterion is fulfilled. After 600 minutes, the failure of Transformer 1 occurred and Transformer 2 must carry the double load, as a result the emergency operational state is reached. To avoid overheating, fans are activated prior to expected grid emergency. Depending on the scenario fan activation starts 400 minutes, 200 minutes or shortly before the grid emergency or load peak (100 minutes).

6.1 Summer

This section contains the analysis of effectiveness of pre-cooling measures by summer ambient temperature. Load profile used as input can be seen in figure 4.3.The grid emergency load profile was artificially generated, by doubling the load from the previous section after 600 minutes.

6.1.1 Scenario 1. Pre-cooling 400 minutes prior grid emergency

In this scenario 4 fans were activated at 200 minutes. Figure 6.1 illustrates HST of different cooling methods after grid emergency.

Die approbierte gedruckte Originalversion dieser Diplomarbeit ist an der TU Wien Bibliothek verfügbar
The approved original version of this thesis is available in print at TU Wien Bibliothek.

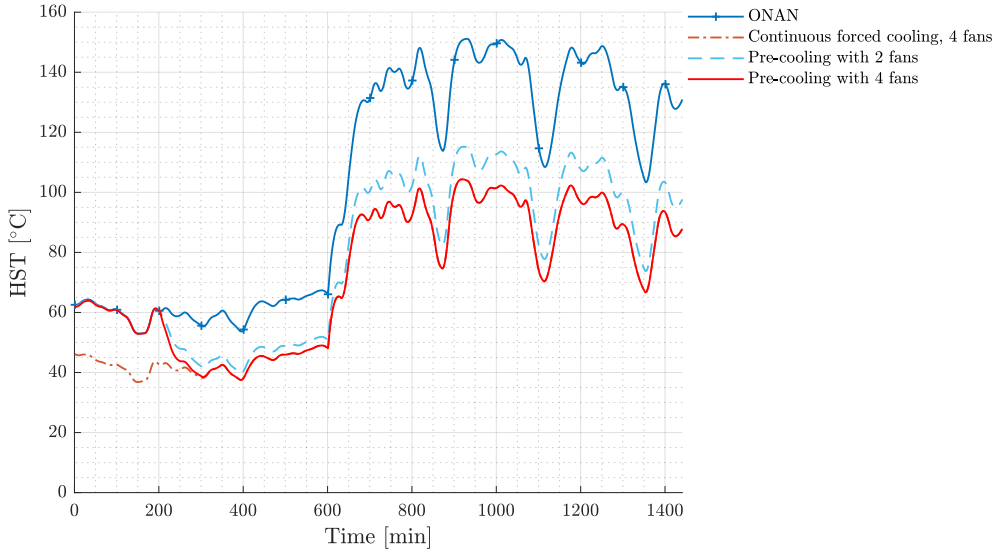

Figure 6.1: HST of different cooling methods after grid emergency. Scenario pre-cooling 400 minutes prior grid emergency, summer

The estimated effective time of pre-cooling is 95 minutes. This means, that after activation of both levels of cooling, the HST remained higher, than the one of a transformer with continuous forced cooling (4 fans) for 95 minutes. The HST dropped from 60.65°C at the beginning of cooling to 41°C. The average HST during the fore-mentioned period of time is 46.56 °C for the pre-cooled transformer against 41.23°C of a transformer with continuous forced cooling.

It can be noticed from figure 6.1, that pre-cooling with 2 fans is less effective compared to pre-cooling with 4 fans. From the moment of activation until the grid emergency temperature difference was not higher than 2 °C, however from minute 600 it steadily grows to 8 °C. On average HST of a transformer pre-cooled with 4 fans is 5 °C lower, than of the one pre-cooled with 2 fans.

6.1.2 Scenario 2. Pre-cooling 200 minutes prior grid emergency

In this scenario pre-cooling begins at 400 minutes. Average HST of different cooling methods after grid emergency can be seen in figure 6.2.

Die approbierte gedruckte Originalversion dieser Diplomarbeit ist an der TU Wien Bibliothek verfügbar
The approved original version of this thesis is available in print at TU Wien Bibliothek.

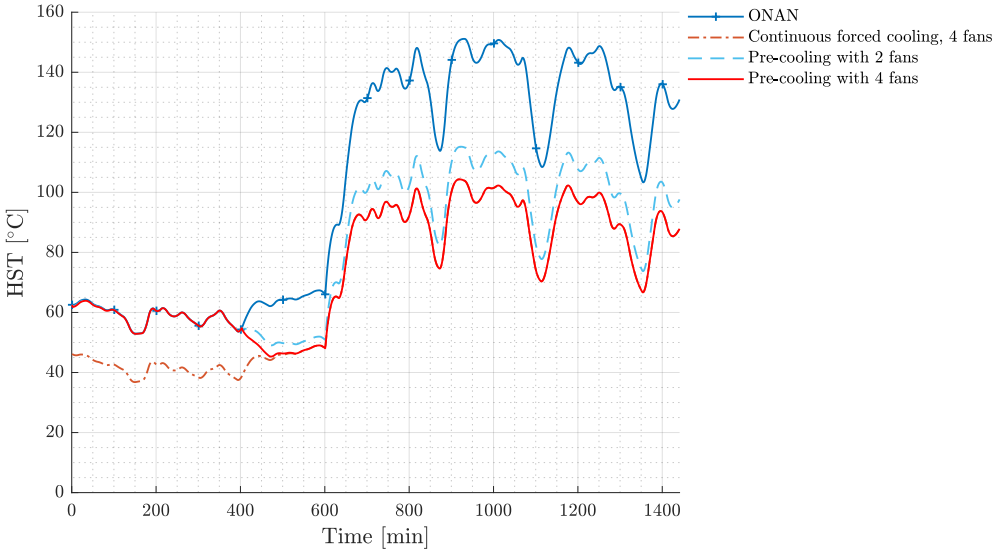

Figure 6.2: HST of different cooling methods. Scenario pre-cooling 200 minutes prior grid emergency, summer

The HST dropped from 53.94°C to 46.34 °C in 94 minutes and afterwards the difference between pre-cooled system and benchmark system can no longer be observed. The average HST during this time is 48°C, whereas the average HST of a transformer with forced cooling is 44°C.

6.1.3 Scenario 3. Pre-cooling 100 minutes prior grid emergency

In this scenario pre-cooling started 100 minutes prior to grid emergency. Figure 6.3 represents HST of different cooling methods after grid emergency.

Die approbierte gedruckte Originalversion dieser Diplomarbeit ist an der TU Wien Bibliothek verfügbar
The approved original version of this thesis is available in print at TU Wien Bibliothek.

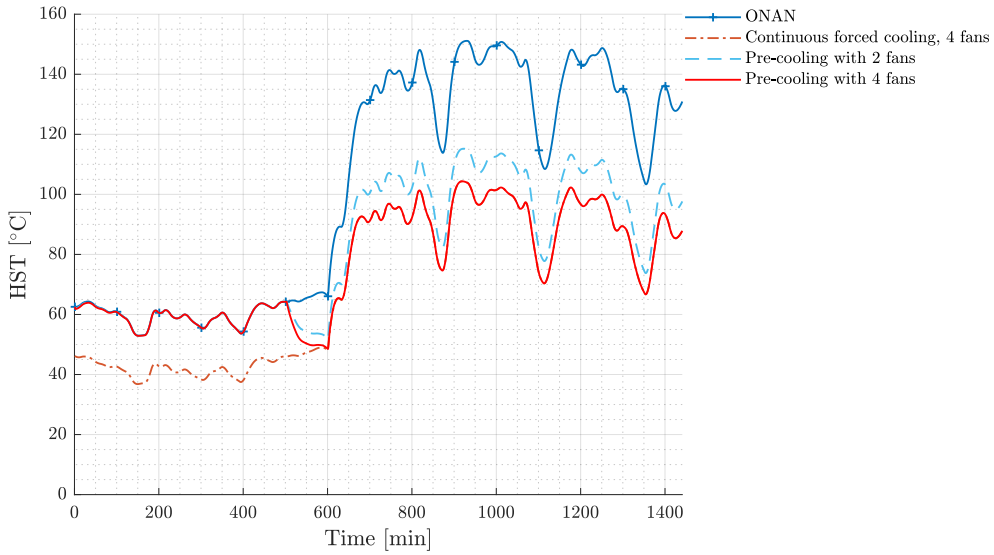

Figure 6.3: HST of different cooling methods after grid emergency. Scenario pre-cooling 100 minutes prior grid emergency, summer

For 97 minutes the HST remained higher than the HST of a transformer with continuous forced cooling. At the moment pre-cooling starts the HST was 64.21°C and after 96 minutes it dropped to 49.07°C. Average HST of a benchmark system during this period of time was 44.38°C and average HST of the pre-cooled system was 47.35°C.

6.1.4 Scenario 4. Cooling after reported emergency

In this scenario the transformer was not pre-cooled and cooling started immediately after reported emergency. Figure 6.4 demonstrates HST of different cooling methods after grid emergency for scenario cooling after reported emergency.

Die approbierte gedruckte Originalversion dieser Diplomarbeit ist an der TU Wien Bibliothek verfügbar
The approved original version of this thesis is available in print at TU Wien Bibliothek.

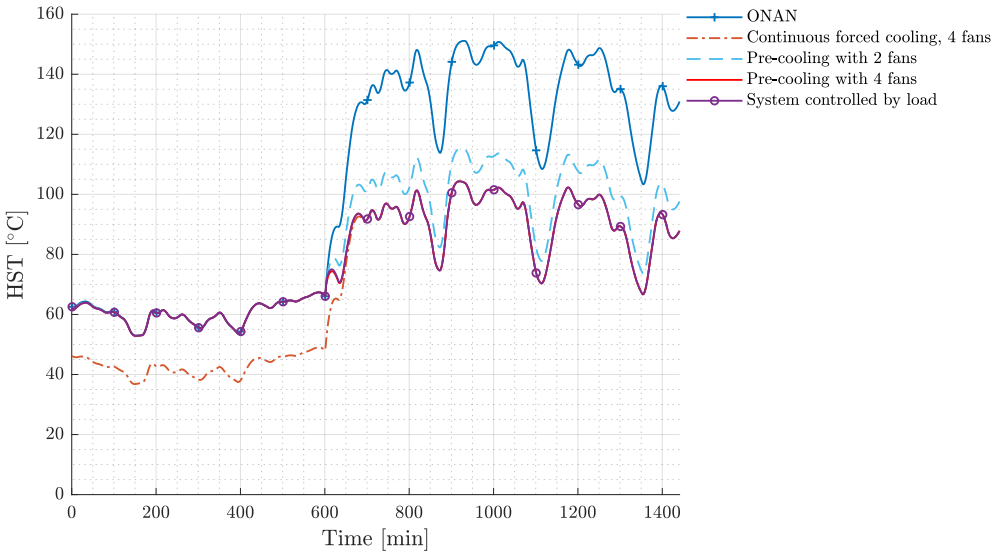

Figure 6.4: HST of different cooling methods and HST of pre-cooled transformer

It is noticeable, that HST after fan activation and forced continuous cooling are different for 97 minutes. The average HST after fan activation was 62.43°C. And for the transformer with forced cooling it was 44.4°C. Due to the fact, that the system controlled by load activated both levels of cooling starting at minute 600 there is no visible difference between the system controlled by load and instant fan activation at the moment of grid emergency. To illustrate this exceptional case, system controlled by load was added to figure 6.4.

6.2 Winter

This section contains the analysis of HST after pre-cooling measures and HST of different automatic systems by low ambient temperature. The temperature profile is illustrated in figure 4.2.

6.2.1 Scenario 1. Pre-cooling 400 minutes prior grid emergency

In this scenario fans were activated after 200 minutes. Figure 6.5 illustrates HST of different cooling methods after grid emergency by winter ambient temperature and the behavior of HST of the pre-cooled system.

Die approbierte gedruckte Originalversion dieser Diplomarbeit ist an der TU Wien Bibliothek verfügbar
The approved original version of this thesis is available in print at TU Wien Bibliothek.

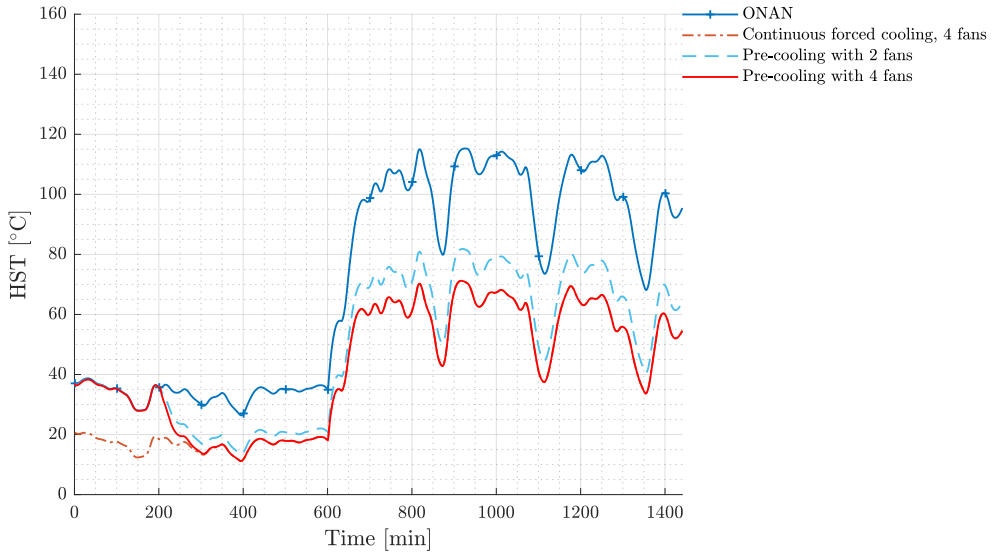

Figure 6.5: HST of different cooling methods. Scenario pre-cooling 400 minutes prior grid emergency

The estimated effective time of pre-cooling is 96 minutes. At the pre-cooling start HST was 35.74°C and after 96 minutes the HST decreased to 17.78°C. Average HST of the pre-cooled system is 25.33 °C.

6.2.2 Scenario 2. Pre-cooling 200 minutes prior grid emergency

Figure 6.6 shows simulation results for scenario pre-cooling 200 minutes prior grid emergency by winter ambient temperature.

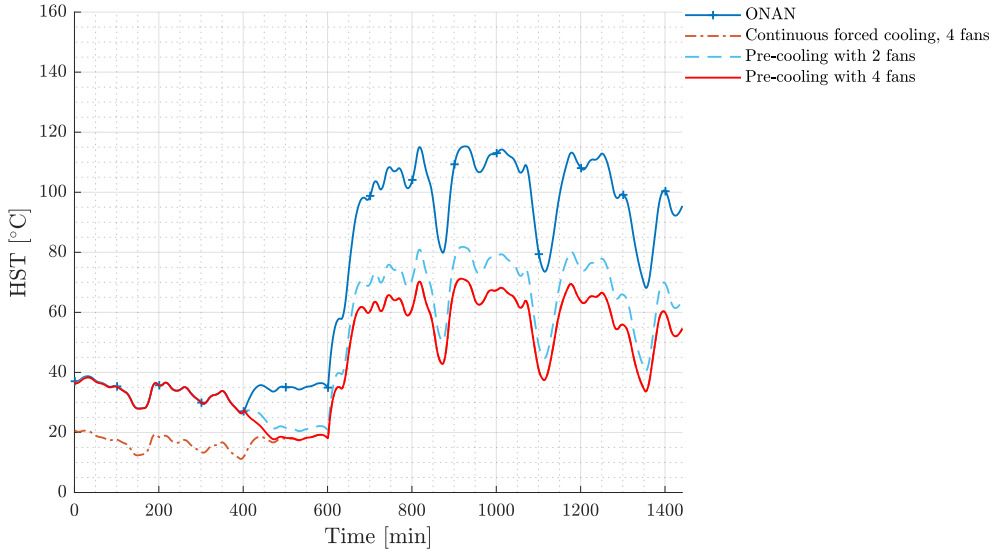

Figure 6.6: HST of different cooling methods. Scenario pre-cooling 200 minutes prior grid emergency, winter

Die approbierte gedruckte Originalversion dieser Diplomarbeit ist an der TU Wien Bibliothek verfügbar
The approved original version of this thesis is available in print at TU Wien Bibliothek.
TU Bibliothek Your knowledge hub WIEN

Following the fan activation at 400 minutes the HST drops to the level of continuous forced cooling in 92 minutes. If at the beginning of cooling HST was 26.83°C, after 92 minutes it decreased to 18.5°C. The average HST during this period of time was 21.5°C.

6.2.3 Scenario 3. Pre-cooling 100 minutes prior grid emergency

Figure 6.7 represents HST of different cooling methods after grid emergency and dynamics of HST after fan activation at 500 minutes.

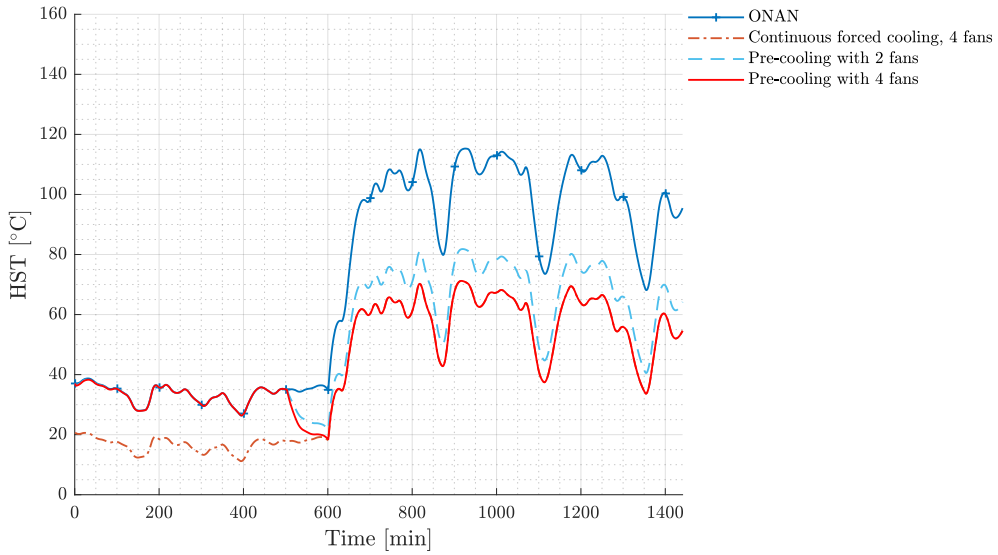

Figure 6.7: HST of different cooling methods after gird emergency. Scenario pre-cooling 100 minutes prior grid emergency, winter

After 500 minutes, a rapid temperature drop can be observed. It required 96 minutes to reach the temperature of transformer with forced cooling. At the start of pre-cooling the HST was 35.08°C and after 96 minutes it was already 19.3°C. The average HST during this time was 23.5°C.

6.3 Pre-cooling and automatic control systems

In this section the effectiveness of pre-cooling is analyzed by comparing it to the automatic control systems. The scenario, where pre-cooling begins 200 minutes before the expected grid emergency was studied during the summer and winter day. Simulation results can be seen in figures 6.8 and 6.10.

6.3.1 Summer

Figure 6.8 illustrates HST of different cooling methods for scenario pre-cooling 200 minutes before the grid emergency. Table 6.2 contains maximum, average HST and TFOT.

Die approbierte gedruckte Originalversion dieser Diplomarbeit ist an der TU Wien Bibliothek verfügbar
The approved original version of this thesis is available in print at TU Wien Bibliothek.

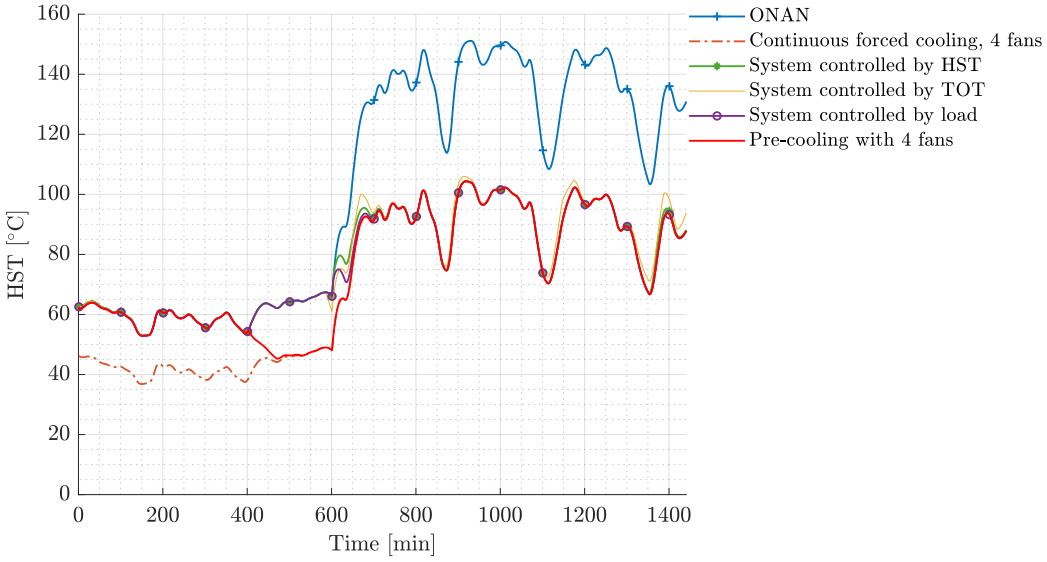

Figure 6.8: HST of different cooling methods after grid emergency. Scenario pre-cooling 200 minutes prior grid emergency, summer

Table 6.1: Maximum, average HST and TFOT of automatic controlled systems after grid emergency. Scenario pre-cooling 200 minutes prior grid emergency, summer

System controlled by	Maximum HST, °C	Average HST,°C	TFOT, hrs
ONAN	151.12	132.31	0
TOT	105.98	92.26	24
HST	104.34	91.07	26.9
Load	104.34	90.47	28
Continuous forced cooling	104.34	89.79	48

The estimated time of pre-cooling exposure for system controlled by HST is 125 minutes. While the average HST of the system controlled by HST was 86.97°C, the average HST of pre-cooled transformer was 79.47°C. The temperature difference between the average HST of pre-cooled transformer and HST of the system controlled by HST is 7.5°C.

The HST of a transformer with system controlled by TOT, the signal required 146 minutes to reach the temperature level of a pre-cooled transformer. So far, this is the slowest automatic control system. The average HST of this control system is 87.82°C against 81.43°C by pre-cooled transformer. In this case the temperature difference is 6.39°C.

The system controlled by load required 99 minutes to cool until pre-cooling HST. The estimated effective time of pre-cooling exposure is 99 minutes. Average HST of a transformer with system controlled by load is 81°C, while for pre-cooled transformer it is 75.9°C. Here, the average temperature difference is 5.1 °C.

Die approbierte gedruckte Originalversion dieser Diplomarbeit ist an der TU Wien Bibliothek verfügbar
The approved original version of this thesis is available in print at TU Wien Bibliothek.

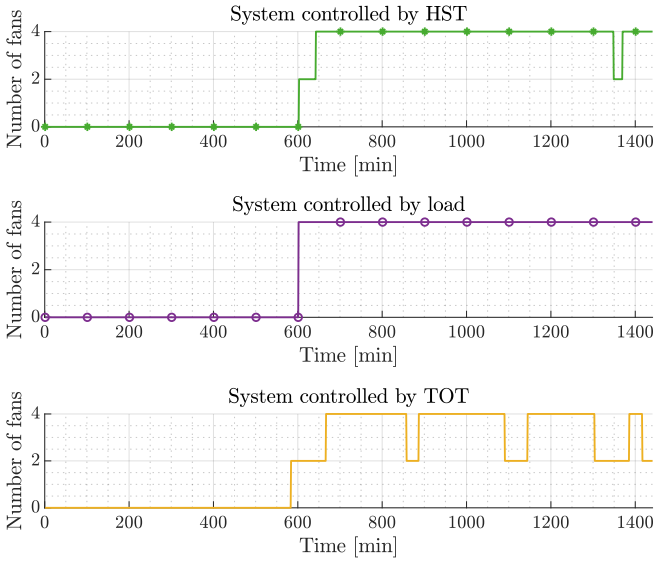

Figure 6.9: HST of different cooling methods after grid emergency. Scenario pre-cooling 200 minutes prior grid emergency, summer

The fan activation pattern can be seen figure 6.9. The system controlled by load activated both cooling levels immediately after grid emergency. The system controlled by TOT activated one level of cooling before emergency, then at 670 minutes it switched to both levels of cooling, afterwards it periodically switched between one and two levels. The system controlled by HST switched one level of cooling at 600 minutes and at 650 minutes, the activation of both levels of cooling followed. Then continuous operation of both levels can be observed until minute 1304, where the system shortly switched to one level of cooling, then continued with both levels of cooling again. All automatic system had durable TFOT, longest was, however by system controlled by load and shortest by system controlled by TOT. The TFOT, has direct impact on average HST. As the system with the longest TFOT tends to have lower HST.

6.3.2 Winter

Figure 6.10 illustrates HST of all automatic systems and of pre-cooled system. Maximum, average HST and TFOT can be found in table 6.2.

Die approbierte gedruckte Originalversion dieser Diplomarbeit ist an der TU Wien Bibliothek verfügbar
The approved original version of this thesis is available in print at TU Wien Bibliothek.

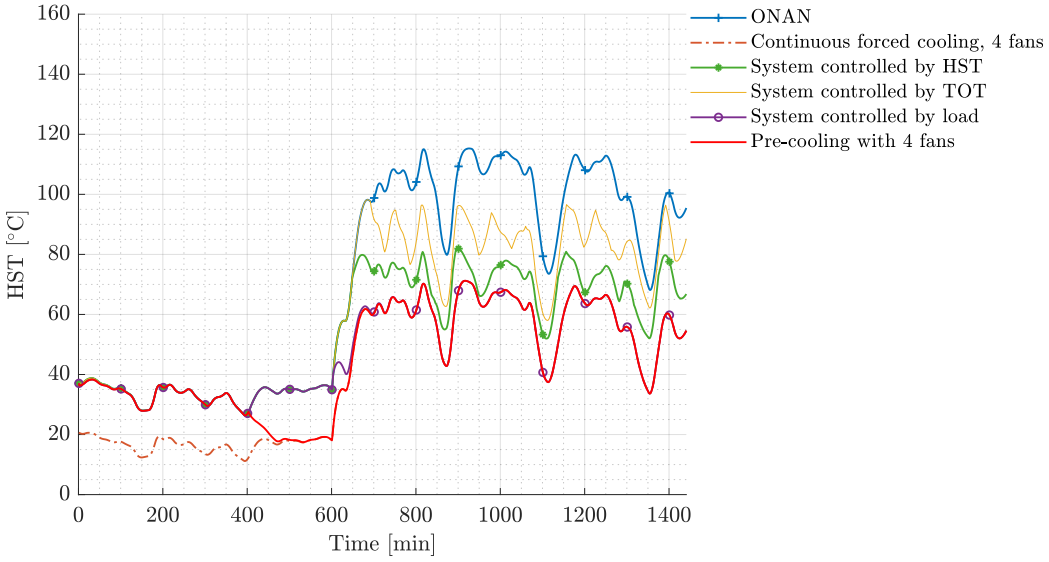

Figure 6.10: HST of different cooling methods after grid emergency. Scenario pre-cooling from 400 minute, winter

Table 6.2: Maximum, average HST and TFOT of automatic controlled systems after grid emergency. Scenario pre-cooling 200 minutes prior grid emergency, winter

System controlled by	Maximum HST, °C	Average HST,°C	TFOT, hrs
ONAN	115.28	97.69	0
TOT	98.19	81.72	5.43
HST	81.95	69.85	12.5
Load	71.21	57.90	28
Continuous forced cooling 4 fans	71.21	57.27	48

It is noticeable, that only the system controlled by load reached the HST of a pre-cooled system, with pre-cooling exposure time 99 minutes and the temperature gain 5.1°C.

For the system controlled by TOT and HST pre-cooling exposure time cannot be determined, as these systems did not reach the HST of pre-cooling. System controlled by TOT has highest average HST after 600 minutes, followed by the system controlled by HST. The effective time of pre-cooling exposure is the same as in the summer scenario.

Die approbierte gedruckte Originalversion dieser Diplomarbeit ist an der TU Wien Bibliothek verfügbar
The approved original version of this thesis is available in print at TU Wien Bibliothek.

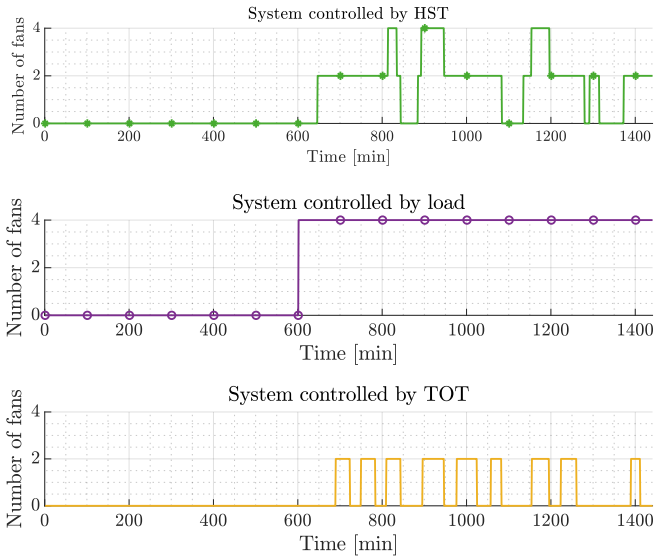

Figure 6.11: HST of different cooling methods after grid emergency. Scenario pre-cooling from 400 minute, summer

Table 6.3: Number of fans activations and de-activations. Scenario pre-cooling 200 minutes prior grid emergency, winter

	System controlled by		
	Load	**HST**	**TOT**
Number of activations	1	5	9
Number of de-activations	0	4	9
Total	1	9	18

The fan activation pattern is illustrated in figure 6.11 and the number of fan activations and de-activations is summarized in table 6.3. It can be seen from figure 6.11, that the system controlled by TOT activates one level of cooling at 700 minutes. Then it frequently switches on and off 2 fans. No continuous cooling was executed. This can be told from total number of activations and de-activation. TFOT of the system controlled by TOT is 12.5 hours. Lack of continuous cooling and frequent switching have direct impact on the value of average HST.

System controlled by load on contrary immediately activated both levels of cooling and 4 fans are operating the entire day. This allowed to achieve more effective cooling.

System controlled by HST switched one level of cooling on at minute 650. One level of cooling is operating until minute 810 then the system shortly activated both levels of cooling and then switched them off. From 900 minutes during 50 minutes longer operation of 4 fans can be observed, then the system switched to one level of cooling and continued with it until minute 1080. At 1100 minutes, a very similar pattern occurred again. Afterwards, the system shortly switched on and off one level of cooling. In total, the system controlled by HST switched on and off 9 times and had 12.5 hours of TFOT.

Die approbierte gedruckte Originalversion dieser Diplomarbeit ist an der TU Wien Bibliothek verfügbar
The approved original version of this thesis is available in print at TU Wien Bibliothek.

6.4 Interpretation of the results

Tables 6.4 and 6.5 contain the following information: effective time of pre-cooling, temperature difference between the pre-cooled and automatic systems for summer and winter, and temperature drop of the automatic control system.

Table 6.4: Effective time of pre-cooling and achieved temperature reserve, summer

Pre-cooling start, min	Temperature drop, °C		Temperature difference, °C	Effective time of pre-cooling, min
	from	to		
200	60.65	41	19.65	95
400	53.94	46.34	7.6	94
500	64.21	49.07	15.14	96

From table 6.4 it can be seen, that effective time of pre-cooling for all scenarios in summer varies between 94 and 96 minutes during this time HST drops by 15-20 °C. This allows to conclude, that long term pre-cooling is not reasonable. It can be recommended to start pre-cooling measures 100 minute prior to expected grid emergency during summer.

Table 6.5: Effective time of pre-cooling and achieved temperature reserve, winter

Pre-cooling start, min	Temperature drop, °C		Temperature reserve, °C	Effective time of pre-cooling, min
	from	to		
200	35.74	17.78	17.96	96
400	26.83	18.5	8.33	92
500	35.08	19.3	15.78	96

Same can be told for pre-cooling in winter. Effective time of pre-cooling varies is 91 or 96 minutes. During this time temperature drop 15-18 °C can achieved. This means, that by winter ambient temperature long-term pre-cooling is not reasonable either.

A summary for the automatic control systems in summer and winter can be found 6.7 and 6.6.

Using the average temperature difference between the HST of a pre-cooled system and the HST of the system controlled by other governing signal ($\Delta\theta_{hs.avg}$) during the exposure time d, the linear temperature gain can be estimated as:

$$\frac{\Delta\theta}{\Delta t} = 0.5 \cdot \frac{\Delta\theta_{hs.avg}}{d} \tag{6.1}$$

Table 6.6: Pre-cooling exposure time, temperature difference between the automatic and pre-cooled system and linear temperature gain, summer

	System controlled by	d, min	$\Delta\theta_{hs.avg}$, $^\circ C$	$\frac{\Delta\theta}{\Delta t}$, °C/min
Summer	TOT	146	6.39	0.02
	HST	125	7.5	0.03
	Load	99	5.1	0.02

Die approbierte gedruckte Originalversion dieser Diplomarbeit ist an der TU Wien Bibliothek verfügbar
The approved original version of this thesis is available in print at TU Wien Bibliothek.
TU Bibliothek Your knowledge hub WIEN

Pre-cooling exposure time in summer varies from 99 to 146 minutes. Systems that activate the fans quickly after load increase, as for example system controlled by load, might not require additional pre-cooling, as average HST of the pre-cooled system is only 5.26°C lower. Pre-cooling average HST was 7.5°C lower than that of automatic system controlled by HST. Pre-cooling can be used as supplementary cooling measure for transformers where the control system uses TOT signal.

From the table 6.6 it can be seen, that system controlled by load and TOT have fast linear temperature gain, whereas the system controlled by HST is the slowest.

Table 6.7: Pre-cooling exposure time and temperature difference between the pre-cooled and automatic control system, winter

	System controlled by	**d, min**	$\Delta\theta_{hs,avg}$,°C
Winter	TOT	-	9.2
	HST	-	8.6
	Load	99	5.1

It can be concluded, that pre-cooling exposure time can be estimated only for the system controlled by load, as the rest of the systems did not reach the HST of pre-cooled system. In table 6.7 the difference between the pre-cooled system and system controlled by HST and TOT was calculated using the pre-cooling exposure time of the system controlled by load. The average HST of system controlled by TOT was 9.2°C higher and the average HST of system controlled by HST was 8.6°C than this of pre-cooled system.

Die approbierte gedruckte Originalversion dieser Diplomarbeit ist an der TU Wien Bibliothek verfügbar
The approved original version of this thesis is available in print at TU Wien Bibliothek.

7 Conclusion

In this work the HST of a power oil-immersed transformer was calculated using the model of M.Djamali and the model provided in IEC 60076-7 loading guide. Different synthetic load profiles and ambient temperatures were used as input. Additionally a method for calculation of bottom-oil temperature was suggested, however this method requires a validation.

The following scenarios were studied: Wind Farm Collector Transformer with a peak load during the mid-day and steadily increasing load, Solar Farm Collector Transformer and interconnecting transformer, which is referred as Grid Transformer in this work.

During writing of this master thesis the following challenges were faced: obtaining the data for the calculation of average oil temperature, since it requires bottom-oil temperature as input, availability of specific geometric parameters of radiators and of fans, lack of information regarding the design dependent parameters for calculation of heat transfer values.

The following insights were gained after conducting the analysis regarding the research questions given in the introduction:

- **Which cooling control strategy is optimal for power transformer depending on the loading and ambient temperature pattern?**

Wind Farm Collector Transformers require a fast cooling control strategy due to the volatile load pattern, such characteristics can be attributed to system controlled by load and by HST.

Summarizing results for both wind load profiles it can be concluded, that the system controlled by load and continuous forced cooling are optimal for both profiles both in summer and winter. By lower ambient temperature further options can be considered as for example continuous forced cooling using only 2 fans or system controlled by HST.

For Solar Farm Collector Transformer by summer ambient temperature all automatic control systems can be applied, however system controlled by TOT can be sufficient, considering the maximum photovoltaic production profile. By winter ambient temperature SFCT does not require any additional cooling.

For interconnecting transformer operating under normal conditions, the system controlled by TOT and by HST can be recommended as optimal. For Grid Transformer by winter ambient temperature no additional cooling is required.

- **How the choice of cooling control strategy influences the maintenance and repair costs of the cooling system?**

To answer this question the two parameters were estimated namely, the Total Fan Operation Time and the number of fans activation and de-activation. The frequent fan activation (de-activation) can be damaging for the equipment, however long operation of

Die approbierte gedruckte Originalversion dieser Diplomarbeit ist an der TU Wien Bibliothek verfügbar
The approved original version of this thesis is available in print at TU Wien Bibliothek.
TU Bibliothek Your knowledge hub WIEN

fans reduces life span of the cooling system too, hence it is important to keep optimal number of switching and operation hours of fans.

While in scenario WFCT1 system controlled by load has optimal number of activations/de-activations and total fan operation time, in scenario WFCT2 system controlled by load activated fans once and they were operating the entire day, so the system controlled by HST looks like a better solution.

In scenario Solar Farm Collector Transformer the number of fan activation/ de-activation is similar for all automatic control systems. More continuous fan operation time can be observed by system controlled by load and the shortest by system controlled by TOT. In this case system controlled by TOT can be referred as optimal.

In scenario where Grid Transformer operates under normal operation conditions system controlled by HST has highest fan activation/de-activation numbers, lowest is by system controlled by load followed by system controlled by TOT. More continuous fan operation can be observed by the system controlled by TOT and shortest by the system controlled by load. Hence, controlling system by TOT in case of the Grid Transformer can be an optimal strategy.

- **What is the effective time of pre-cooling and how high is the achievable temperature reserve by using the pre-cooling?**

Effective time of pre- cooling is the time that the pre-cooled system required to achieve HST of the benchmark system. The temperature reserve can be defined as a temperature drop from the pre-cooling start until the moment when the pre-cooled system reached HST of the benchmark.

To answer these questions the following scenarios were simulated: pre-cooling 400 minutes, 200 minutes and 100 minutes prior grid emergency. All scenarios were studied by summer and winter ambient temperatures, before the grid emergency using the continuous forced cooling by 4 fans as a benchmark.

The estimated effective time of pre-cooling ranges between 94-96 minutes by summer and winter temperature by rated oil time constant 150 minutes for the specified transformer. Generally the temperature reserve ranges between 7°C and 19 °C for all scenarios in summer and winter.

- **What is the pre-cooling exposure time and maximum achieved temperature gain?**

To answer these questions pre-cooling 200 minutes before grid emergency was studied by both summer and winter ambient temperature.

Time that automatic system required to reach the HST of a pre-cooled system is defined as pre-cooling exposure time. The temperature gain is average difference between HST of a pre-cooled system and automatic control system during the pre-cooling exposure time.

Pre-cooling exposure time was calculated by comparing the HST of system controlled by TOT, HST, load to the HST of a pre-cooled system after grid emergency. Additionally, linear temperature gain was calculated using the obtained pre-cooling exposure time and temperature difference.

Pre-cooling exposure time by summer ambient temperature varies between 99 and 146 minutes and the temperature gain varies from 5°C to 7 °C. Maximum linear temperature gain was achieved by applying pre-cooling with system controlled by HST 0.03 °C/min.

Die approbierte gedruckte Originalversion dieser Diplomarbeit ist an der TU Wien Bibliothek verfügbar
The approved original version of this thesis is available in print at TU Wien Bibliothek.
TU Bibliothek Your knowledge hub WIEN

Hence, by using pre-cooling method together with system controlled by HST even better cooling effect can be achieved.

Pre-cooling exposure time by winter can only be calculated for the system controlled by load, as the system controlled by HST and TOT did not achieve the HST of the pre-cooled system. As average HST after grid emergency without any fan activation was 97 °C, the transformer does not require any pre-cooling.

For the reference transformer it can be concluded, that pre-cooling effect lasts 92-96 minutes by rated oil-time constant 150 minutes irrespective of the fan activation start time and ambient temperature. Hence, it is reasonable to start pre-cooling shortly before (for example 100 minutes) before contingency. It is only applicable against the short-term peak load. Applying pre-cooling against long-term peak load is rather redundant. The achieved temperature reserve can be up to 19 °C. Pre-cooling by winter ambient temperature is not required, as the temperature drops below 20 °C in all scenarios.

Since the major part of this master thesis was the modelling and parametrization of the model some questions remained open. These are for example: a maximum peak load, that a transformer can withstand by applied pre-cooling, a validation of the model, applying model on other transformer with different cooling types and comparing the results, the behavior of the thermal resistance etc.

Die approbierte gedruckte Originalversion dieser Diplomarbeit ist an der TU Wien Bibliothek verfügbar
The approved original version of this thesis is available in print at TU Wien Bibliothek.

Annex A

Table 7.1: Empirical and design dependent parameters used in the model

	Description	Value	Units
s_{oil}	surface of convection heat transfer on the oil side	0.3	m
A_{oil}	characteristic length of oil convection	10	cm^2
p_{oil}	empirical factor of oil natural convection	0.191	-
q_{oil}	empirical factor of oil natural convection	8.152	-
u_{air}	proportionality constant of air	4.8	-
d_{air}	characteristic diameter of air path	0.152	m
s_{air}	characteristic length of air convection	0.1	m
A_{rad}	effective surface of radiation	0.5	cm^2
A_{air}	sufrace of convection heat transfer on the air side	7	cm^2
m	empirical factor of forced air convection	0.5	-
n	empirical factor of forced air convection	0.33	-
C_{air}	empirical factor of forced air convection	0.085	-
p_{air}	empirical factor of air natural convection	0.25	-
q_{air}	empirical factor of air natural convection	0.858	-

Die approbierte gedruckte Originalversion dieser Diplomarbeit ist an der TU Wien Bibliothek verfügbar
The approved original version of this thesis is available in print at TU Wien Bibliothek.

Table 7.2: The parameters of the reference transformer

Parameter	Value	Unit
S_n	58/45/40	MVA
U_n	225/26.4	kV
R_{bo}	0.09	K/W
$\theta_{bo,r}$	46.7	$°C$
$P_{no_load_loss}$	46.32	kW
P_{load_loss}	370.9	kW
x	0.8	
y	1.3	
R	8.0	
k_{11}	1	
k_{21}	2.0	
k_{22}	2.0	
τ_o	150	min
τ_w	7	min
$\Delta\theta_{to,r}$	52	$°C$
R_{thr}	0.89	K/W
$\Delta\theta_{hr}$	26	$°C$

Table 7.3: The empirical coefficients for estimation of the heat transfer coefficient [44]

	Forced convective cooling		Natural convective cooling	
Winding type	C	m	C	m
Layer winding, axial	0.0834	0.213	9.05	0.61
Layer winding, radial	0.0834	0.213	8.152	0.191
Disc winding, radial	0.0834	0.213	8.152	0.191
Disc winding, axial	0.61	0.210	9.05	0.61
Disc winding radial and axial	0.0148	0.210	9.05	0.61
	0.0148	0.47	0.262	0.346

Die approbierte gedruckte Originalversion dieser Diplomarbeit ist an der TU Wien Bibliothek verfügbar
The approved original version of this thesis is available in print at TU Wien Bibliothek.

Table 7.4: Power transformer radiator parameters [45]

Symbol	**Radiator design parameters**	**Parameter values**
h	Radiator height	2600 mm
Δy	The height between the radiator and the winding	450 mm
W	Radiator width	520 mm
N	Number of panels	22
b_{oil}/a_{oil}	Ratio of length to width of rectangular oil channel	14.29
s_c	Oil flow channel area	$3.25 \times 10^{-4} m^2$
d_c	Perimeter of oil flow channel	0.3045 m
α_{air}	Radiator spacing	50 mm
V_{air}	Wind speed	1 m/s

Die approbierte gedruckte Originalversion dieser Diplomarbeit ist an der TU Wien Bibliothek verfügbar
The approved original version of this thesis is available in print at TU Wien Bibliothek.

List of Figures

2.1 WPP grid topology [8] . . . 7
2.2 SPP grid topology [10] . . . 8
2.3 Transformer cooling modes [12] . . . 9
2.4 Dependency of oil density from the temperature [14] . . . 10
2.5 High mounted radiator [15] . . . 10
2.6 Operation principle of ONAN cooling method [15] . . . 11
2.7 Operation principle of ONAF cooling method [15] . . . 12
2.8 Thermal diagram of a transformer with ONAN and additional ONAF cooling methods [11] . . . 13
2.9 Vertical and horizontal mounted fans [16] . . . 14
2.10 The scheme of a control cabinet [11] . . . 15
2.11 The effect of pre-cooling on the insulation aging [17] . . . 16
2.12 Traditional gauge [20] . . . 17
2.13 Scheme of WTI and OTI [21] . . . 18

3.1 Linear thermal diagram of oil cooled transformer [1] . . . 24
3.2 Thermo-electric analogy [29] . . . 27
3.3 Circuit for calculation of TOT in Swift model [32] . . . 28
3.4 Circuit for calculation of TOT in Susa model [33] . . . 29
3.5 Circuit for calculation of HST in Susa model [33] . . . 30
3.6 Circuit for calculation of TOT in Djamali model [36] . . . 32

4.1 Simplified model block diagram . . . 33
4.2 Ambient temperature in winter and summer . . . 34
4.3 Load profiles used for different scenarios . . . 36
4.4 Bottom-oil circuit . . . 42

5.1 HST of different cooling methods. WFCT 1, summer . . . 46
5.2 Fan activation pattern. Scenario WFCT 1, summer . . . 47
5.3 HST of different cooling methods. Scenario WFCT 1, winter . . . 48
5.4 Fan activation pattern. Scenario WFCT 1, winter . . . 49
5.5 HST of different cooling methods. Scenario WFCT 2, summer . . . 51
5.6 Fan activation pattern. Scenario WFCT 2, summer . . . 52
5.7 HST temperatures of different cooling methods. Scenario WFCT 2, winter . . . 53
5.8 Fan activation pattern. Scenario WFCT 2,winter . . . 54
5.9 HST of different cooling methods. Scenario SFCT, summer . . . 55
5.10 Fan activation pattern. Scenario SFCT, summer . . . 56
5.11 HST of different cooling methods. Scenario SFCT, winter . . . 57
5.12 HST of different cooling methods. Scenario grid transformer, summer . . . 58
5.13 Fan activation pattern. Scenario grid transformer, summer . . . 59
5.14 HST of different cooling methods. Scenario grid transformer, winter . . . 60

Die approbierte gedruckte Originalversion dieser Diplomarbeit ist an der TU Wien Bibliothek verfügbar
The approved original version of this thesis is available in print at TU Wien Bibliothek.
TU Bibliothek Your knowledge hub WIEN

6.1 HST of different cooling methods after grid emergency. Scenario pre-cooling 400 minutes prior grid emergency, summer 62
6.2 HST of different cooling methods. Scenario pre-cooling 200 minutes prior grid emergency, summer 63
6.3 HST of different cooling methods after grid emergency. Scenario pre-cooling 100 minutes prior grid emergency, summer 64
6.4 HST of different cooling methods and HST of pre-cooled transformer 65
6.5 HST of different cooling methods. Scenario pre-cooling 400 minutes prior grid emergency 66
6.6 HST of different cooling methods. Scenario pre-cooling 200 minutes prior grid emergency, winter 66
6.7 HST of different cooling methods after gird emergency. Scenario pre-cooling 100 minutes prior grid emergency, winter 67
6.8 HST of different cooling methods after grid emergency. Scenario pre-cooling 200 minutes prior grid emergency, summer 68
6.9 HST of different cooling methods after grid emergency. Scenario pre-cooling 200 minutes prior grid emergency, summer 69
6.10 HST of different cooling methods after grid emergency. Scenario pre-cooling from 400 minute, winter 70
6.11 HST of different cooling methods after grid emergency. Scenario pre-cooling from 400 minute, summer 71

Die approbierte gedruckte Originalversion dieser Diplomarbeit ist an der TU Wien Bibliothek verfügbar
The approved original version of this thesis is available in print at TU Wien Bibliothek.

List of Tables

3.1 Analogy between the thermal and electrical variables [32] 27

4.1 Minimum, maximum and average temperatures for winter and summer temperature profiles 34
4.2 Maximum, minimum and average load factors 36
4.3 Fan switch on and off points for different automatic systems 43

5.1 Maximum, average HST and TFOT of different cooling methods. Scenario WFCT 1, summer 46
5.2 Number of fan activations and de-activations. Scenario WFCT 1, summer . 47
5.3 Maximum, average HST and TFOT of different cooling methods. Scenario WFCT 1, winter 49
5.4 Number of fan activations and de-activations for all automatic systems. Scenario WFCT 1, winter 50
5.5 Maximum, average HST and TFOT of different cooling methods. Scenario WFCT 2, summer 51
5.6 Number of fan activations and de-activations. Scenario WFCT 2, summer . 52
5.7 Maximum, average HST and TFOT of different cooling methods. Scenario WFCT 2, winter 53
5.8 Number of fan activations. Scenario WFCT 2, winter 54
5.9 Maximum, average HST and TFOT of different cooling methods. Scenario SFCT, summer 55
5.10 Maximum, average HST and TFOT. Scenario grid transformer, summer . . 58
5.11 Number of fans activations and de-activations. Scenario grid transformer, summer 59

6.1 Maximum, average HST and TFOT of automatic controlled systems after grid emergency. Scenario pre-cooling 200 minutes prior grid emergency, summer 68
6.2 Maximum, average HST and TFOT of automatic controlled systems after grid emergency. Scenario pre-cooling 200 minutes prior grid emergency, winter 70
6.3 Number of fans activations and de-activations. Scenario pre-cooling 200 minutes prior grid emergency, winter 71
6.4 Effective time of pre-cooling and achieved temperature reserve, summer . . 72
6.5 Effective time of pre-cooling and achieved temperature reserve, winter . . . 72
6.6 Pre-cooling exposure time, temperature difference between the automatic and pre-cooled system and linear temperature gain, summer 72
6.7 Pre-cooling exposure time and temperature difference between the pre-cooled and automatic control system, winter 73

Die approbierte gedruckte Originalversion dieser Diplomarbeit ist an der TU Wien Bibliothek verfügbar
The approved original version of this thesis is available in print at TU Wien Bibliothek.
TU Bibliothek Your knowledge hub WIEN

7.1 Empirical and design dependent parameters used in the model 77
7.2 The parameters of the reference transformer 78
7.3 The empirical coefficients for estimation of the heat transfer coefficient [44] 78
7.4 Power transformer radiator parameters [45] 79

Die approbierte gedruckte Originalversion dieser Diplomarbeit ist an der TU Wien Bibliothek verfügbar
The approved original version of this thesis is available in print at TU Wien Bibliothek.

Bibliography

[1] "Power transformers – part 7: Loading guide for mineral-oil-immersed power transformers, 60076-7," International Electrotechnical Comission, Tech. Rep., 2008. 1, 3, 23, 24, 25, 26, 37, 80

[2] E. Amoiralis, M. A. Tsili, and P. S. Georgilakis, "The state of the art in engineering methods for transformer design and optimization: a survey," *Journal of optoelectronics and advanced materials*, vol. 10, no. 5, pp. 1149–1158, May 2008. 3, 4, 5

[3] R. Feinberg, Ed., *Modern power transformer practice*, repr ed., London, 1980. 4, 6

[4] Z. Melhem, Ed., *Electricity transmission, distribution and storage systems*, ser. Woodhead publishing series in energy. Oxford: Woodhead Publishing, 2013, no. Number 38. 4

[5] L. F. Blume, *Transformer engineering: a treatise on the theory, operation and application of transformers*, 2nd ed. New York: John Wiley, 1951, oCLC: 318318406. 5

[6] W. Hofbauer, "Thermische Modellierung von Leistungstransformatoren zur Integration in ein dynamisches Verfügbarkeitsmanagement - Evaluierung von Konzepten," Ph.D. dissertation, 2017. [Online]. Available: https://repositum.tuwien.at/handle/20.500.12708/3775 5, 11, 25

[7] "Power Transformer Application for Wind Plant Substations." New Jersey: IEEE, 2010. 6

[8] "Wind Plant Power Flow Modeling Guide - ESIG." [Online]. Available: https://www.esig.energy/wiki-main-page/wind-plant-power-flow-modeling-guide/ 6, 7, 80

[9] H. A. Halim, B.T. Phung, and John Fletcher, "Energizing inrush current transients in parallel connected transformers," 2015. 6

[10] *IEEE Std C57.159-2016: IEEE Guide on Transformers for Application in Distributed Photovoltaic (DPV) Power Generation Systems*. IEEE, 2016, oCLC: 972624534. 7, 8, 80

[11] H. Vosen, *Kühlung und Belastbarkeit von Transformatoren: Erläuterungen zu DIN VDE 0532*, ser. VDE-Schriftenreihe. Berlin: VDE-Verl, 1997, no. 72. 8, 9, 13, 14, 15, 16, 18, 20, 80

[12] L. Borowik, R. Włodarz, and K. Chwastek, "Eco-efficient control of the cooling systems for power transformers," *Journal of Cleaner Production*, vol. 139, pp. 1551–1562, 2022. [Online]. Available: https://linkinghub.elsevier.com/retrieve/pii/S0959652615019198 8, 9, 80

Die approbierte gedruckte Originalversion dieser Diplomarbeit ist an der TU Wien Bibliothek verfügbar
The approved original version of this thesis is available in print at TU Wien Bibliothek.
TU Bibliothek Your knowledge hub WIEN

[13] Conseil international des grands réseaux électriques, Ed., *Transformer thermal modelling*. Paris: Cigré, 2016. 9, 23, 25, 33

[14] F. Zhu and B. Yang, *Power transformer design practices*, first edition ed. Boca Raton, FL: CRC Press/Taylor & Francis Group, LLC, 2021. 10, 11, 80

[15] L. Kish, *Heating and cooling of transformers*. Moscow: Energy, 1980. 10, 11, 12, 80

[16] S. B. Paramane, W. Van Der Veken, A. Sharma, and J. Coddé, "Effect of fan arrangement and air flow direction on thermal performance of radiators in a power transformer," *Journal of Power Technologies 97*, vol. 2, pp. 127–134, 2017. 14, 80

[17] C. Kane, "Monitoring technologies for large power transformers," IEE, Tech. Rep. 16, 80

[18] "Transformer Temperature Monitoring | Dynamic Ratings." [Online]. Available: https://www.dynamicratings.com/solutions/transformer-monitoring/temperature-monitoring/ 16

[19] "Oil and Winding temperature Indicator of the transformer." [Online]. Available: https://vietnamtransformer.com/our-news/oil-and-winding-temperature-indicator-of-the-transformer 17

[20] "Oil and Winding temperature Indicator of the transformer." [Online]. Available: https://vietnamtransformer.com/our-news/oil-and-winding-temperature-indicator-of-the-transformer 17, 18, 80

[21] B. D. Sparling, "Transformers Journal," *Improved transformer temperature monitoring*, vol. 4, no. 4, pp. 22–26. 18, 19, 80

[22] "Transformer Winding Temperature Sensor, Indicator, Monitoring." [Online]. Available: https://www.orionitalia.com/applications/industrial/transformer-winding-temperature-sensor-monitoring-indicator 19

[23] R. Smith, H. Inomata, and C. Peters, "Heat Transfer and Finite-Difference Methods," in *Supercritical Fluid Science and Technology*. Elsevier, 2013, vol. 4, pp. 557–615. [Online]. Available: https://linkinghub.elsevier.com/retrieve/pii/B9780444522153000088 20, 21, 22

[24] VDI-Gesellschaft Verfahrenstechnik und Chemieingenieurwesen, Ed., *VDI heat atlas*, 2nd ed., ser. VDI-buch. Berlin ; New York: Springer, 2010, oCLC: ocn489638163. 20, 22, 40

[25] "Majid Bahrami - Teaching - ENSC 388." [Online]. Available: https://www.sfu.ca/~mbahrami/ensc388.html 20

[26] E. Shashi Menon, "Fluid Flow in Pipes," in *Transmission Pipeline Calculations and Simulations Manual*. Elsevier, 2015, pp. 149–234. [Online]. Available: https://linkinghub.elsevier.com/retrieve/pii/B9781856178303000055 21

[27] B. E. Rapp, "Fluids," in *Microfluidics: Modelling, Mechanics and Mathematics*. Elsevier, 2017, pp. 243–263. [Online]. Available: https://linkinghub.elsevier.com/retrieve/pii/B9781455731411500095 22

Die approbierte gedruckte Originalversion dieser Diplomarbeit ist an der TU Wien Bibliothek verfügbar
The approved original version of this thesis is available in print at TU Wien Bibliothek.
TU Bibliothek Your knowledge hub WIEN

[28] M. Djamali, "Thermal monitoring of power transformers," PhD, Universität Stuttgart, Stuttgart, Jan. 2018. 22, 23

[29] M. Djamali and S. Tenbohlen, "Hundred years of experience in the dynamic thermal modelling of power transformers," *IET Generation, Transmission & Distribution*, vol. 11, no. 11, pp. 2731–2739, Aug. 2017. [Online]. Available: https://onlinelibrary.wiley.com/doi/10.1049/iet-gtd.2016.1321 22, 27, 28, 29, 80

[30] *IEEE guide for loading mineral-oil-immersed transformers.* New York: Institute of Electrical and Electronics Engineers, 1996, oCLC: 326336179. 23, 26

[31] W. H. Tang and Q. H. Wu, *Condition monitoring and assessment of power transformers using computational intelligence*, ser. Power systems. London ; New York: Springer, 2011, oCLC: ocn722305754. 26

[32] G. Swift, T. Molinski, and W. Lehn, "A fundamental approach to transformer thermal modeling. I. Theory and equivalent circuit," *IEEE Transactions on Power Delivery*, vol. 16, no. 2, pp. 171–175, Apr. 2001. [Online]. Available: http://ieeexplore.ieee.org/document/915478/ 27, 28, 80, 82

[33] D. Susa, M. Lehtonen, and H. Nordman, "Dynamic Thermal Modelling of Power Transformers," *IEEE Transactions on Power Delivery*, vol. 20, no. 1, pp. 197–204, Jan. 2005. [Online]. Available: http://ieeexplore.ieee.org/document/1375095/ 29, 30, 31, 80

[34] D. Susa, J. Palola, M. Lehtonen, and M. Hyvarinen, "Temperature Rises in an OFAF Transformer at OFAN Cooling Mode in Service," *IEEE Transactions on Power Delivery*, vol. 20, no. 4, pp. 2517–2525, Oct. 2005. [Online]. Available: http://ieeexplore.ieee.org/document/1514499/ 29

[35] D. Susa and M. Lehtonen, "Dynamic Thermal Modeling of Power Transformers: Further Development—Part I," *IEEE Transactions on Power Delivery*, vol. 21, no. 4, pp. 1961–1970, Oct. 2006. [Online]. Available: http://ieeexplore.ieee.org/document/1705556/ 29

[36] M. Djamali and S. Tenbohlen, "Malfunction Detection of the Cooling System in Air-Forced Power Transformers Using Online Thermal Monitoring," *IEEE Transactions on Power Delivery*, vol. 32, no. 2, pp. 1058–1067, Apr. 2017. [Online]. Available: http://ieeexplore.ieee.org/document/7529157/ 31, 32, 38, 80

[37] "ZAMG Data Hub." [Online]. Available: https://data.hub.zamg.ac.at/dataset/klima-v1-10min 34

[38] M. Weigl, "Abschätzung der Unsicherheiten von Belastungsszenarien einer Ortnetzstation mittels maschinellen Lernens für ein dezentrales Verfügbarkeitsmanagement," Ph.D. dissertation, 2022. [Online]. Available: https://repositum.tuwien.at/handle/20.500.12708/19705 35

[39] S. Meinecke, D. Sarajlić, S. R. Drauz, A. Klettke, L.-P. Lauven, C. Rehtanz, A. Moser, and M. Braun, "SimBench—A Benchmark Dataset of Electric Power Systems to Compare Innovative Solutions Based on Power Flow

Die approbierte gedruckte Originalversion dieser Diplomarbeit ist an der TU Wien Bibliothek verfügbar
The approved original version of this thesis is available in print at TU Wien Bibliothek.
TU Bibliothek Your knowledge hub WIEN

Analysis," *Energies*, vol. 13, no. 12, p. 3290, Jun. 2020. [Online]. Available: https://www.mdpi.com/1996-1073/13/12/3290 35

[40] "SimBench – Benchmark-Datensatz für Netzanalyse, Netzplanung und Netzbetriebsführung." [Online]. Available: https://simbench.de/en/ 35

[41] L. Wang, L. Zhou, H. Tang, D. Wang, and Y. Cui, "Numerical and experimental validation of variation of power transformers' thermal time constants with load factor," *Applied Thermal Engineering*, vol. 126, pp. 939–948, Nov. 2017. [Online]. Available: https://linkinghub.elsevier.com/retrieve/pii/S1359431117327357 37

[42] R. McCluney, "Radiometry and Photometry," in *Encyclopedia of Physical Science and Technology*. Elsevier, 2003, pp. 731–758. [Online]. Available: https://linkinghub.elsevier.com/retrieve/pii/B0122274105006487 40

[43] "IEEE Guide for Loading Mineral-Oil-Immersed Transformers and Step-Voltage Regulators," IEEE, Tech. Rep. [Online]. Available: http://ieeexplore.ieee.org/document/6166928/ 44

[44] K. Eckholz, W. Knorr, and M. Schäfer, "NEW DEVELOPMENTS IN TRANSFORMER COOLING CALCULATIONS," 2006. 78, 83

[45] L. Wang, W. Zuo, Z.-X. Yang, J. Zhang, and Z. Cai, "A Method for Fans' Potential Malfunction Detection of ONAF Transformer Using Top-Oil Temperature Monitoring," *IEEE Access*, vol. 9, pp. 129 881–129 889, 2021. [Online]. Available: https://ieeexplore.ieee.org/document/9541383/ 79, 83

Die approbierte gedruckte Originalversion dieser Diplomarbeit ist an der TU Wien Bibliothek verfügbar
The approved original version of this thesis is available in print at TU Wien Bibliothek.